

Two-Gluon Correlations in Heavy-Light Ion Collisions: Energy and Geometry Dependence, IR Divergences, and k_T -Factorization

Yuri V. Kovchegov,^a Douglas E. Wertepny^b

Department of Physics, The Ohio State University, Columbus, OH 43210, USA

We study the properties of the cross section for two-gluon production in heavy-light ion collisions derived in our previous paper [1] in the saturation/Color Glass Condensate framework. Concentrating on the energy and geometry dependence of the corresponding correlation functions we find that the two-gluon correlator is a much slower function of the center-of-mass energy than the one- and two-gluon production cross sections. The geometry dependence of the correlation function leads to stronger azimuthal near- and away-side correlations in the tip-on-tip U+U collisions than in the side-on-side U+U collisions, an exactly opposite behavior from the correlations generated by the elliptic flow of the quark-gluon plasma: a study of azimuthal correlations in the U+U collisions may thus help to disentangle the two sources of correlations.

We demonstrate that the cross section for two-gluon production in heavy-light ion collisions contains a power-law infrared (IR) divergence even for fixed produced gluon momenta: while saturation effects in the target regulate some of the power-law IR divergent terms in the lowest-order expression for the two-gluon correlator, other power-law IR divergent terms remain, possibly due to absence of saturation effects in the dilute projectile. Finally we rewrite our result for the two-gluon production cross-section in a k_T -factorized form, obtaining a new factorized expression involving a convolution of one- and two-gluon Wigner distributions over both the transverse momenta and impact parameters. We show that the two-gluon production cross-section depends on two different types of unintegrated two-gluon Wigner distribution functions.

PACS numbers: 25.75.-q, 25.75.Gz, 12.38.Bx, 12.38.Cy

I. INTRODUCTION

The discovery of the long-range rapidity correlation known as the 'ridge' in heavy ion collisions at the Relativistic Heavy Ion Collider (RHIC) [2–5] spurred, among other things, a flurry of activity [6–21] aimed at better understanding two-particle correlations in the parton saturation/Color Glass Condensate (CGC) physics framework (see [22–27] for reviews of the saturation/CGC field). Apart from quantifying how much of the 'ridge' dynamics, which in the meantime was also observed by experiments at the Large Hadron Collider (LHC) in proton–proton (pp) and proton–nucleus (pA) collisions [28–31], is due to the initial-state saturation effects, the problem of two-gluon production in nucleus–nucleus (AA) collisions is an important theoretical problem in its own right, allowing us to gain a new insight in the nonlinear dynamics of strong gluon fields in the initial stages of heavy ion collisions.

The strategy for tackling the two-gluon production problem closely parallels that of the single-gluon production. Any observable in the saturation/CGC framework is calculated in three stages: (i) First the observable is evaluated in the quasi-classical Glauber–Mueller (GM) [32] / McLerran–Venugopalan (MV) [33–35] approximation; (ii) then the small- x Balitsky–Kovchegov (BK) [36–39] and Jalilian-Marian–Iancu–McLerran–Weigert–Leonidov–Kovner (JIMWLK) [40–43] nonlinear evolution corrections are included into the expression; (iii) finally, phenomenological applications [44–46] demand that the scale of the running coupling is fixed [47–50] using, e.g., Brodsky–Lepage–Mackenzie (BLM) prescription [51]. Indeed higher-order perturbative corrections (beyond the running coupling corrections) need to be included as well [52], though at this point they have not been implemented in the existing phenomenology.

While the steps (i), (ii) and (iii) have been fully implemented for the total cross section in deep inelastic scattering (DIS) and for the corresponding structure functions, the situation is more complicated for particle production. The classical gluon production cross section (step (i) in the above classification) is known analytically in pp collisions (dilute–dilute scattering) [53–55] and in pA collisions (dilute–dense scattering) [56, 57], while only numerical solution [58, 59] exists for the classical gluon field in AA collisions (dense–dense scattering). Leading- $\ln 1/x$ evolution corrections (step (ii)) have been included into the pA gluon production cross section in [60, 61]. (The analogous pp result can be obtained from pA by expansion to the lowest order in saturation effects in the nucleus.) Running coupling corrections for the gluon production (step (i)) have only been resummed for the pp case [50].

^a kovchegov.1@asc.ohio-state.edu

^b wertepny.1@osu.edu

Our understanding of the two-gluon production in the saturation/CGC framework is somewhat less developed, chiefly due to the complexity of the problem. The problem of two-gluon production in DIS and pA (dilute–dense) collisions was solved in [61–65] for the gluons produced with the large separation in rapidity, $\Delta y \gtrsim 1/\alpha_s$ with α_s the strong coupling constant. To describe two-gluon production in AA collisions one needs to include higher-order density effects in the projectile. The lowest-order quasi-classical two-gluon production cross section in AA was derived in the original paper [8], with the gluons close to each other in rapidity, $\Delta y \lesssim 1/\alpha_s$. The corresponding two-gluon production cross section for the semi-dilute–dense scattering case (which we will refer to as heavy-light ion collisions) was found only recently in [1, 16]. (Note that the pA scattering is not a good model for two-gluon production in dense–dense collisions in the CGC framework, since in AA collisions the two gluons are produced mainly from different nucleons: replacing one of the nuclei by a proton would force two gluons to be emitted off of the same proton, which is subleading in the AA case. Here we model AA collisions by considering the case when one nucleus is much smaller than another one, while still having a significant number of nucleons [1]: these are the heavy-light ion collisions.) Since the cross section in [1, 16] expresses the interaction with the dense target nucleus via Wilson lines, small- x evolution between the produced gluons and the target can be automatically included into it: however, unlike the pA case of [61–63, 65], no one has yet included the evolution between the projectile and the produced gluons in heavy-light ion collisions, allowing the gluons to be produced at mid-rapidity in RHIC or LHC kinematics. Two-gluon production in the dense–dense (AA) case has so far been tackled only numerically [66] in the quasi-classical limit.

All the above-mentioned results for two-gluon production [1, 8, 16, 66] indicate that the corresponding cross section exhibits long-range rapidity correlations, along with enhancement of correlations at the azimuthal opening angles $\Delta\phi = 0$ and $\Delta\phi = \pi$ between the gluons. A saturation-inspired generalization of the lowest-order result [8] allowed for successful pp and pA phenomenology [12, 17–19]. However, further theoretical advances are needed to improve the precision of CGC predictions for di-hadron correlations.

The goal of this paper is to study the properties of the two-gluon production cross section in heavy-light ion collisions found in [1]. While we begin the paper by reviewing the main results of [1] in Sec. II, our paper is best read in conjunction with [1].

The scope of our paper covers a wide range of issues in our understanding of two-gluon correlations. Recently there was a significant amount of discussion in the community of whether the ‘ridge’ correlations seen in pp and pA collisions at the LHC [28–31] have hydrodynamic or CGC origin [67]. It appears important to find an experiment being able to disentangle the two mechanism generating azimuthal correlations. In Sec. III we show that such an experiment could be the study of long-range rapidity correlations in the $U + U$ collisions. We show that the CGC correlations are stronger in the tip-on-tip $U + U$ collisions than in the side-on-side ones. Such behavior is the exact opposite of the ellipticity-driven hydrodynamic correlations [68–70]. Perhaps the two effects could be disentangled by studying the $U + U$ collisions data.

It has been known since the original calculation of [8] that the two-gluon production cross section in CGC contains power-law infrared (IR) divergences, even for fixed momenta of the produced gluons (see Eq. (16) below). This is in stark contrast to the single-gluon production cross section, which only contains weak logarithmic IR divergences. The authors of [8] conjectured that saturation effects in both colliding nuclei, when included, would regulate this divergence: this assumption appears to be confirmed by numerical simulations of [66]. The analytical expression for two-gluon production in heavy-light ion collisions obtained in [1] contains all-order saturation effects in one of the nuclei (the target nucleus). In Sec. IV we study the result of [1] to explore whether the saturation effects in one of the nuclei are sufficient to regulate the power-law IR divergence of [8]. We find that, while some of the power-law IR divergent terms are regulated by saturation effects in the target, other terms with the same divergence remain, rendering the whole cross-section power-law IR-divergent (see Eq. (40) below). Such result is indeed worrisome, since it questions our ability to make controlled phenomenological predictions for di-hadron correlations: however we find that the IR-divergent piece does not contain any azimuthally-nontrivial correlations. Hence the $\Delta\phi$ -dependent part of the correlations is not affected and is safe from this IR divergence.

The cross section for single-gluon production in pA collisions calculated in approximations (i) and (ii) described above can be cast in a k_T -factorized form [60, 63]. Recently, k_T -factorization at the JIMWLK functional level has been proven (in the leading- $\ln 1/x$ approximation) for local in rapidity particle production in dense–dense collisions in [10, 71, 72]. Motivated by these results we try obtaining a k_T -factorized form for two-gluon production cross section in Sec. V. The final result, given in Eq. (72), is a k_T -factorized expression, whose form is more complicated than that for the single-gluon production [60, 63]. The expression (72) contains not only a convolution over transverse momenta, but also over impact parameters. The objects being convoluted are not the unintegrated gluon distributions, but rather one- and two-gluon Wigner distributions, containing the information about both the gluons momenta and impact parameters. Note that the production cross section employs two types of two-gluon Wigner distributions: double-trace (48) and quadrupole (50) ones, introduced for the first time in this paper. (This is to be compared with the dipole single-gluon distribution entering the single-gluon production [60, 63].)

Another important question concerning the energy-dependence of the two-gluon production cross section is studied

in Sec. VI. We find that, in the leading power-of-energy approximation, the two-gluon correlation function in heavy-light ion collisions is independent of the center-of-mass energy of the collision. This is a prediction which can be verified experimentally. Note that, as we have mentioned above, the two-gluon production cross section of [1] was derived without any evolution corrections between the projectile and the produced gluons. Hence, in this approximation, the net rapidity interval is equal to the rapidity interval between the produced gluons and the target. Further studies of energy and rapidity dependence of two-gluon production should be carried out improving upon our approximation.

We conclude in Sec. VII by summarizing our main results and discussing future avenues of research on correlations in the CGC framework.

II. BRIEF SUMMARY OF THE RESULTS FOR THE TWO-GLUON PRODUCTION CROSS SECTION

In [1] we considered two-gluon production in a collision of a large heavy ion (target) with a lighter nucleus (projectile). The projectile was considered to be smaller than the target, but still large enough a nucleus for the two gluons to be produced in collisions of different nucleons in the projectile with the target nucleus. Formally we assume that $A_2 \gg A_1 \gg 1$, where A_1 and A_2 are respectively the atomic numbers of the projectile and the target. The target was large enough for the saturation effects to be important, such that $\alpha_s^2 A_2^{1/3} \sim 1$. The saturation effects in the projectile were kept at the lowest order with $\alpha_s^2 A_1^{1/3} \ll 1$. In terms of momentum scales the regime of interest is $k_T \gtrsim Q_{s1}$, with k_T the transverse momentum of either one of the produced gluons (k_1 or k_2) and Q_{s1} the saturation scale of the projectile which is much smaller than the saturation scale of the target, $Q_{s2} \gg Q_{s1} \gg \Lambda_{QCD}$. The approximation used in [1] corresponds to calculating the two-gluon production in nucleus-nucleus ($A+A$) collisions in the McLerran-Venugopalan (MV) model [33–35] while keeping interactions with the projectile nucleus to the lowest non-trivial order of two interacting nucleons. This setup may not directly describe the bulk of proton-nucleus ($p+A$) collisions (also known as the dense-dilute collisions); note however that if one triggers on the high-multiplicity $p+A$ events one is then probing rare high-parton-number fluctuations in the proton wave function, which make the parton density in the proton appear more like that in a small nucleus. Hence our setup may be relevant for high-multiplicity $p+A$ collisions as well.

The resulting two-gluon production cross section was written in [1] as a sum of two terms corresponding to two different classes of diagrams (labeled 'square' and 'crossed'),

$$\frac{d\sigma}{d^2k_1 dy_1 d^2k_2 dy_2} = \frac{d\sigma_{square}}{d^2k_1 dy_1 d^2k_2 dy_2} + \frac{d\sigma_{crossed}}{d^2k_1 dy_1 d^2k_2 dy_2}, \quad (1)$$

with

$$\begin{aligned} \frac{d\sigma_{square}}{d^2k_1 dy_1 d^2k_2 dy_2} &= \frac{\alpha_s^2 C_F^2}{16 \pi^8} \int d^2B d^2b_1 d^2b_2 T_1(\mathbf{B} - \mathbf{b}_1) T_1(\mathbf{B} - \mathbf{b}_2) d^2x_1 d^2y_1 d^2x_2 d^2y_2 e^{-i \mathbf{k}_1 \cdot (\mathbf{x}_1 - \mathbf{y}_1) - i \mathbf{k}_2 \cdot (\mathbf{x}_2 - \mathbf{y}_2)} \\ &\times \frac{\mathbf{x}_1 - \mathbf{b}_1}{|\mathbf{x}_1 - \mathbf{b}_1|^2} \cdot \frac{\mathbf{y}_1 - \mathbf{b}_1}{|\mathbf{y}_1 - \mathbf{b}_1|^2} \frac{\mathbf{x}_2 - \mathbf{b}_2}{|\mathbf{x}_2 - \mathbf{b}_2|^2} \cdot \frac{\mathbf{y}_2 - \mathbf{b}_2}{|\mathbf{y}_2 - \mathbf{b}_2|^2} \\ &\times \left\langle \left(\frac{1}{N_c^2 - 1} \text{Tr}[U_{\mathbf{x}_1} U_{\mathbf{y}_1}^\dagger] - \frac{1}{N_c^2 - 1} \text{Tr}[U_{\mathbf{x}_1} U_{\mathbf{b}_1}^\dagger] - \frac{1}{N_c^2 - 1} \text{Tr}[U_{\mathbf{b}_1} U_{\mathbf{y}_1}^\dagger] + 1 \right) \right. \\ &\times \left. \left(\frac{1}{N_c^2 - 1} \text{Tr}[U_{\mathbf{x}_2} U_{\mathbf{y}_2}^\dagger] - \frac{1}{N_c^2 - 1} \text{Tr}[U_{\mathbf{x}_2} U_{\mathbf{b}_2}^\dagger] - \frac{1}{N_c^2 - 1} \text{Tr}[U_{\mathbf{b}_2} U_{\mathbf{y}_2}^\dagger] + 1 \right) \right\rangle \end{aligned} \quad (2)$$

and

$$\begin{aligned} \frac{d\sigma_{crossed}}{d^2k_1 dy_1 d^2k_2 dy_2} &= \frac{1}{[2(2\pi)^3]^2} \int d^2B d^2b_1 d^2b_2 T_1(\mathbf{B} - \mathbf{b}_1) T_1(\mathbf{B} - \mathbf{b}_2) d^2x_1 d^2y_1 d^2x_2 d^2y_2 \\ &\times \left[e^{-i \mathbf{k}_1 \cdot (\mathbf{x}_1 - \mathbf{y}_2) - i \mathbf{k}_2 \cdot (\mathbf{x}_2 - \mathbf{y}_1)} + e^{-i \mathbf{k}_1 \cdot (\mathbf{x}_1 - \mathbf{y}_2) + i \mathbf{k}_2 \cdot (\mathbf{x}_2 - \mathbf{y}_1)} \right] \frac{16 \alpha_s^2 C_F}{\pi^2 2N_c} \frac{\mathbf{x}_1 - \mathbf{b}_1}{|\mathbf{x}_1 - \mathbf{b}_1|^2} \cdot \frac{\mathbf{y}_2 - \mathbf{b}_2}{|\mathbf{y}_2 - \mathbf{b}_2|^2} \frac{\mathbf{x}_2 - \mathbf{b}_2}{|\mathbf{x}_2 - \mathbf{b}_2|^2} \cdot \frac{\mathbf{y}_1 - \mathbf{b}_1}{|\mathbf{y}_1 - \mathbf{b}_1|^2} \\ &\times \left[Q(\mathbf{x}_1, \mathbf{y}_1, \mathbf{x}_2, \mathbf{y}_2) - Q(\mathbf{x}_1, \mathbf{y}_1, \mathbf{x}_2, \mathbf{b}_2) - Q(\mathbf{x}_1, \mathbf{y}_1, \mathbf{b}_2, \mathbf{y}_2) + S_G(\mathbf{x}_1, \mathbf{y}_1) - Q(\mathbf{x}_1, \mathbf{b}_1, \mathbf{x}_2, \mathbf{y}_2) + Q(\mathbf{x}_1, \mathbf{b}_1, \mathbf{x}_2, \mathbf{b}_2) \right. \\ &+ Q(\mathbf{x}_1, \mathbf{b}_1, \mathbf{b}_2, \mathbf{y}_2) - S_G(\mathbf{x}_1, \mathbf{b}_1) - Q(\mathbf{b}_1, \mathbf{y}_1, \mathbf{x}_2, \mathbf{y}_2) + Q(\mathbf{b}_1, \mathbf{y}_1, \mathbf{x}_2, \mathbf{b}_2) + Q(\mathbf{b}_1, \mathbf{y}_1, \mathbf{b}_2, \mathbf{y}_2) - S_G(\mathbf{b}_1, \mathbf{y}_1) + S_G(\mathbf{x}_2, \mathbf{y}_2) \\ &\left. - S_G(\mathbf{x}_2, \mathbf{b}_2) - S_G(\mathbf{b}_2, \mathbf{y}_2) + 1 \right]. \end{aligned} \quad (3)$$

We denote two-dimensional vectors in the transverse plane by $\mathbf{v} = (v^x, v^y)$ with their length $v_T \equiv v_\perp \equiv |\mathbf{v}|$. As usual, α_s is the strong coupling constant, N_c is the number of quark colors, and $C_F = (N_c^2 - 1)/2N_c$ is the Casimir operator of $SU(N_c)$ in the fundamental representation. The center of the projectile nucleus is located at impact parameter \mathbf{B} with respect to the center of the target nucleus, with \mathbf{b}_1 and \mathbf{b}_2 the impact parameters of the two interacting nucleons in the projectile, also measured with respect to the center of the target. The nuclear profile function $T_1(\mathbf{b})$ describes the distribution of nucleons in the projectile. Angle brackets $\langle \dots \rangle$ denote averaging in the target wave function squared.

The interactions with the target are described using

$$U_{\mathbf{x}} = \text{P exp} \left\{ i g \int_{-\infty}^{\infty} dx^+ \mathcal{A}^-(x^+, x^- = 0, \mathbf{x}) \right\}, \quad (4)$$

which is the Wilson line taken along the x^+ light cone with \mathcal{A}^- the gluon field of the target nucleus in the adjoint representation. The contribution (3) depends on the S -matrices for the adjoint color-dipole

$$S_G(\mathbf{x}_1, \mathbf{x}_2, Y) \equiv \frac{1}{N_c^2 - 1} \langle \text{Tr}[U_{\mathbf{x}_1} U_{\mathbf{x}_2}^\dagger] \rangle (Y) \quad (5)$$

and adjoint color-quadrupole

$$Q(\mathbf{x}_1, \mathbf{x}_2, \mathbf{x}_3, \mathbf{x}_4, Y) \equiv \frac{1}{N_c^2 - 1} \langle \text{Tr}[U_{\mathbf{x}_1} U_{\mathbf{x}_2}^\dagger U_{\mathbf{x}_3} U_{\mathbf{x}_4}^\dagger] \rangle (Y), \quad (6)$$

where, for the future purposes, we now explicitly show the rapidity (Y) dependence of the matrix elements.

We impose no ordering on the rapidities y_1 and y_2 of the two produced gluons. (We do assume that $|y_1 - y_2| \ll 1/\alpha_s$ and $0 < Y - y_{1,2} \ll 1/\alpha_s$, with Y the rapidity of the projectile, such that no small- x evolution corrections need to be included in the rapidity intervals between the gluons and between the projectile and the gluons.) In the case of rapidity-ordered two-gluon production (say, $y_2 \gg y_1$) the corresponding cross section was found previously in [14] (see also [15, 64]), in apparent agreement with our Eq. (2) (modulo the nuclear profile functions $T_1(\mathbf{b})$ we included in the projectile nucleus). An expression for two-gluon production without rapidity ordering containing both the double-trace and quadrupole structures of Eqs. (2) and (3) was obtained in [16] shortly before our work [1].

The matrix elements of the double-trace, dipole and quadrupole operators entering Eqs. (2) and (3) were evaluated in [1] using the Gaussian approximation (the MV model). When using this approximation one treats both the projectile and the target in the same consistent way, including only multiple interactions with target and projectile nucleons in the cross section. The drawback is, of course, that the resulting two-gluon production cross section is energy- and rapidity-independent, just like all other observables in the quasi-classical approximation. Inclusion of the full energy and rapidity dependence goes beyond the scope of the present work. However, evolution corrections can be readily included in the rapidity interval between the produced gluons and the target by evolving the double-trace, dipole and quadrupole operators using the BK [36–39] and JIMWLK [40–43] evolution equations. This would make the two-gluon production cross section energy-dependent: the effect of such evolution corrections will be explored below in Sec. VI.

In the MV model and in the large- N_c approximation¹ the double-trace and quadrupole operators entering Eqs. (2) and (3) were found in [1] (cf. [62]). The results are as follows. For the double-trace operator we write

$$\frac{1}{(N_c^2 - 1)^2} \langle \text{Tr}[U_{\mathbf{x}_1} U_{\mathbf{x}_2}^\dagger] \text{Tr}[U_{\mathbf{x}_3} U_{\mathbf{x}_4}^\dagger] \rangle = \frac{1}{(N_c^2 - 1)^2} \langle \text{Tr}[U_{\mathbf{x}_1} U_{\mathbf{x}_2}^\dagger] \rangle \langle \text{Tr}[U_{\mathbf{x}_3} U_{\mathbf{x}_4}^\dagger] \rangle + \Delta(\mathbf{x}_1, \mathbf{x}_2, \mathbf{x}_3, \mathbf{x}_4), \quad (7)$$

where Δ represents the subleading in $\frac{1}{N_c^2}$ terms in the matrix element. To leading order in $\frac{1}{N_c^2}$ in the MV model it is given by

$$\Delta(\mathbf{x}_1, \mathbf{x}_2, \mathbf{x}_3, \mathbf{x}_4) = \frac{(D_3 - D_2)^2}{N_c^2} \left[\frac{e^{D_1}}{D_1 - D_2} - \frac{2e^{D_1}}{(D_1 - D_2)^2} + \frac{e^{D_1}}{D_1 - D_3} - \frac{2e^{D_1}}{(D_1 - D_3)^2} \right. \\ \left. + \frac{2e^{\frac{1}{2}(D_1 + D_2)}}{(D_1 - D_2)^2} + \frac{2e^{\frac{1}{2}(D_1 + D_3)}}{(D_1 - D_3)^2} \right] + O\left(\frac{1}{N_c^4}\right), \quad (8)$$

¹ Note that the large- N_c approximation here implies a regular 't Hooft large- N_c limit taken while keeping the saturation scale Q_s fixed: this Q_s fixing can be achieved within the standard large- N_c limit by assuming that nucleons are made out of $\sim N_c^2$ valence quarks.

where we have defined

$$D_1 = -\Gamma_G(\mathbf{x}_1, \mathbf{x}_2, Y=0) - \Gamma_G(\mathbf{x}_3, \mathbf{x}_4, Y=0) \quad (9a)$$

$$D_2 = -\Gamma_G(\mathbf{x}_1, \mathbf{x}_3, Y=0) - \Gamma_G(\mathbf{x}_2, \mathbf{x}_4, Y=0) \quad (9b)$$

$$D_3 = -\Gamma_G(\mathbf{x}_1, \mathbf{x}_4, Y=0) - \Gamma_G(\mathbf{x}_2, \mathbf{x}_3, Y=0). \quad (9c)$$

In the MV model used in [1]

$$\Gamma_G(\mathbf{x}_1, \mathbf{x}_2, Y=0) = \frac{Q_{s2}^2}{4} |\mathbf{x}_1 - \mathbf{x}_2|^2 \ln\left(\frac{1}{|\mathbf{x}_1 - \mathbf{x}_2| \Lambda}\right) \quad (10)$$

with Q_{s2} the target saturation scale for gluons in the quasi-classical (MV) limit [32] and Λ an infrared (IR) cutoff. (Note that our notation here is slightly different from [1]: we use Q_{s2} instead of Q_{s0} used in [1] to denote the same MV saturation scale of the target nucleus.)

The S -matrix S_G for the gluon color dipole interaction with the target and in the MV model is [32]

$$S_G(\mathbf{x}_1, \mathbf{x}_2, Y=0) = e^{-\Gamma_G(\mathbf{x}_1, \mathbf{x}_2, Y=0)}. \quad (11)$$

The gluon color-quadrupole S -matrix in the MV model and in the large- N_c approximation is

$$Q(\mathbf{x}_1, \mathbf{x}_2, \mathbf{x}_3, \mathbf{x}_4, Y=0) = \left[e^{D_1/2} + \frac{D_3 - D_2}{D_1 - D_3} \left(e^{D_1/2} - e^{D_3/2} \right) \right]^2. \quad (12)$$

The correlation function is defined by

$$C(\mathbf{k}_1, y_1, \mathbf{k}_2, y_2) = \mathcal{N} \frac{\frac{d\sigma}{d^2k_1 dy_1 d^2k_2 dy_2}}{\frac{d\sigma}{d^2k_1 dy_1} \frac{d\sigma}{d^2k_2 dy_2}} - 1 \quad (13)$$

where the normalization factor \mathcal{N} is usually fixed by requiring that the numerator of C (after reducing both terms in (13) to the common denominator) integrates out to zero when integrating over the whole sample defined by the cuts. (Our \mathcal{N} here is defined differently from that in Eq. (1) of [1].) For instance, the correlator as a function of gluon rapidities y_1, y_2 and azimuthal angles ϕ_1, ϕ_2 for gluons with fixed magnitudes of their transverse momenta k_1, k_2 is given by

$$C(\mathbf{k}_1, y_1, \mathbf{k}_2, y_2) = \frac{\left[\int d\phi_1 dy_1 \frac{d\sigma}{d^2k_1 dy_1} \int d\phi_2 dy_2 \frac{d\sigma}{d^2k_2 dy_2} \right]}{\left[\int d\phi_1 dy_1 \frac{d\sigma}{d^2k_1 dy_1} \int d\phi_2 dy_2 \frac{d\sigma}{d^2k_2 dy_2} \right]} \frac{\frac{d\sigma}{d^2k_1 dy_1 d^2k_2 dy_2}}{\frac{d\sigma}{d^2k_1 dy_1} \frac{d\sigma}{d^2k_2 dy_2}} - 1. \quad (14)$$

In [1] it was shown that the correlations contained in the cross sections (1), (2) and (3) are symmetric under $\mathbf{k}_1 \leftrightarrow \mathbf{k}_2$ and $\mathbf{k}_2 \rightarrow -\mathbf{k}_2$. This implies that the correlation function contains only even Fourier harmonics in its Fourier decomposition over the azimuthal opening angle $\Delta\phi = \phi_1 - \phi_2$: therefore the near- and away-side correlations (that is, correlations around $\Delta\phi = 0$ and $\Delta\phi = \pi$ respectively) resulting from the calculation [1] are identical. The correlations are also flat in rapidity up to $|y_1 - y_2| \lesssim 1/\alpha_s$, making them a plausible contributor to the 'ridge' correlation observed in $A + A$, $p + A$ and $p + p$ collisions at RHIC and LHC.

Substituting Eqs. (1), (2) and (3) along with the lowest-order single-gluon production cross section

$$\frac{d\sigma^{pA_2}}{d^2k dy d^2b} = \frac{\alpha_s C_F}{\pi^2} \frac{Q_{s2}^2(\mathbf{b})}{k_T^4} \ln \frac{k_T^2}{\Lambda^2} \quad (15)$$

into Eq. (14) and expanding the resulting correlator to the lowest non-trivial order in multiple rescattering in the target (lowest non-trivial order in Q_{s2}) one obtains [1]

$$\begin{aligned} C(\mathbf{k}_1, y_1, \mathbf{k}_2, y_2) \Big|_{LO} &= \frac{1}{N_c^2} \frac{\int d^2B d^2b [T_1(\mathbf{B} - \mathbf{b})]^2 Q_{s2}^4(\mathbf{b})}{\int d^2B d^2b_1 d^2b_2 T_1(\mathbf{B} - \mathbf{b}_1) T_1(\mathbf{B} - \mathbf{b}_2) Q_{s2}^2(\mathbf{b}_1) Q_{s2}^2(\mathbf{b}_2)} \\ &\times \frac{k_1^2 k_2^2}{\ln \frac{k_1^2}{\Lambda^2} \ln \frac{k_2^2}{\Lambda^2}} \left\{ 2 \int_{\Lambda} \frac{d^2l}{(l^2)^2} \left[\frac{1}{(\mathbf{k}_1 - \mathbf{l})^2 (\mathbf{k}_2 + \mathbf{l})^2} + \frac{1}{(\mathbf{k}_1 - \mathbf{l})^2 (\mathbf{k}_2 - \mathbf{l})^2} \right] \right. \\ &+ \frac{1}{8} \left[\int_{\Lambda} \frac{d^2l}{(l^2)^2 ((\mathbf{l} - \mathbf{k}_1 + \mathbf{k}_2)^2 ((\mathbf{k}_1 - \mathbf{l})^2 ((\mathbf{k}_2 + \mathbf{l})^2)^2} \right. \\ &\times \left. \left. \left[l^2 (\mathbf{k}_2 + \mathbf{l})^2 + (\mathbf{k}_1 - \mathbf{l})^2 (\mathbf{l} - \mathbf{k}_1 + \mathbf{k}_2)^2 - k_1^2 (\mathbf{k}_2 - \mathbf{k}_1 + 2\mathbf{l})^2 \right] \right. \right. \\ &\times \left. \left. \left[l^2 (\mathbf{k}_1 - \mathbf{l})^2 + (\mathbf{k}_2 + \mathbf{l})^2 (\mathbf{l} - \mathbf{k}_1 + \mathbf{k}_2)^2 - k_2^2 (\mathbf{k}_2 - \mathbf{k}_1 + 2\mathbf{l})^2 \right] + (\mathbf{k}_2 \rightarrow -\mathbf{k}_2) \right] \right\}. \quad (16) \end{aligned}$$

The momentum-space part of the expression (16) reproduces that derived in the original analyses of the ridge correlations in the saturation picture [8, 11, 12]. The prefactor of Eq. (16) containing impact parameter integrations brings in a non-trivial dependence of the resulting correlations on geometry, which will be investigated below in Sec. III. The correlator (16) also contains a power-law IR divergence at $l = 0$ with the integrand scaling as $\sim 1/l^4$ in that region. This is a stronger divergence than $\sim 1/l^2$ divergences usually encountered in single-gluon production cross section calculations. Elucidating how a part of this divergence is removed by saturation effects in the target nucleus will be one of the topics presented below in Sec. IV.

III. GEOMETRY-DEPENDENT CORRELATIONS

In [1] we pointed out that the geometry of the collision can have an effect on the correlation function, both through the so-called geometric correlations introduced in [1] (see also [73, 74] for a discussion of the role of geometry in di-jet production in $p + p$ collisions) and through a collision geometry-dependent prefactor of the correlator, like that in Eq. (16). Note also that in the approximation considered, the two-gluon production cross section contains only the even Fourier harmonics in the azimuthal opening angle $\Delta\phi$: it would be important to better understand the effect of geometry on the Fourier expansion coefficients. We know that even Fourier harmonics in the di-hadron correlators are also generated by the event-averaged hydrodynamics, describing the flow of the quark-gluon plasma. (The odd harmonics are generated by the event-by-event hydrodynamic simulations, including geometry fluctuations [75].) It would be interesting to understand the differences and similarities of the two types of correlations.

Let us concentrate specifically on the elliptic flow observable v_2 , resulting from the 2nd Fourier harmonic of the correlation function. The value of v_2 in the event-averaged hydrodynamics is driven by the ellipticity of the overlap region of the colliding nuclei: the larger the ellipticity, the larger is v_2 . In contrast to this behavior, the non-flow correlations in Eqs. (2) and (3) do not seem to require any ellipticity at all to produce a second harmonic (and other even harmonics) in the correlator, resulting in the geometry-dependent non-flow contribution to v_2 which is not ellipticity-driven. This can be seen from the lowest-order correlator in Eq. (16): there the geometry-dependent factor factorizes from the momentum-dependent term which contains the azimuthal angle dependence of the correlations. The strength of the correlations in (16) is indeed dependent on the geometry-dependent prefactor: however, it is not *a priori* clear whether this factor depends on the ellipticity of the overlap region.

To elucidate this issue let us consider uranium-uranium ($U + U$) collisions. Data from such collisions have been collected at RHIC, in order to study the properties of hydrodynamic evolution, which predicts stronger elliptic flow (larger v_2) in the side-on-side collisions (bottom panel in Fig. 1) than in the tip-on-tip collisions (top panel in Fig. 1), since the ellipticity in the former case is much larger than that in the latter case [68–70].

To compare this with the behavior of the correlations in the CGC dynamics we will employ the lowest-order correlator (16). Note that the higher-order corrections to this correlator, which are contained in Eqs. (2) and (3), are likely to regulate some of the IR singularities present in (16), introducing new factors of the saturation scale $Q_{s2}(\mathbf{b})$, which may modify the geometry-dependence of the lowest-order correlator (16). However, as we will see below, the power-law IR divergences in (16) do not affect the azimuthal angle-dependent correlations; hence our estimate of the magnitude of the Fourier harmonics with index $n \geq 2$ should not be affected qualitatively by higher-order corrections.

To see how the geometry of the collision affects the correlation we take the ratio of two correlation functions which have different geometries associated with the $U + U$ collision illustrated in Fig. 1: tip-on-tip (top panel) and side-on-side (bottom panel). This requires fixing the impact parameter between the two nuclei, \mathbf{B} , which, in this case, is fixed to $\mathbf{0}$ for both correlations. In the MV model which we have used here $Q_{s2}^2 = 4\pi\alpha_s^2 T_2(\mathbf{b})$. In our case the two nuclei involved in a collision are identical and, hence, have the same nuclear profile functions, $T_1(\mathbf{b}) = T_2(\mathbf{b})$. (Note that, while the gluon production cross section in Eqs. (2) and (3) was derived in the $A_2 \gg A_1 \gg 1$ limit with $k_1, k_2 \gtrsim Q_{s1}$, the lowest-order correlator (16) is valid for $k_1, k_2 \gg Q_{s1}, Q_{s2}$ with the ordering condition relaxed on $A_1, A_2 \gg 1$.) The difference between the two geometries in Fig. 1 is governed by the nuclear profile function. The ratio between the tip-on-tip and side-on-side correlation functions (16) can be written as

$$\frac{C_{tip-on-tip}(\mathbf{k}_1, y_1, \mathbf{k}_2, y_2)|_{LO}}{C_{side-on-side}(\mathbf{k}_1, y_1, \mathbf{k}_2, y_2)|_{LO}} = \frac{\int d^2b [T_{tip-on-tip}(\mathbf{b})]^4}{[\int d^2b [T_{tip-on-tip}(\mathbf{b})]^2]^2} \frac{[\int d^2b [T_{side-on-side}(\mathbf{b})]^2]^2}{\int d^2b [T_{side-on-side}(\mathbf{b})]^4}. \quad (17)$$

Note that the momentum dependence cancels out in the ratio of two lowest-order correlators.

For the analytical estimate we are about to perform here we employ a toy model of a uranium nucleus as a prolate spheroid with the Gaussian distribution of the nucleon number density

$$\rho(\vec{\mathbf{r}}) = \rho_0 e^{-\frac{x^2}{R^2} - \frac{y^2}{R^2} - \frac{\lambda^2}{R^2} z^2} \quad (18)$$

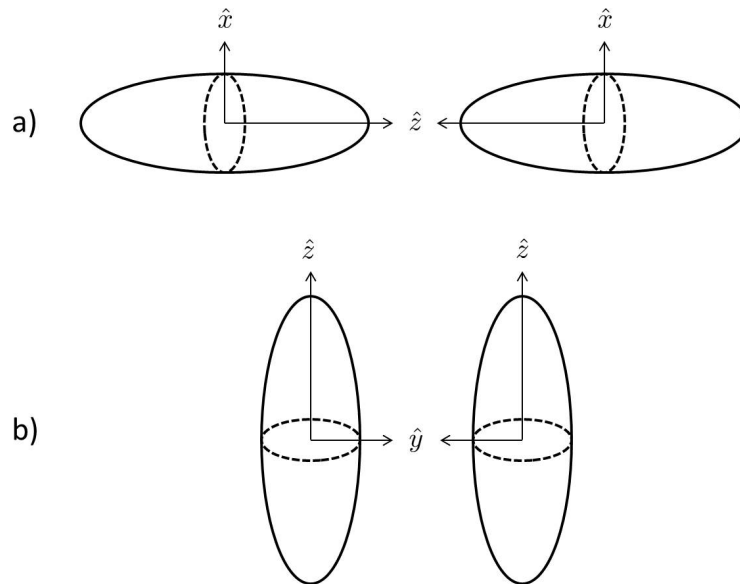


FIG. 1. The layout of two possible geometries for the $U + U$ collisions. The top panel is the tip-on-tip collision, which has the z-axis of the two nuclei anti-parallel to each other and (anti)parallel to the collision axis. The bottom diagram is the side-on collision, which has the z-axis of the two nuclei parallel to each other and perpendicular to the collision axis.

where $\lambda \approx 0.79$ is related to the ellipticity ϵ of the spheroid by $\lambda = \sqrt{1 - \epsilon^2}$. To translate this into a nuclear profile function we integrate over one of the spatial coordinates: z for the tip-on-tip collisions and y for the side-on-side collisions (see Fig. 1). Thus we have

$$\begin{aligned}
 T_{tip-on-tip}(\mathbf{b} = (x, y)) &= \int_{-\infty}^{\infty} dz \rho(\vec{\mathbf{r}}) = \sqrt{\pi} \frac{R}{\lambda} \rho_0 e^{-\frac{b^2}{R^2}} \\
 T_{side-on-side}(\mathbf{b} = (z, x)) &= \int_{-\infty}^{\infty} dy \rho(\vec{\mathbf{r}}) = \sqrt{\pi} R \rho_0 e^{-\frac{x^2}{R^2} - \frac{\lambda^2}{R^2} z^2}.
 \end{aligned}
 \tag{19}$$

Plugging these results into Eq. (17) and integrating we arrive at

$$\frac{C_{tip-on-tip}(\mathbf{k}_1, y_1, \mathbf{k}_2, y_2)|_{LO}}{C_{side-on-side}(\mathbf{k}_1, y_1, \mathbf{k}_2, y_2)|_{LO}} = \frac{1}{\lambda} \approx 1.26 \quad (\text{for } U + U).
 \tag{20}$$

Thus a tip-on-tip collision enhances the initial-state (CGC) correlation between two gluons as compared to the side-on-side collision. We have checked this conclusion numerically by using more realistic nuclear density profiles in Eq. (17), invariably getting stronger correlations in the tip-on-tip versus side-on-side collisions.

We conclude that, at least at the lowest order, the two-gluon correlations behave in an exactly opposite way from hydrodynamics: while hydrodynamic contribution to v_2 is ellipticity-driven, and is hence larger in the side-on-side $U + U$ collisions, the CGC correlations considered here give stronger correlations for the tip-on-tip $U + U$ collisions. This difference in geometry dependence should allow these two effects to be experimentally distinguishable. Further work is needed to understand the geometry dependence of the full correlator resulting from the two-gluon production cross section in Eqs. (2) and (3).

IV. IR DIVERGENCES

Saturation effects are known to regulate IR divergences in total and production cross sections, along with related observables. For instance, the unintegrated gluon distribution function at the lowest order has a power-law IR divergence, $\phi(k_T) \sim 1/k_T^2$ for $k_T \rightarrow 0$; saturation effects in the MV model reduce this IR divergence to a logarithmic integrable singularity [76], $\phi(k_T) \sim \ln(Q_s^2/k_T^2)$. It is likely that similar IR screening takes place in the two-gluon production cross section at hand.

An analysis of the pole structure in the lowest-order correlator of Eq. (16) reveals poles at

$$\mathbf{l} = \mathbf{0}, \mathbf{k}_1, \mathbf{k}_2, -\mathbf{k}_2, \mathbf{k}_1 - \mathbf{k}_2. \quad (21)$$

Taking a closer look at these poles we see that the majority of them are proportional to $\frac{1}{p^2}$ as $p \rightarrow 0$ which, after integration over momentum p , gives rise to logarithmic divergences, likely to be absorbed into gluon distributions of the nucleons [32]. However, the pole at $\mathbf{l} = \mathbf{0}$ in the first term in the curly brackets scales proportional to $\frac{1}{l^4}$ which, after integration, gives rise to a power-law IR divergence. Such power-law divergence is quite rare in the quasi-classical MV limit, and it appears important to us to verify that it is indeed regulated by the saturation effects in the full cross section given by Eqs. (2) and (3), such that the corresponding correlator, which would include all-order saturation effects in the target nucleus, would not depend on the IR cutoff in the power-law way. We will show in this Section that saturation effects in the target do indeed regulate the IR power-law divergence present in Eq. (2). However, the IR power-law divergence from Eq. (3) is not regularized by the saturation effects in the target, and is probably regularized by the projectile saturation effects not included in our analysis [1].

There are two different classes of diagrams contributing to the cross section associated with the correlation (16), the 'square' (separated) diagrams and the 'crossed' diagrams, with examples of both shown in Fig. 2 in $A^+ = 0$ gauge (with the projectile moving in the light-cone "+" direction) and contributing the expressions (2) and (3) correspondingly to the two-gluon production cross section. To analyze the IR divergences it is necessary to look at each diagram class individually. First we start with the 'square' cross section.

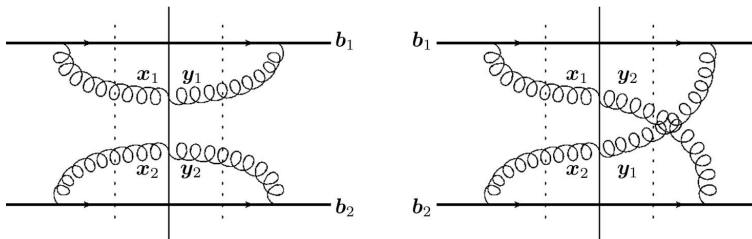


FIG. 2. Examples of a 'square' diagram (left panel) and a 'crossed' diagram (right panel) with corresponding two-vectors $\mathbf{x}_1, \mathbf{x}_2, \mathbf{y}_1$, and \mathbf{y}_2 labeling the transverse positions of the gluons and with $\mathbf{b}_1, \mathbf{b}_2$ denoting the transverse locations of the projectile valence quarks. The interaction with the target is shown by the vertical dotted lines.

The cross section for the 'square' diagrams is given by Eq. (2). The connected part of this cross section that contributes the (non-geometric) correlations is obtained by keeping only the Δ -labeled parts of the double-trace correlators using Eq. (7). This gives [1]

$$\begin{aligned} \frac{d\sigma_{square}^{(corr)}}{d^2k_1 dy_1 d^2k_2 dy_2} &= \frac{\alpha_s^2 C_F^2}{16\pi^8} \int d^2B d^2b_1 d^2b_2 T_1(\mathbf{B} - \mathbf{b}_1) T_1(\mathbf{B} - \mathbf{b}_2) d^2x_1 d^2y_1 d^2x_2 d^2y_2 e^{-i\mathbf{k}_1 \cdot (\mathbf{x}_1 - \mathbf{y}_1) - i\mathbf{k}_2 \cdot (\mathbf{x}_2 - \mathbf{y}_2)} \\ &\times \frac{\mathbf{x}_1 - \mathbf{b}_1}{|\mathbf{x}_1 - \mathbf{b}_1|^2} \cdot \frac{\mathbf{y}_1 - \mathbf{b}_1}{|\mathbf{y}_1 - \mathbf{b}_1|^2} \frac{\mathbf{x}_2 - \mathbf{b}_2}{|\mathbf{x}_2 - \mathbf{b}_2|^2} \cdot \frac{\mathbf{y}_2 - \mathbf{b}_2}{|\mathbf{y}_2 - \mathbf{b}_2|^2} \\ &\times [\Delta(\mathbf{x}_1, \mathbf{y}_1, \mathbf{x}_2, \mathbf{y}_2) - \Delta(\mathbf{x}_1, \mathbf{y}_1, \mathbf{x}_2, \mathbf{b}_2) - \Delta(\mathbf{x}_1, \mathbf{y}_1, \mathbf{b}_2, \mathbf{y}_2) - \Delta(\mathbf{x}_1, \mathbf{b}_1, \mathbf{x}_2, \mathbf{y}_2) - \Delta(\mathbf{b}_1, \mathbf{y}_1, \mathbf{x}_2, \mathbf{y}_2) \\ &+ \Delta(\mathbf{x}_1, \mathbf{b}_1, \mathbf{x}_2, \mathbf{b}_2) + \Delta(\mathbf{x}_1, \mathbf{b}_1, \mathbf{b}_2, \mathbf{y}_2) + \Delta(\mathbf{b}_1, \mathbf{y}_1, \mathbf{x}_2, \mathbf{b}_2) + \Delta(\mathbf{b}_1, \mathbf{y}_1, \mathbf{b}_2, \mathbf{y}_2)]. \end{aligned} \quad (22)$$

Let us introduce the variable $\mathbf{b} = \frac{1}{2}(\mathbf{b}_1 + \mathbf{b}_2)$, which is the transverse position of the center of mass of the two quarks, and $\mathbf{\Delta b} = \mathbf{b}_1 - \mathbf{b}_2$, which is the transverse separation between the two quarks. We also shift the coordinates of the gluons such that

$$\tilde{\mathbf{x}}_1 = \mathbf{x}_1 - \mathbf{b}_1, \tilde{\mathbf{y}}_1 = \mathbf{y}_1 - \mathbf{b}_1, \tilde{\mathbf{x}}_2 = \mathbf{x}_2 - \mathbf{b}_2, \tilde{\mathbf{y}}_2 = \mathbf{y}_2 - \mathbf{b}_2. \quad (23)$$

For connected diagrams like those that gave rise to Eq. (22) the distance $\mathbf{\Delta b}$ has to be perturbatively small: we assume that $\Delta b \ll 1/\Lambda$ with Λ some IR cutoff of the order of the QCD confinement scale Λ_{QCD} . Since the corresponding distance $1/\Lambda$ is of the order of a nucleon size, it is much smaller than the radius of a large projectile nucleus, $1/\Lambda \ll R_1 \approx A_1^{1/3}/\Lambda$, such that the nuclear profile function does not vary much over the distances of the order of Δb . This allows for the approximation

$$T_1(\mathbf{B} - \mathbf{b}_1)T_1(\mathbf{B} - \mathbf{b}_2) = T_1\left(\mathbf{B} - \mathbf{b} - \frac{\mathbf{\Delta b}}{2}\right) T_1\left(\mathbf{B} - \mathbf{b} + \frac{\mathbf{\Delta b}}{2}\right) \approx [T_1(\mathbf{B} - \mathbf{b})]^2. \quad (24)$$

With this approximation and employing coordinate redefinitions outlined above, the cross-section (22) can be written as

$$\begin{aligned}
\frac{d\sigma_{square}^{(corr)}}{d^2k_1 dy_1 d^2k_2 dy_2} &= \frac{\alpha_s^2 C_F^2}{16 \pi^8} \int d^2B d^2b d^2\Delta b [T_1(\mathbf{B} - \mathbf{b})]^2 d^2\tilde{x}_1 d^2\tilde{y}_1 d^2\tilde{x}_2 d^2\tilde{y}_2 e^{-i\mathbf{k}_1 \cdot (\tilde{\mathbf{x}}_1 - \tilde{\mathbf{y}}_1) - i\mathbf{k}_2 \cdot (\tilde{\mathbf{x}}_2 - \tilde{\mathbf{y}}_2)} \\
&\times \frac{\tilde{\mathbf{x}}_1}{|\tilde{\mathbf{x}}_1|^2} \cdot \frac{\tilde{\mathbf{y}}_1}{|\tilde{\mathbf{y}}_1|^2} \frac{\tilde{\mathbf{x}}_2}{|\tilde{\mathbf{x}}_2|^2} \cdot \frac{\tilde{\mathbf{y}}_2}{|\tilde{\mathbf{y}}_2|^2} \left[\Delta \left(\tilde{\mathbf{x}}_1 + \mathbf{b} + \frac{1}{2} \Delta b, \tilde{\mathbf{y}}_1 + \mathbf{b} + \frac{1}{2} \Delta b, \tilde{\mathbf{x}}_2 + \mathbf{b} - \frac{1}{2} \Delta b, \tilde{\mathbf{y}}_2 + \mathbf{b} - \frac{1}{2} \Delta b \right) \right. \\
&\quad - \Delta \left(\tilde{\mathbf{x}}_1 + \mathbf{b} + \frac{1}{2} \Delta b, \tilde{\mathbf{y}}_1 + \mathbf{b} + \frac{1}{2} \Delta b, \tilde{\mathbf{x}}_2 + \mathbf{b} - \frac{1}{2} \Delta b, \mathbf{b} - \frac{1}{2} \Delta b \right) \\
&\quad - \Delta \left(\tilde{\mathbf{x}}_1 + \mathbf{b} + \frac{1}{2} \Delta b, \tilde{\mathbf{y}}_1 + \mathbf{b} + \frac{1}{2} \Delta b, \mathbf{b} - \frac{1}{2} \Delta b, \tilde{\mathbf{y}}_2 + \mathbf{b} - \frac{1}{2} \Delta b \right) \\
&\quad - \Delta \left(\tilde{\mathbf{x}}_1 + \mathbf{b} + \frac{1}{2} \Delta b, \mathbf{b} + \frac{1}{2} \Delta b, \tilde{\mathbf{x}}_2 + \mathbf{b} - \frac{1}{2} \Delta b, \tilde{\mathbf{y}}_2 + \mathbf{b} - \frac{1}{2} \Delta b \right) \\
&\quad - \Delta \left(\mathbf{b} + \frac{1}{2} \Delta b, \tilde{\mathbf{y}}_1 + \mathbf{b} + \frac{1}{2} \Delta b, \tilde{\mathbf{x}}_2 + \mathbf{b} - \frac{1}{2} \Delta b, \tilde{\mathbf{y}}_2 + \mathbf{b} - \frac{1}{2} \Delta b \right) \\
&\quad + \Delta \left(\tilde{\mathbf{x}}_1 + \mathbf{b} + \frac{1}{2} \Delta b, \mathbf{b} + \frac{1}{2} \Delta b, \tilde{\mathbf{x}}_2 + \mathbf{b} - \frac{1}{2} \Delta b, \mathbf{b} - \frac{1}{2} \Delta b \right) \\
&\quad + \Delta \left(\tilde{\mathbf{x}}_1 + \mathbf{b} + \frac{1}{2} \Delta b, \mathbf{b} + \frac{1}{2} \Delta b, \mathbf{b} - \frac{1}{2} \Delta b, \tilde{\mathbf{y}}_2 + \mathbf{b} - \frac{1}{2} \Delta b \right) \\
&\quad + \Delta \left(\mathbf{b} + \frac{1}{2} \Delta b, \tilde{\mathbf{y}}_1 + \mathbf{b} + \frac{1}{2} \Delta b, \tilde{\mathbf{x}}_2 + \mathbf{b} - \frac{1}{2} \Delta b, \mathbf{b} - \frac{1}{2} \Delta b \right) \\
&\quad \left. + \Delta \left(\mathbf{b} + \frac{1}{2} \Delta b, \tilde{\mathbf{y}}_1 + \mathbf{b} + \frac{1}{2} \Delta b, \mathbf{b} - \frac{1}{2} \Delta b, \tilde{\mathbf{y}}_2 + \mathbf{b} - \frac{1}{2} \Delta b \right) \right]. \quad (25)
\end{aligned}$$

The advantage of this form of the cross section is that all the Δb -dependence is now in the Δ -terms.

Our next step is to identify the coordinate-space IR divergence corresponding to the $l = 0$ singularity in Eq. (16). The cross sections in Eqs. (2) and (3), and, therefore, the cross section in Eq. (25) are all written as convolutions in the transverse coordinate space. We need to identify which transverse coordinate integral in Eq. (25) corresponds to the $1/l^4$ divergence in Eq. (16).

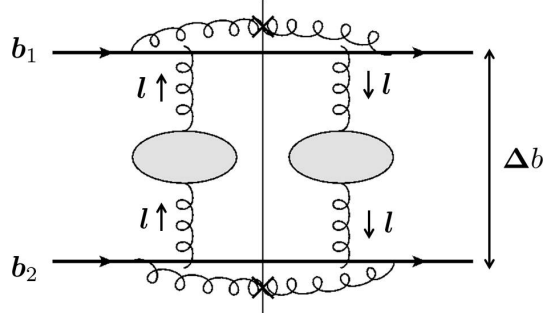


FIG. 3. A pictorial representation of the quadratic IR divergence in Eq. (16): here l is the transverse momentum transferred between the two quarks in the amplitude. It is conjugate to Δb , the separation between the two quarks. Gray ovals denote two nucleons in the target nucleus. Disconnected t -channel gluon lines indicate that the t -channel gluons can couple to either the s -channel gluons or to valence quarks.

Such identification can be done by analyzing the lowest-order diagrams giving rise to the correlation (16): the diagrams are shown in [1] (see Fig. 8 there). Studying those diagrams we see that the transverse momentum l corresponds to the momentum transferred between the two 'systems' or 'clusters' consisting of the valence quarks along with the produced gluons, as seen in Fig. 3. Already in the left panel of Fig. 2 we see that the two-gluon production in this channel consists of two independent quark-gluon 'clusters', with the correlation (cross-talk) between them generated through the interaction with the target. As illustrated in Fig. 3, l is conjugate to the separation between the two quarks, Δb : this momentum flows through a nucleon from one quark-gluon 'system' to another in the amplitude, and in the opposite direction in the complex conjugate amplitude. (Note that the diagram in Fig. 3 is only one example of a set of diagrams generating the two-gluon correlations at hand.) Thus the large Δb limit corresponds

to the IR divergence at $l \approx 0$ in (16). (The four t -channel gluon propagators in Fig. 3 give us a $\sim 1/(l^2)^4$ contribution, with the gauge-invariance of the coupling of these t -channel gluons to the color-neutral quark-gluon system giving a factor of $(l^2)^2$ at small- l , resulting in the net $1/(l^2)^2$ infrared divergence, as seen in Eq. (16).) To study the effects of saturation corrections on this divergence we need to study the large- Δb behavior of Eq. (25) (and, in the next step, of Eq. (3)).

As we have already noted, the Δb -dependence of the integrand in Eq. (25) is now purely in the Δ -terms. To cross-check our conclusion identifying the power-law IR divergence with the large- Δb behavior of that integrand, we need to make sure that to lowest order in saturation effects this cross-section has a quadratic IR divergence. Our goal after that would be to verify that if we include saturation effects in the target to all orders the divergence would become at most logarithmic.

At lowest order in multiple rescatterings in the MV model we have

$$\Delta_{LO}(\mathbf{x}_1, \mathbf{x}_2, \mathbf{x}_3, \mathbf{x}_4) = \frac{(D_3 - D_2)^2}{2N_c^2}. \quad (26)$$

which is obtained by expanding Eq. (8) to the lowest order in D_i 's defined in Eq. (9) [1]. Our next step is to substitute this into Eq. (25) and integrate over Δb concentrating on the large- Δb behavior. To do this we use the large- Δb expansion

$$(\mathbf{x} + \Delta \mathbf{b})^2 \ln \frac{1}{|\mathbf{x} + \Delta \mathbf{b}| \Lambda} = \Delta b^2 \ln \frac{1}{\Delta b \Lambda} + 2 \mathbf{x} \cdot \Delta \mathbf{b} \left(\ln \frac{1}{\Delta b \Lambda} - \frac{1}{2} \right) + \mathbf{x}^2 \left(\ln \frac{1}{\Delta b \Lambda} - \frac{1}{2} \right) - \frac{[\mathbf{x} \cdot \Delta \mathbf{b}]^2}{\Delta b^2} + \mathcal{O} \left(\frac{1}{\Delta b} \right) \quad (27)$$

to write the D_i 's entering the expression for, say, $\Delta(\mathbf{x}_1, \mathbf{y}_1, \mathbf{x}_2, \mathbf{y}_2)$ as

$$D_1 = -\frac{Q_{s2}^2}{4} \left[(\tilde{\mathbf{x}}_1 - \tilde{\mathbf{y}}_1)^2 \ln \frac{1}{|\tilde{\mathbf{x}}_1 - \tilde{\mathbf{y}}_1| \Lambda} + (\tilde{\mathbf{x}}_2 - \tilde{\mathbf{y}}_2)^2 \ln \frac{1}{|\tilde{\mathbf{x}}_2 - \tilde{\mathbf{y}}_2| \Lambda} \right] \quad (28a)$$

$$D_2 = -\frac{Q_{s2}^2}{4} \left[2 \Delta b^2 \ln \frac{1}{\Delta b \Lambda} + 2(\tilde{\mathbf{x}}_1 - \tilde{\mathbf{x}}_2 + \tilde{\mathbf{y}}_1 - \tilde{\mathbf{y}}_2) \cdot \Delta \mathbf{b} \left(\ln \frac{1}{\Delta b \Lambda} - \frac{1}{2} \right) + [(\tilde{\mathbf{x}}_1 - \tilde{\mathbf{x}}_2)^2 + (\tilde{\mathbf{y}}_1 - \tilde{\mathbf{y}}_2)^2] \left(\ln \frac{1}{\Delta b \Lambda} - \frac{1}{2} \right) - \frac{[(\tilde{\mathbf{x}}_1 - \tilde{\mathbf{x}}_2) \cdot \Delta \mathbf{b}]^2}{\Delta b^2} - \frac{[(\tilde{\mathbf{y}}_1 - \tilde{\mathbf{y}}_2) \cdot \Delta \mathbf{b}]^2}{\Delta b^2} + \mathcal{O} \left(\frac{1}{\Delta b} \right) \right] \quad (28b)$$

$$D_3 = -\frac{Q_{s2}^2}{4} \left[2 \Delta b^2 \ln \frac{1}{\Delta b \Lambda} + 2(\tilde{\mathbf{x}}_1 - \tilde{\mathbf{y}}_2 + \tilde{\mathbf{y}}_1 - \tilde{\mathbf{x}}_2) \cdot \Delta \mathbf{b} \left(\ln \frac{1}{\Delta b \Lambda} - \frac{1}{2} \right) + [(\tilde{\mathbf{x}}_1 - \tilde{\mathbf{y}}_2)^2 + (\tilde{\mathbf{y}}_1 - \tilde{\mathbf{x}}_2)^2] \left(\ln \frac{1}{\Delta b \Lambda} - \frac{1}{2} \right) - \frac{[(\tilde{\mathbf{x}}_1 - \tilde{\mathbf{y}}_2) \cdot \Delta \mathbf{b}]^2}{\Delta b^2} - \frac{[(\tilde{\mathbf{y}}_1 - \tilde{\mathbf{x}}_2) \cdot \Delta \mathbf{b}]^2}{\Delta b^2} + \mathcal{O} \left(\frac{1}{\Delta b} \right) \right]. \quad (28c)$$

Using these in Eq. (26) we see that

$$\Delta_{LO}(\mathbf{x}_1, \mathbf{y}_1, \mathbf{x}_2, \mathbf{y}_2) = \frac{Q_{s2}^4}{8N_c^2} \left[(\tilde{\mathbf{x}}_1 - \tilde{\mathbf{y}}_1) \cdot (\tilde{\mathbf{x}}_2 - \tilde{\mathbf{y}}_2) \left(\ln \frac{1}{\Delta b \Lambda} - \frac{1}{2} \right) - \frac{(\tilde{\mathbf{x}}_1 - \tilde{\mathbf{y}}_1) \cdot \Delta \mathbf{b} (\tilde{\mathbf{x}}_2 - \tilde{\mathbf{y}}_2) \cdot \Delta \mathbf{b}}{\Delta b^2} \right]^2 + \mathcal{O} \left(\frac{1}{\Delta b} \right) \quad (29)$$

such that when we integrate Δ_{LO} over Δb up to some IR cutoff $1/\Lambda_{\text{IR}}$ we arrive at an IR-divergent expression

$$\int^{1/\Lambda_{\text{IR}}^2} d^2 \Delta b \Delta_{LO}(\mathbf{x}_1, \mathbf{y}_1, \mathbf{x}_2, \mathbf{y}_2) = \frac{Q_{s2}^4}{64N_c^2} \frac{\pi}{\Lambda_{\text{IR}}^2} \left[(\tilde{\mathbf{x}}_1 - \tilde{\mathbf{y}}_1)^2 (\tilde{\mathbf{x}}_2 - \tilde{\mathbf{y}}_2)^2 + 4 \left(2 \ln^2 \left(\frac{\Lambda_{\text{IR}}}{\Lambda} \right) - 2 \ln \left(\frac{\Lambda_{\text{IR}}}{\Lambda} \right) + 1 \right) [(\tilde{\mathbf{x}}_1 - \tilde{\mathbf{y}}_1) \cdot (\tilde{\mathbf{x}}_2 - \tilde{\mathbf{y}}_2)]^2 \right]. \quad (30)$$

Note that since expressions like Eq. (10) are valid for distances much smaller than $1/\Lambda$ we assume that $1/\Lambda_{\text{IR}} < 1/\Lambda$. It is easy to generalize the expression (10) to the case of larger distances (as long as perturbation theory applies), making the $1/\Lambda_{\text{IR}} < 1/\Lambda$ condition not necessary: however, such generalization would complicate the algebra and would not bring any new physics insight. Therefore we will proceed here with the unmodified expression along with the $\Lambda_{\text{IR}} > \Lambda$ assumption.

Inserting Eq. (30) along with the similar Δb -integrals for other Δ 's into Eq. (25) gives

$$\begin{aligned} \frac{d\sigma_{square,LO}^{(corr)}}{d^2k_1 dy_1 d^2k_2 dy_2} &\approx \frac{\alpha_s^2 C_F^2}{16\pi^8} \int d^2B d^2b [T_1(\mathbf{B} - \mathbf{b})]^2 d^2\tilde{x}_1 d^2\tilde{y}_1 d^2\tilde{x}_2 d^2\tilde{y}_2 e^{-i\mathbf{k}_1 \cdot (\tilde{\mathbf{x}}_1 - \tilde{\mathbf{y}}_1) - i\mathbf{k}_2 \cdot (\tilde{\mathbf{x}}_2 - \tilde{\mathbf{y}}_2)} \frac{\tilde{\mathbf{x}}_1}{|\tilde{\mathbf{x}}_1|^2} \cdot \frac{\tilde{\mathbf{y}}_1}{|\tilde{\mathbf{y}}_1|^2} \\ &\times \frac{\tilde{\mathbf{x}}_2}{|\tilde{\mathbf{x}}_2|^2} \cdot \frac{\tilde{\mathbf{y}}_2}{|\tilde{\mathbf{y}}_2|^2} \frac{Q_{s2}^4}{16N_c^2} \frac{\pi}{\Lambda_{IR}^2} \left[\tilde{\mathbf{x}}_1 \cdot \tilde{\mathbf{y}}_1 \tilde{\mathbf{x}}_2 \cdot \tilde{\mathbf{y}}_2 + 2 \left(2 \ln^2 \left(\frac{\Lambda_{IR}}{\Lambda} \right) - 2 \ln \left(\frac{\Lambda_{IR}}{\Lambda} \right) + 1 \right) (\tilde{\mathbf{x}}_1 \cdot \tilde{\mathbf{y}}_2 \tilde{\mathbf{x}}_2 \cdot \tilde{\mathbf{y}}_1 + \tilde{\mathbf{x}}_1 \cdot \tilde{\mathbf{x}}_2 \tilde{\mathbf{y}}_1 \cdot \tilde{\mathbf{y}}_2) \right]. \end{aligned} \quad (31)$$

This expression diverges as $\sim 1/\Lambda_{IR}^2$ in the IR, as we expected from the lowest-order contribution.

Now let us see whether this power-law IR divergence is cured by saturation effects. From Eqs. (28) and (29) we conclude that at large Δb the quantities D_2 and D_3 are large and negative, while D_1 is constant and $D_2 - D_3$ is approximately constant (up to a logarithm). Even though this was shown for the D_i 's contributing to $\Delta_{LO}(\mathbf{x}_1, \mathbf{y}_1, \mathbf{x}_2, \mathbf{y}_2)$, these conclusions are also true for all other Δ 's in Eq. (25). Employing Eq. (8) we can approximate any of these Δ 's as

$$\Delta \approx -\frac{(D_3 - D_2)^2}{N_c^2} e^{D_1} \left(\frac{1}{D_2} + \frac{1}{D_3} \right) \approx \frac{(D_3 - D_2)^2}{N_c^2} e^{D_1} \frac{4}{Q_{s2}^2} \frac{1}{\Delta b^2 \ln \left(\frac{1}{\Delta b \Lambda} \right)}. \quad (32)$$

We see right away that, neglecting logarithms, $\Delta \sim 1/\Delta b^2$, such that the Δb -integral of Δ is only logarithmically divergent in the IR and the power-law divergence is regulated!

A more detailed calculation yields the same conclusion:

$$\begin{aligned} \int_{1/\mu^2}^{1/\Lambda_{IR}^2} d^2\Delta b \Delta(\mathbf{x}_1, \mathbf{y}_1, \mathbf{x}_2, \mathbf{y}_2) &\approx \frac{Q_{s2}^2}{4N_c^2} e^{D_1} \pi \left[(\tilde{\mathbf{x}}_1 - \tilde{\mathbf{y}}_1)^2 (\tilde{\mathbf{x}}_2 - \tilde{\mathbf{y}}_2)^2 \ln \frac{\ln \mu/\Lambda}{\ln \Lambda_{IR}/\Lambda} \right. \\ &\left. + [(\tilde{\mathbf{x}}_1 - \tilde{\mathbf{y}}_1) \cdot (\tilde{\mathbf{x}}_2 - \tilde{\mathbf{y}}_2)]^2 \left(\ln \frac{\mu^2}{\Lambda_{IR}^2} \ln \frac{\mu^2 \Lambda_{IR}^2}{\Lambda^4} - 8 \ln \frac{\mu^2}{\Lambda_{IR}^2} + 8 \ln \frac{\ln \mu/\Lambda}{\ln \Lambda_{IR}/\Lambda} \right) \right], \end{aligned} \quad (33)$$

where μ is an ultraviolet (UV) cutoff, $\mu \gg \Lambda_{IR} > \Lambda$. Typically the role of μ will be played by the perturbatively short inverse transverse distances $1/\tilde{x}_i$ or $1/\tilde{y}_i$, while after the transverse coordinate integrations are carried out μ would be a combination of k_1 , k_2 and Q_{s2} . The exact value of μ , while important for the exact evaluation of the integrals in Eq. (25), is not important for our goal of determining the degree of the IR divergence in the expression.

Substituting Eq. (33) along with the similar Δb -integrals for other Δ 's into Eq. (25) we would obtain a cross section containing at most $\ln \Lambda_{IR}$ divergences. Since the corresponding expression is rather cumbersome, we do not show it here explicitly: instead, to demonstrate that these $\ln \Lambda_{IR}$ divergences do not cancel out, we present the $k_1, k_2 \gg Q_{s2}$ limit of the 'square' diagrams cross section:

$$\begin{aligned} \left. \frac{d\sigma_{square}^{(corr)}}{d^2k_1 dy_1 d^2k_2 dy_2} \right|_{k_1, k_2 \gg Q_{s2}} &\approx \frac{\alpha_s^2 C_F^2}{16\pi^8} \int d^2B d^2b [T_1(\mathbf{B} - \mathbf{b})]^2 d^2\tilde{x}_1 d^2\tilde{y}_1 d^2\tilde{x}_2 d^2\tilde{y}_2 e^{-i\mathbf{k}_1 \cdot (\tilde{\mathbf{x}}_1 - \tilde{\mathbf{y}}_1) - i\mathbf{k}_2 \cdot (\tilde{\mathbf{x}}_2 - \tilde{\mathbf{y}}_2)} \frac{\tilde{\mathbf{x}}_1}{|\tilde{\mathbf{x}}_1|^2} \cdot \frac{\tilde{\mathbf{y}}_1}{|\tilde{\mathbf{y}}_1|^2} \\ &\times \frac{\tilde{\mathbf{x}}_2}{|\tilde{\mathbf{x}}_2|^2} \cdot \frac{\tilde{\mathbf{y}}_2}{|\tilde{\mathbf{y}}_2|^2} \frac{\pi Q_{s2}^4}{N_c^2} \left[\tilde{\mathbf{x}}_1 \cdot \tilde{\mathbf{y}}_1 \tilde{\mathbf{x}}_2 \cdot \tilde{\mathbf{y}}_2 \ln \frac{\ln \mu/\Lambda}{\ln \Lambda_{IR}/\Lambda} + \frac{1}{2} (\tilde{\mathbf{x}}_1 \cdot \tilde{\mathbf{y}}_2 \tilde{\mathbf{x}}_2 \cdot \tilde{\mathbf{y}}_1 + \tilde{\mathbf{x}}_1 \cdot \tilde{\mathbf{x}}_2 \tilde{\mathbf{y}}_1 \cdot \tilde{\mathbf{y}}_2) \right. \\ &\left. \times \left(\ln \frac{\mu^2}{\Lambda_{IR}^2} \ln \frac{\mu^2 \Lambda_{IR}^2}{\Lambda^4} - 8 \ln \frac{\mu^2}{\Lambda_{IR}^2} + 8 \ln \frac{\ln \mu/\Lambda}{\ln \Lambda_{IR}/\Lambda} \right) \right]. \end{aligned} \quad (34)$$

Noticing that the IR divergence in Eq. (34) is at most logarithmic in Λ_{IR} (and in Λ) we conclude that the all-order multiple rescatterings in the target nucleus regulate the power-law IR divergence of Eqs. (31) and Eq. (16). (One should not worry about the potential singularity of Eq. (34) in the $\Lambda_{IR} \rightarrow \Lambda$ limit: as we mentioned above, since Eq. (34) was derived in the $\Lambda_{IR} \gg \Lambda$ approximation, the $\Lambda_{IR} \rightarrow \Lambda$ divergence is regularized if one includes a more careful treatment for the scattering on a single nucleon than in Eq. (10).)

Unfortunately similar screening of the IR power-law divergence does not take place in the second part of the two-gluon production cross section (3) corresponding to the sum of the 'crossed' diagrams. To show this we will use a diagrammatic argument. Start by noticing that the origin of the divergence in the 'square' diagrams at the lowest order, as shown in Fig. 3, is in the four gluon propagators connected to two nucleons in the target carrying the same momentum l . From this we surmise that the IR divergence in the 'crossed' case originates from four gluon propagators with the same momentum connecting to the two nucleons in the projectile nucleus. (At the lowest order the 'square' and 'crossed' diagrams are related to each other by interchanging the target and the projectile.) An example of the

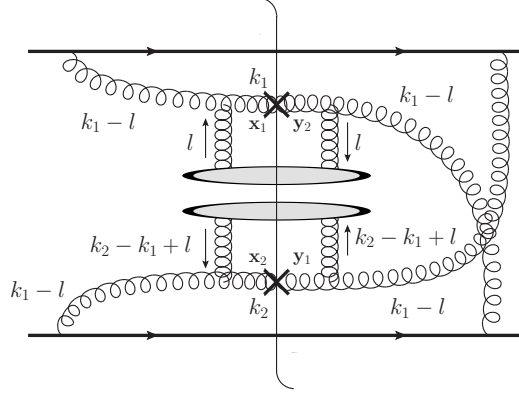


FIG. 4. An examples of a 'crossed' diagram containing a power-law IR divergence, as described in the text.

'crossed' diagram with the IR divergence is shown in Fig. 4, where the momentum labeling clearly demonstrates that the four gluon propagators attached to the projectile quark lines carry the same momentum $k_1 - l$. Each of those propagators gives a factor of $(\mathbf{k}_1 - l)/(\mathbf{k}_1 - l)^2$ in the projectile ($A^+ = 0$) light-cone gauge. These factors are dotted pairwise with each other, giving

$$\left[\frac{\mathbf{k}_1 - l}{(\mathbf{k}_1 - l)^2} \cdot \frac{\mathbf{k}_1 - l}{(\mathbf{k}_1 - l)^2} \right]^2 = \frac{1}{[(\mathbf{k}_1 - l)^2]^2}, \quad (35)$$

containing the power-law IR divergence in question (at $l = \mathbf{k}_1$ instead of $l = 0$ due to a different choice of momentum labeling from that in Eq. (16)).

For the divergence to appear it is essential that the target nucleons interact only with the s -channel gluons: one can easily see that if either nucleon interacts with the valence quarks the power-law IR divergence disappears, since we would not have four gluon propagators with identical momenta in such a case. This implies that of all the terms in the square brackets of Eq. (3) containing quadrupole and dipole interactions with the target, the IR divergence may only come from the first quadrupole term, $Q(\mathbf{x}_1, \mathbf{y}_1, \mathbf{x}_2, \mathbf{y}_2)$. The Fourier exponentials in Eq. (3) make sure that $|\mathbf{x}_1 - \mathbf{y}_2| < 1/k_1$ and $|\mathbf{x}_2 - \mathbf{y}_1| < 1/k_2$: therefore, the IR divergence may only arise from keeping the distances $|\mathbf{x}_1 - \mathbf{y}_2|$ and $|\mathbf{x}_2 - \mathbf{y}_1|$ fixed, while sending the pairs $\mathbf{x}_1, \mathbf{y}_2$ and $\mathbf{x}_2, \mathbf{y}_1$ far apart from each other (cf. the analysis of the IR divergences in Eq. (2)). This limit corresponds to keeping D_3 fixed while taking D_1, D_2 to be large, such that (see Eq. (12))

$$Q(\mathbf{x}_1, \mathbf{y}_1, \mathbf{x}_2, \mathbf{y}_2) \approx e^{D_3} = \exp \left[-\frac{1}{4} (\mathbf{x}_1 - \mathbf{y}_2)^2 Q_{s2}^2 \ln \frac{1}{|\mathbf{x}_1 - \mathbf{y}_2| \Lambda} - \frac{1}{4} (\mathbf{x}_2 - \mathbf{y}_1)^2 Q_{s2}^2 \ln \frac{1}{|\mathbf{x}_2 - \mathbf{y}_1| \Lambda} \right]. \quad (36)$$

Defining

$$\mathbf{r}_1 = \mathbf{x}_1 - \mathbf{y}_2, \quad \mathbf{r}_2 = \mathbf{x}_2 - \mathbf{y}_1 \quad (37)$$

and using the approximation (24) we rewrite the potentially IR-divergent part of Eq. (3) as

$$\begin{aligned} \frac{d\sigma_{crossed}}{d^2k_1 dy_1 d^2k_2 dy_2} \Big|_{IR-div} &= \int \frac{d^2B d^2b}{[2(2\pi)^3]^2} d^2\Delta b [T_1(\mathbf{B} - \mathbf{b})]^2 d^2r_1 d^2r_2 d^2y_1 d^2y_2 [e^{-i\mathbf{k}_1 \cdot \mathbf{r}_1 - i\mathbf{k}_2 \cdot \mathbf{r}_2} + e^{-i\mathbf{k}_1 \cdot \mathbf{r}_1 + i\mathbf{k}_2 \cdot \mathbf{r}_2}] \\ &\times \frac{16 \alpha_s^2 C_F}{\pi^2 2N_c} \frac{\mathbf{r}_1 + \mathbf{y}_2 - \mathbf{b} - \frac{1}{2} \Delta \mathbf{b}}{|\mathbf{r}_1 + \mathbf{y}_2 - \mathbf{b} - \frac{1}{2} \Delta \mathbf{b}|^2} \cdot \frac{\mathbf{y}_2 - \mathbf{b} + \frac{1}{2} \Delta \mathbf{b}}{|\mathbf{y}_2 - \mathbf{b} + \frac{1}{2} \Delta \mathbf{b}|^2} \frac{\mathbf{r}_2 + \mathbf{y}_1 - \mathbf{b} + \frac{1}{2} \Delta \mathbf{b}}{|\mathbf{r}_2 + \mathbf{y}_1 - \mathbf{b} + \frac{1}{2} \Delta \mathbf{b}|^2} \cdot \frac{\mathbf{y}_1 - \mathbf{b} - \frac{1}{2} \Delta \mathbf{b}}{|\mathbf{y}_1 - \mathbf{b} - \frac{1}{2} \Delta \mathbf{b}|^2} \\ &\times e^{-\frac{1}{4} \mathbf{r}_1^2 Q_{s2}^2 \ln \frac{1}{|\mathbf{r}_1| \Lambda} - \frac{1}{4} \mathbf{r}_2^2 Q_{s2}^2 \ln \frac{1}{|\mathbf{r}_2| \Lambda}}. \end{aligned} \quad (38)$$

Integrating (38) over \mathbf{y}_1 and \mathbf{y}_2 yields

$$\begin{aligned} \frac{d\sigma_{crossed}}{d^2k_1 dy_1 d^2k_2 dy_2} \Big|_{IR-div} &= \int \frac{d^2B d^2b}{[2(2\pi)^3]^2} d^2\Delta b [T_1(\mathbf{B} - \mathbf{b})]^2 d^2r_1 d^2r_2 [e^{-i\mathbf{k}_1 \cdot \mathbf{r}_1 - i\mathbf{k}_2 \cdot \mathbf{r}_2} + e^{-i\mathbf{k}_1 \cdot \mathbf{r}_1 + i\mathbf{k}_2 \cdot \mathbf{r}_2}] \\ &\times 32 \alpha_s^2 \frac{C_F}{N_c} \ln(|\mathbf{r}_1 - \Delta \mathbf{b}| \Lambda) \ln(|\mathbf{r}_2 + \Delta \mathbf{b}| \Lambda) e^{-\frac{1}{4} \mathbf{r}_1^2 Q_{s2}^2 \ln \frac{1}{|\mathbf{r}_1| \Lambda} - \frac{1}{4} \mathbf{r}_2^2 Q_{s2}^2 \ln \frac{1}{|\mathbf{r}_2| \Lambda}}. \end{aligned} \quad (39)$$

We see that the $d^2\Delta b$ -integral in Eq. (39) diverges as a power of the IR cutoff, such that

$$\left. \frac{d\sigma_{crossed}}{d^2k_1 dy_1 d^2k_2 dy_2} \right|_{IR-div} \sim \frac{1}{\Lambda_{IR}^2}. \quad (40)$$

Since the expression (39) contains the only potentially-divergent term in Eq. (3), we see that the divergence (40) is not canceled by other terms in Eq. (3). We conclude that the saturation effects in the target nucleus do not regulate a part of the IR divergence present in the lowest-order result (16) that originates in (3).

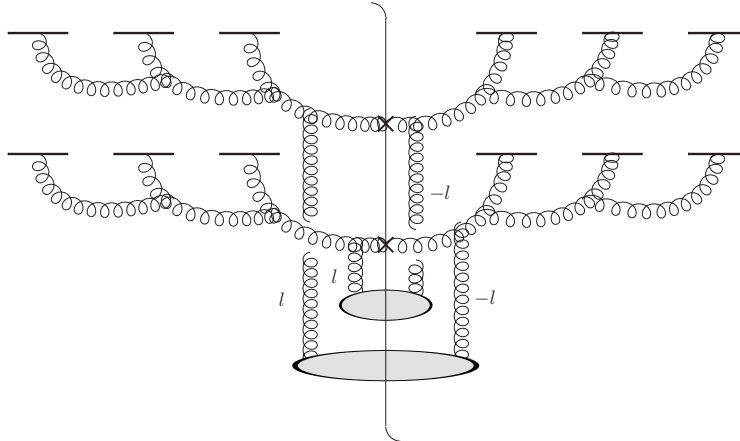


FIG. 5. A diagram in the light-cone gauge of the target containing the power-law IR divergence of Eq. (40).

We would like to propose a possible physical interpretation of this divergence illustrated in Fig. 5, which shows a diagram contributing to the two-gluon production cross section in the $A^- = 0$ light-cone gauge of the target nucleus. The target nucleus is shown at the top of Fig. 5, while the projectile nucleus is at the bottom. We assume that the saturation effects come into the two-gluon production cross section as the non-Abelian Weizsäcker-Williams (WW) gluon fields [56, 76–78], responsible for the gluon mergers in the top part of Fig. 5. If the extra nucleons (and the gluon mergers) are removed in Fig. 5, we would readily recover one of the original graphs considered in [8] giving long-range rapidity correlations.

The graph in Fig. 5 diverges for the same reason as Fig. 3: four t -channel gluon propagators give $1/(\mathbf{l}^2)^4$, while the color-neutrality of the target gives a factor of $(\mathbf{l}^2)^2$, altogether resulting in $1/(\mathbf{l}^2)^2$ factor in the \mathbf{l} -integral at small- l_T . At any order in the target saturation effects we still have this IR divergence, with the degree of divergence being the same at any order in the powers of $\alpha_s^2 A_2^{1/3}$ (the parameter corresponding to resumming the WW saturation effects in the target [78]). This is why the IR divergence (40) survives the inclusion of saturation effects in the target wave function.

The interpretation proposed in Fig. 5 allows one to hope that the IR divergence would be removed after inclusion of multiple rescatterings in the projectile wave function, similar to how the IR divergence of Fig. 3 was regulated by the multiple rescatterings in the target. Numerical simulations of the classical two-gluon correlations in the nucleus-nucleus collisions [66] appear to support this conjecture.

To conclude this section let us note that, as follows from Eq. (39), the \mathbf{k}_1 - and \mathbf{k}_2 -dependences factorize in the coefficient of $1/\Lambda_{IR}^2$ in (40). Hence the IR-divergent term from (3) does not generate two-gluon correlations with a non-trivial azimuthal angular dependence. This conclusion is consistent with the same azimuthal angle-independence of the power-law IR-divergent part of the lowest-order correlator (16), generalizing the latter to all orders in the multiple rescatterings in the target. Thus, while the power-law IR divergence of Eq. (40) does present a theoretical problem for the quasi-classical two-gluon production cross section in heavy-light ion collisions, such divergence does not affect the azimuthal angle-dependent part of the correlation function needed for phenomenology of the ‘ridge’ correlations.

V. k_T -FACTORIZATION

It is a well-known result of saturation physics that the single-gluon production cross section in the proton-nucleus (pA) collisions calculated either in the quasi-classical or leading- $\ln 1/x$ evolution approximations can be cast in the

form consistent with k_T -factorization [60, 63, 79] (see [24, 27] for pedagogical presentations of these results). By proton-nucleus collisions we denote dilute-dense scattering where the projectile wave function contains no saturation effects. Such scattering is slightly different from the two-gluon production in heavy-light ion collisions at hand: in obtaining Eqs. (2) and (3) we considered two gluons originating in the projectile wave function, which could be deemed a “saturation effect” compared to the single gluon needed for quasi-classical gluon production in pA collisions. It appears to be interesting to investigate whether the two-gluon production cross section (1) could also be written in a k_T -factorized form.

The cross-section for the production of a single gluon in a pA collision, calculated in the quasi-classical and/or leading- $\ln 1/x$ approximations, can be written as a convolution of two different unintegrated gluon distributions [60]²

$$\frac{d\sigma_g}{d^2k dy} = \frac{2\alpha_s}{C_F} \frac{1}{k^2} \int d^2q \langle \phi_{A_1}(\mathbf{q}, Y - y) \rangle_{A_1} \langle \phi_{A_2}(\mathbf{k} - \mathbf{q}, y) \rangle_{A_2} \quad (41)$$

where we replaced the proton by the light ion A_1 , implying that no saturation effects are included in the light ion wave function, which makes it equivalent to a proton for the purpose of the single-gluon production calculation. The angle brackets $\langle \dots \rangle_{A_1}$ and $\langle \dots \rangle_{A_2}$ denote averaging in the projectile and target wave functions respectively.

The unintegrated gluon distribution for the light ion is

$$\langle \phi_{A_1}(\mathbf{q}, y) \rangle_{A_1} = \frac{C_F}{\alpha_s(2\pi)^3} \int d^2b d^2r e^{-i\mathbf{q}\cdot\mathbf{r}} \nabla_{\mathbf{r}}^2 n_G(\mathbf{b} + \mathbf{r}, \mathbf{b}, y), \quad (42)$$

where $n_G(\mathbf{b} + \mathbf{r}, \mathbf{b}, y)$ is the gluon dipole scattering amplitude on the projectile evaluated without saturation effects (no multiple rescatterings, only linear BFKL evolution). The two gluons in the dipole are located at transverse positions $\mathbf{b} + \mathbf{r}$ and \mathbf{b} , and the rapidity interval for the scattering is y . In the quasi-classical limit one has

$$n_G(\mathbf{b} + \mathbf{r}, \mathbf{b}, y = 0) = \pi \alpha_s^2 r_{\perp}^2 \ln \left(\frac{1}{|\mathbf{r}| \Lambda} \right) T_1(\mathbf{b}). \quad (43)$$

The unintegrated gluon distribution for the heavy ion is defined as

$$\langle \phi_{A_2}(\mathbf{q}, y) \rangle_{A_2} = \frac{C_F}{\alpha_s(2\pi)^3} \int d^2b d^2r e^{-i\mathbf{q}\cdot\mathbf{r}} \nabla_{\mathbf{r}}^2 N_G(\mathbf{b} + \mathbf{r}, \mathbf{b}, y) \quad (44)$$

where we use the following convention for the imaginary part of the forward scattering amplitude for the gluon dipole on the target nucleus,

$$N_G(\mathbf{x}, \mathbf{y}, Y) = \frac{1}{N_c^2 - 1} \langle \text{Tr} [\mathbb{1} - U_{\mathbf{x}} U_{\mathbf{y}}^\dagger] \rangle_{A_2}(Y). \quad (45)$$

The correlator in Eq. (45) is evaluated either in the MV model (classical limit) or with the full nonlinear BK/JIMWLK evolution.

In Eqs. (43) and (45) the vector \mathbf{r} is the transverse size of the gluon dipole and \mathbf{b} can be thought of as the impact parameter of the dipole. Normally the impact parameter is defined as the transverse position of the center of mass of the dipole: we introduced a slightly different notation here for the future convenience.

The distribution functions (42) and (44) defined above are needed for the k_T factorization expression (41) of the single gluon production cross-section in pA (or heavy-light ion) collisions. However, when we are dealing with the two-gluon production cross-section (1), these distribution function are likely not to be adequate. First we notice that the only Wilson line operator in the single-gluon production case is the gluon dipole (45). In the expression for the two-gluon production cross section (1) we have both the quadruple operator (6), and the double trace operator (7), which would lead to different distribution functions.

Secondly, the two gluon production cross-section has geometric correlations [1], which arise purely from the integration over the impact parameters B , b_1 and b_2 in Eqs. (2) and (3). This prevents the integrals over the impact parameters from being contained within the distribution functions themselves. This will end up drastically changing the nature of the distribution functions and thus the final factorized form.

² The normalization of this result has recently been questioned in [80]. The worry of [80] is, however, unjustified: the factor of π^2 difference between Eq. (41) and the corresponding result of [80] (given by Eq. (A21) there) is due to the difference in the definitions of gluon distributions. The unintegrated gluon distributions ϕ used in Eq. (41) are normalized to give the number of gluons per dk_T^2 element of transverse momentum phase space, whereas the gluon transverse momentum distributions (TMDs) used in [80] are defined to give the number of gluons per d^2k phase space. The resulting factor of π difference in each distribution function leads to an overall factor of π^2 difference in the normalizations of Eq. (41) and Eq. (A21) from [80]. Thus the discrepancy is entirely due to a different convention.

The last major difference comes from the 'crossed' diagrams. These diagrams contain the interference of the wave functions of the incoming nucleons, which generates a significant "cross-talk" between different parts of the diagram; it is, therefore, *a priori* unlikely that factorization would take place. As we will see below, the factorized form of the expression cannot be written purely as a convolution of distribution functions without additional factors, like in Eq. (41). While factorized form can be achieved, it would also contain an extra factor (a "coefficient function") in the final result for the convolution.

With these considerations in mind we first should take a look at the nature of the distribution functions needed for the k_T -factorized expression for the two-gluon production.

A. One- and Two-Gluon Distribution Functions

As we mentioned above, the impact parameter convolutions in Eqs. (2) and (3) do not appear to be factorizable into the integral over the distances between the gluons and the projectile and a separate integral over the distances between the gluons and the target, in stark contrast to the single-gluon production case [60, 63]. Therefore, any factorization expression we could obtain for the two-gluon production has to have an explicit convolution over the impact parameters. Therefore, we first need to rewrite the single-gluon distribution functions introduced above for the fixed impact parameter. We can easily recast Eqs. (42) and (44) as

$$\left\langle \frac{d\phi_{A_1}(\mathbf{q}, y)}{d^2b} \right\rangle_{A_1} = \frac{C_F}{\alpha_s(2\pi)^3} \int d^2r e^{-i\mathbf{q}\cdot\mathbf{r}} \nabla_{\mathbf{r}}^2 n_G(\mathbf{b} + \mathbf{r}, \mathbf{b}, y) \quad (46)$$

and

$$\left\langle \frac{d\phi_{A_2}(\mathbf{q}, y)}{d^2b} \right\rangle_{A_2} = \frac{C_F}{\alpha_s(2\pi)^3} \int d^2r e^{-i\mathbf{q}\cdot\mathbf{r}} \nabla_{\mathbf{r}}^2 N_G(\mathbf{b} + \mathbf{r}, \mathbf{b}, y). \quad (47)$$

Since now these distribution functions fix both the momentum of the gluon \mathbf{q} and its (approximate) position in the transverse coordinate space \mathbf{b} , along with its rapidity y specifying the value of Bjorken- x variable, we identify the differential unintegrated gluon distribution functions in Eqs. (46) and (47) with the Wigner distribution [81] for gluons (see [82, 83] and references therein for applications of Wigner distributions in perturbative QCD).

Here we introduce two different distribution functions which are associated with the two Wilson line operators entering the two-gluon production cross-section (1), the gluon quadrupole and the double-trace operators. The two-gluon distribution function associated with the gluon double-trace operator is

$$\left\langle \frac{d\phi_{A_2}^D(\mathbf{q}_1, \mathbf{q}_2, y)}{d^2b_1 d^2b_2} \right\rangle_{A_2} = \left(\frac{C_F}{\alpha_s(2\pi)^3} \right)^2 \int d^2r_1 d^2r_2 e^{-i\mathbf{q}_1\cdot\mathbf{r}_1 - i\mathbf{q}_2\cdot\mathbf{r}_2} \nabla_{\mathbf{r}_1}^2 \nabla_{\mathbf{r}_2}^2 N_D(\mathbf{b}_1 + \mathbf{r}_1, \mathbf{b}_1, \mathbf{b}_2 + \mathbf{r}_2, \mathbf{b}_2, y), \quad (48)$$

where

$$N_D(\mathbf{x}, \mathbf{y}, \mathbf{z}, \mathbf{w}, Y) = \frac{1}{(N_c^2 - 1)^2} \langle \text{Tr} [\mathbb{1} - U_{\mathbf{x}} U_{\mathbf{y}}^\dagger] \text{Tr} [\mathbb{1} - U_{\mathbf{z}} U_{\mathbf{w}}^\dagger] \rangle_{A_2}(Y). \quad (49)$$

The correlator N_D is illustrated diagrammatically in the top panel of Fig. 6 for the quasi-classical approximation. The distribution function (48) gives us the number density for pairs of gluons, with the transverse momenta $\mathbf{q}_1, \mathbf{q}_2$ and positions $\mathbf{b}_1, \mathbf{b}_2$ of the gluons fixed and with the rapidity of both gluons being close to y (up to $\ll 1/\alpha_s$ variations): we can think of this distribution function as a two-gluon Wigner distribution.

The distribution function associated with the gluon quadrupole operator is

$$\left\langle \frac{d\phi_{A_2}^Q(\mathbf{q}_1, \mathbf{q}_2, y)}{d^2b_1 d^2b_2} \right\rangle_{A_2} = \left(\frac{C_F}{\alpha_s(2\pi)^3} \right)^2 \int d^2r_1 d^2r_2 e^{-i\mathbf{q}_1\cdot\mathbf{r}_1 - i\mathbf{q}_2\cdot\mathbf{r}_2} \nabla_{\mathbf{r}_1}^2 \nabla_{\mathbf{r}_2}^2 N_Q(\mathbf{b}_1 + \mathbf{r}_1, \mathbf{b}_1, \mathbf{b}_2 + \mathbf{r}_2, \mathbf{b}_2, y) \quad (50)$$

with

$$N_Q(\mathbf{x}, \mathbf{y}, \mathbf{z}, \mathbf{w}, Y) = \frac{1}{N_c^2 - 1} \langle \text{Tr} [(\mathbb{1} - U_{\mathbf{x}} U_{\mathbf{y}}^\dagger) (\mathbb{1} - U_{\mathbf{z}} U_{\mathbf{w}}^\dagger)] \rangle_{A_2}(Y). \quad (51)$$

The definition (50) is illustrated diagrammatically in the lower panel of Fig. 6 in the quasi-classical approximation. The object defined in (50) can, similar to (48), be thought of as a (different) two-gluon Wigner distribution.

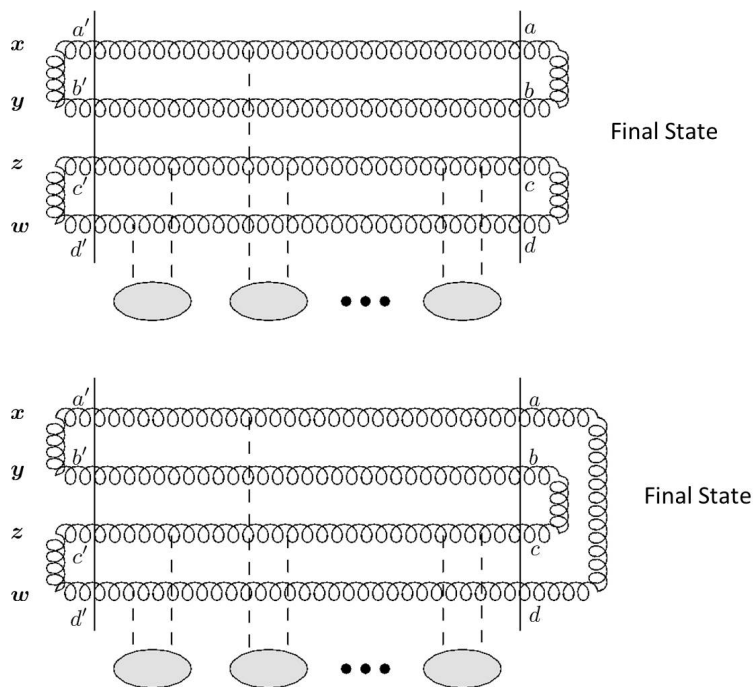


FIG. 6. The top panel represents the forward amplitude for the scattering of two gluon dipoles on a target nucleus in the quasi-classical approximation: this is an essential contribution to the definition of the two-gluon distribution in Eq. (48). The bottom panel represents the quadrupole scattering on the target, as in the definition of the two-gluon distribution in Eq. (50). The vectors \mathbf{x} , \mathbf{y} , \mathbf{z} , and \mathbf{w} label the positions of the gluon Wilson lines. Vertical solid lines denote the initial (left) and final (right) states. The final state of the gluons is labeled to stress that the difference between the two panels is in the color configurations of the final state.

Notice how both the two-dipole (48) and quadrupole (50) two-gluon distribution are composed of Wilson line operators. This is natural for distribution functions entering production cross section, since in high energy scattering all cross sections are expressed in terms of Wilson lines. This is in exact parallel to the single-gluon distribution (47), which is related to the adjoint dipole operator. Note that since the single-gluon production cross section depends only on the adjoint dipole operator, one can express it only in terms of the single-gluon distribution (44). For the two-gluon production (1), which contains both the double-trace and quadrupole operators, we end up with two different two-gluon distributions (48) and (50).

There is also an alternative single-gluon distribution, the so-called Weizsäcker-Williams (WW) distribution [56, 60, 76, 79], which was found to be related to the $q\bar{q}$ back-to-back jet production in DIS [84]. In the quasi-classical MV picture the Weizsäcker-Williams two-gluon distribution, given by the correlator of four different gluon fields, would simply factorize into a product of two single-gluon WW distributions. It is possible, however, that beyond the quasi-classical limit the two-gluon WW distribution (properly defined in terms of Wilson line operators along the lines of the single-gluon WW distribution from [84]) would constitute an independent new object, related to some observables. Investigating this possibility further is beyond the scope of this work.

Since there exists more experience in the field with dipole distribution functions (47), it would be nice to be able to write the two-gluon distributions (48) and (50) as combinations of dipole distributions. Unfortunately this is not possible in general; however each distribution does contain a piece that can be written in terms of dipole distributions.

The most obvious is the double-trace two-gluon distribution function (48). Since in the large- N_c limit

$$N_D(\mathbf{x}, \mathbf{y}, \mathbf{z}, \mathbf{w}) \Big|_{\text{large-}N_c} = N_G(\mathbf{x}, \mathbf{y}) N_G(\mathbf{z}, \mathbf{w}) \quad (52)$$

with $N_G = 1 - S_G$, we can see by plugging this result into Eq. (48) and comparing to Eq. (47) that

$$\left\langle \frac{d\phi_{A_2}^D(\mathbf{q}_1, \mathbf{q}_2, y)}{d^2b_1 d^2b_2} \right\rangle_{A_2} \Big|_{\text{large-}N_c} = \left\langle \frac{d\phi_{A_2}(\mathbf{q}_1, y)}{d^2b_1} \right\rangle_{A_2} \left\langle \frac{d\phi_{A_2}(\mathbf{q}_2, y)}{d^2b_2} \right\rangle_{A_2}. \quad (53)$$

The double-trace two-gluon distribution function factorizes into two dipole distribution functions only in the large- N_c limit. Unfortunately, the only correlations left in the two-gluon production cross section (1) evaluated in the large- N_c limit are the geometric correlations [1]. All of the other correlations contained in (1) are subleading in N_c ; for instance, the correlations (16) are explicitly $\mathcal{O}(1/N_c^2)$.

In order to isolate the dipole contribution to the two-gluon quadrupole distribution (50) we cannot just take the large- N_c limit like we did for the singlet distribution. (In addition the whole corresponding contribution to the cross section (3) is $\mathcal{O}(1/N_c^2)$ when compared to Eq. (2).) Instead we can single out the part of the two-gluon quadrupole distribution which is expressible in terms of single-gluon dipole distributions: we will show later that this is exactly the part that gives rise to the early-time Hanbury-Brown-Twiss (HBT) correlations [85] discussed in [1].

First let us analyze the quadrupole operator (cf. Eq. (6))

$$Q(\mathbf{x}, \mathbf{y}, \mathbf{z}, \mathbf{w}, Y) = \frac{1}{N_c^2 - 1} \langle \text{Tr} [U_{\mathbf{x}} U_{\mathbf{y}}^\dagger U_{\mathbf{z}} U_{\mathbf{w}}^\dagger] \rangle_{A_2} (Y) = \frac{1}{N_c^2 - 1} \left\langle \delta^{ad} \delta^{bc} U_{\mathbf{x}}^{aa'} U_{\mathbf{y}}^{bb'} U_{\mathbf{z}}^{cc'} U_{\mathbf{w}}^{dd'} \delta^{a'b'} \delta^{c'd'} \right\rangle_{A_2} (Y). \quad (54)$$

Here we have written out the color structure implied by the trace notation in terms of the adjoint color indices a, b, c, d (and the corresponding primed variables) shown in the lower panel of Fig. 6. The four gluon lines in the final state in Fig. 6 carrying indices a, b, c, d are in a net color-neutral state. This allows us to classify the color states in the quadrupole operator by the color states of the two gluons with indices a and b . Choosing the color state of gluons a and b sets the color state of gluons c and d due to the color neutrality of all four gluons in the final state. The same applies to the initial state gluons with the color indices a', b', c' , and d' .

A pair of gluons may be found in either of the following irreducible representations of $\text{SU}(N_c)$

$$\begin{aligned} (N_c^2 - 1) \otimes (N_c^2 - 1) &= V_1 \oplus V_2 \oplus V_3 \oplus V_4 \oplus V_5 \oplus V_6 \oplus V_7 \\ &= \mathbf{1} \oplus (N_c^2 - 1) \oplus \frac{N_c^2(N_c - 3)(N_c + 1)}{4} \oplus \frac{N_c^2(N_c + 3)(N_c - 1)}{4} \oplus (N_c^2 - 1) \oplus \frac{(N_c^2 - 1)(N_c^2 - 4)}{4} \oplus \frac{(N_c^2 - 1)(N_c^2 - 4)}{4}. \end{aligned} \quad (55)$$

In Eq. (55) we follow the notation for the irreducible representations introduced in [86], see page 120 there. We will, however, use a different normalization scheme from the projection operators P_i^{abcd} 's. We normalize the states such that $P_i^{abcd} P_i^{abcd} = 1$ (summation over repeated indices is implied), which implies, due to the orthonormality of the projection operators,

$$\mathbb{1}^{abcd, a'b'c'd'} = \sum_{i=1}^7 P_i^{abcd} P_i^{a'b'c'd'}. \quad (56)$$

The only projection operator we need to know explicitly for the following calculation is the singlet projector,

$$P_1^{abcd} = \frac{1}{N_c^2 - 1} \delta^{ab} \delta^{cd}. \quad (57)$$

Using the singlet projection and the unit operator (56) we can rewrite Eq. (54) as (dropping the A_2 subscript and not showing rapidity dependence for brevity)

$$\frac{1}{N_c^2 - 1} \langle \text{Tr} [U_{\mathbf{x}} U_{\mathbf{y}}^\dagger U_{\mathbf{z}} U_{\mathbf{w}}^\dagger] \rangle = \sum_{i=1}^7 P_i^{a''b''b''a''} \left\langle P_i^{abcd} U_{\mathbf{x}}^{aa'} U_{\mathbf{y}}^{bb'} U_{\mathbf{z}}^{cc'} U_{\mathbf{w}}^{dd'} P_1^{a'b'c'd'} \right\rangle. \quad (58)$$

We can isolate the part that gives the factorized dipole contribution in the sum of Eq. (58). This contribution comes from the large- N_c part of the double-dipole operator, which, in turn, originates in the P_1 -term in the sum in (58). Isolating the double trace operator from the rest of the expression in Eq. (58) we arrive at

$$\begin{aligned} \frac{1}{N_c^2 - 1} \langle \text{Tr} [U_{\mathbf{x}} U_{\mathbf{y}}^\dagger U_{\mathbf{z}} U_{\mathbf{w}}^\dagger] \rangle &= \frac{1}{(N_c^2 - 1)^2} \langle \text{Tr} [U_{\mathbf{x}} U_{\mathbf{y}}^\dagger] \text{Tr} [U_{\mathbf{z}} U_{\mathbf{w}}^\dagger] \rangle \\ &\quad + \sum_{i=2}^7 P_i^{a''b''b''a''} \left\langle P_i^{abcd} U_{\mathbf{x}}^{aa'} U_{\mathbf{y}}^{bb'} U_{\mathbf{z}}^{cc'} U_{\mathbf{w}}^{dd'} P_1^{a'b'c'd'} \right\rangle. \end{aligned} \quad (59)$$

The double trace operator comes with a prefactor of $\frac{1}{(N_c^2 - 1)^2}$, which means that when we combine Eq. (59) with Eq. (51) we arrive at

$$N_Q(\mathbf{x}, \mathbf{y}, \mathbf{z}, \mathbf{w}) = N_G(\mathbf{x}, \mathbf{y}) N_G(\mathbf{z}, \mathbf{w}) + \dots \quad (60)$$

The ellipses in (60) represent the remaining contributions which are not contained in the factorized gluon dipoles, the P_2 through P_7 terms and the sub-leading in N_c terms from the double trace operator in Eq. (59). Plugging Eq. (60) into Eq. (50) we arrive at

$$\left\langle \frac{d\phi_{A_2}^Q(\mathbf{q}_1, \mathbf{q}_2, y)}{d^2b_1 d^2b_2} \right\rangle_{A_2} = \left\langle \frac{d\phi_{A_2}(\mathbf{q}_1, y)}{d^2b_1} \right\rangle_{A_2} \left\langle \frac{d\phi_{A_2}(\mathbf{q}_2, y)}{d^2b_2} \right\rangle_{A_2} + \dots, \quad (61)$$

where we have isolated the factorized dipole distributions from the rest of the expression. Let us stress that the terms represented by ellipsis in Eq. (61) are not suppressed by any parameter involved in the problem: these corrections are comparable to the term shown explicitly on the right of (61). Hence even if we took the leading- N_c limit of the two-gluon quadrupole distribution there would still be terms that would not be contained inside the two factorized gluon distributions of (61).

B. Derivation of the Factorized Forms

Now that we have defined the necessary distribution functions we can start constructing the factorized form of the two-gluon production cross-section. Each of the parts of the cross section (1) given by Eqs. (2) and (3) factorizes differently.

The easiest case to factorize, and thus the first one we will cover, is the 'square' diagram component (2). Separating the transverse vectors associated with either one of the valence quarks and emitted gluons, we can write Eq. (2) in the following form,

$$\begin{aligned} \frac{d\sigma_{square}}{d^2k_1 dy_1 d^2k_2 dy_2} &= \frac{\alpha_s^2 C_F^2}{16 \pi^8} \int d^2B \left\langle \int d^2x_1 d^2y_1 d^2b_1 T_1(\mathbf{B} - \mathbf{b}_1) e^{-i \mathbf{k}_1 \cdot (\mathbf{x}_1 - \mathbf{y}_1)} \frac{\mathbf{x}_1 - \mathbf{b}_1}{|\mathbf{x}_1 - \mathbf{b}_1|^2} \cdot \frac{\mathbf{y}_1 - \mathbf{b}_1}{|\mathbf{y}_1 - \mathbf{b}_1|^2} \right. \\ &\times \left(\frac{1}{N_c^2 - 1} \text{Tr}[U_{\mathbf{x}_1} U_{\mathbf{y}_1}^\dagger] - \frac{1}{N_c^2 - 1} \text{Tr}[U_{\mathbf{x}_1} U_{\mathbf{b}_1}^\dagger] - \frac{1}{N_c^2 - 1} \text{Tr}[U_{\mathbf{b}_1} U_{\mathbf{y}_1}^\dagger] + 1 \right) \\ &\times \int d^2x_2 d^2y_2 d^2b_2 T_1(\mathbf{B} - \mathbf{b}_2) e^{-i \mathbf{k}_2 \cdot (\mathbf{x}_2 - \mathbf{y}_2)} \frac{\mathbf{x}_2 - \mathbf{b}_2}{|\mathbf{x}_2 - \mathbf{b}_2|^2} \cdot \frac{\mathbf{y}_2 - \mathbf{b}_2}{|\mathbf{y}_2 - \mathbf{b}_2|^2} \\ &\times \left. \left(\frac{1}{N_c^2 - 1} \text{Tr}[U_{\mathbf{x}_2} U_{\mathbf{y}_2}^\dagger] - \frac{1}{N_c^2 - 1} \text{Tr}[U_{\mathbf{x}_2} U_{\mathbf{b}_2}^\dagger] - \frac{1}{N_c^2 - 1} \text{Tr}[U_{\mathbf{b}_2} U_{\mathbf{y}_2}^\dagger] + 1 \right) \right\rangle_{A_2}. \quad (62) \end{aligned}$$

Notice that the first two lines in Eq. (62) are the only two lines that contain the variables \mathbf{x}_1 , \mathbf{y}_1 , \mathbf{b}_1 , while the next two lines are the only ones that contain the variables \mathbf{x}_2 , \mathbf{y}_2 , \mathbf{b}_2 . In the limit we are dealing with \mathbf{x}_1 , \mathbf{y}_1 , \mathbf{b}_1 are perturbatively close to each other. Since $T_1(\mathbf{b})$ is slowly varying it is approximately constant over perturbatively short scales. Thus we can make the approximation

$$T_1(\mathbf{B} - \mathbf{b}_1) \approx T_1(\mathbf{B} - \mathbf{x}_1) \approx T_1(\mathbf{B} - \mathbf{y}_1). \quad (63)$$

This same approximation also applies to \mathbf{x}_2 , \mathbf{y}_2 , \mathbf{b}_2 . Notice that the second line of (62) has four different terms in the parentheses, each of which is at most a function of two of the three variables \mathbf{x}_1 , \mathbf{y}_1 , \mathbf{b}_1 . Combining this fact with the approximation (63) we can perform one of the \mathbf{x}_1 , \mathbf{y}_1 , \mathbf{b}_1 integrals over a different variable for each term in the second line depending on which variable is not in the trace. A similar thing is done with the \mathbf{x}_2 , \mathbf{y}_2 , \mathbf{b}_2 integral. After doing this and integrating by parts we arrive at

$$\begin{aligned} \frac{d\sigma_{square}}{d^2k_1 dy_1 d^2k_2 dy_2} &= \frac{\alpha_s^2 C_F^2}{4 \pi^6} \frac{1}{\mathbf{k}_1^2 \mathbf{k}_2^2} \int d^2B d^2b_1 d^2b_2 d^2x_1 d^2x_2 T_1(\mathbf{B} - \mathbf{b}_1) T_1(\mathbf{B} - \mathbf{b}_2) \ln \left(\frac{1}{|\mathbf{x}_1 - \mathbf{b}_1| \Lambda} \right) \ln \left(\frac{1}{|\mathbf{x}_2 - \mathbf{b}_2| \Lambda} \right) \\ &\times e^{-i \mathbf{k}_1 \cdot (\mathbf{x}_1 - \mathbf{b}_1) - i \mathbf{k}_2 \cdot (\mathbf{x}_2 - \mathbf{b}_2)} \nabla_{\mathbf{x}_1}^2 \nabla_{\mathbf{x}_2}^2 \frac{1}{(N_c^2 - 1)^2} \left\langle \text{Tr} [\mathbb{1} - U_{\mathbf{x}_1} U_{\mathbf{b}_1}^\dagger] \text{Tr} [\mathbb{1} - U_{\mathbf{x}_2} U_{\mathbf{b}_2}^\dagger] \right\rangle_{A_2}. \quad (64) \end{aligned}$$

From here we can manipulate this expression into a form reminiscent of Eq. (41) but not quite the same. As mentioned in the discussion at the beginning of Sec. V, the integrals over the impact parameters cannot be absorbed into the distribution functions. This is now manifest in Eq. (64): we have three integrals (over \mathbf{B} , \mathbf{b}_1 and \mathbf{b}_2) and four impact parameter-related distances ($\mathbf{B} - \mathbf{b}_1$, $\mathbf{B} - \mathbf{b}_2$, \mathbf{b}_1 and \mathbf{b}_2). We conclude that we must use the new distribution functions defined in Eqs. (46) and (48) while convoluting them over the impact parameters \mathbf{B} , \mathbf{b}_1 and \mathbf{b}_2 . Employing Eqs. (46) and (48) we can rewrite the 'square' diagrams contribution to the two-gluon production cross section (2) in

the factorized form

$$\begin{aligned} \frac{d\sigma_{square}}{d^2k_1 dy_1 d^2k_2 dy_2} &= \left(\frac{2\alpha_s}{C_F} \right)^2 \frac{1}{k_1^2 k_2^2} \int d^2B d^2b_1 d^2b_2 \int d^2q_1 d^2q_2 \\ &\times \left\langle \frac{d\phi_{A_1}(\mathbf{q}_1, y=0)}{d^2(\mathbf{B}-\mathbf{b}_1)} \right\rangle_{A_1} \left\langle \frac{d\phi_{A_1}(\mathbf{q}_2, y=0)}{d^2(\mathbf{B}-\mathbf{b}_2)} \right\rangle_{A_1} \left\langle \frac{d\phi_{A_2}^D(\mathbf{q}_1-\mathbf{k}_1, \mathbf{q}_2-\mathbf{k}_2, y \approx y_1 \approx y_2)}{d^2b_1 d^2b_2} \right\rangle_{A_2}. \end{aligned} \quad (65)$$

The asymmetry in rapidity arguments of the distribution entering Eq. (65) is due to the fact that the projectile in the original Eq. (2) was treated in the lowest-order quasi-classical approximation, while the whole non-linear evolution [36–43] is included in the rapidity interval between the produced gluons and the target by the use of the Wilson lines. As mentioned previously, Eq. (65) is similar to Eq. (41) but has a few key differences. Eq. (41) employs unintegrated gluon distributions (gluon transverse momentum distributions (TMDs)), while Eq. (65) uses one- and two-gluon Wigner distributions. Related to that, in Eq. (41) the convolution happens only over transverse momentum, while Eq. (65) also contains integrals over impact parameters \mathbf{B} , \mathbf{b}_1 , and \mathbf{b}_2 .

One may also note that Eq. (65) is not target-projectile symmetric: the target is described by a single two-gluon distribution, while the projectile is represented by two single-gluon distributions. In contrast, Eq. (41) is completely target-projectile symmetric. In fact, Eq. (41) is often generalized to the case of nucleus–nucleus (AA) collisions by using Eq. (44) for both unintegrated gluon distributions in it. While such generalization allows for successful phenomenology (see e.g. [45]), it is theoretically not justified below the saturation scales of both nuclei. Moreover, there is numerical evidence [87] demonstrating that the k_T -factorization formula (41) is not valid in AA collisions. Therefore, it appears that the apparent target-projectile symmetry of Eq. (41) is, in fact, somewhat misleading: the equation was derived in the limit where the projectile is dilute, while the target may or may not be dense, leading to the difference in the definitions of the unintegrated gluon distributions of the target and the projectile in Eqs. (42) and (44). It is likely that Eq. (41) is not valid for dense-dense scattering [87], and is thus not truly target-projectile symmetric due to the underlying assumptions.

With the ‘square’ diagrams contribution to the cross section cast in a factorized form we now turn our attention to the ‘crossed’ diagrams contribution (3). It is helpful to write out the crossed diagrams part of the cross section, Eq. (3), in the following form,

$$\begin{aligned} \frac{d\sigma_{crossed}}{d^2k_1 dy_1 d^2k_2 dy_2} &= \frac{\alpha_s^2 C_F^2}{16\pi^8} \int d^2B \left\langle \int d^2x_1 d^2y_1 d^2b_1 T_1(\mathbf{B}-\mathbf{b}_1) e^{-i\mathbf{k}_1 \cdot \mathbf{x}_1 + i\mathbf{k}_2 \cdot \mathbf{y}_1} \left[\frac{\mathbf{x}_1 - \mathbf{b}_1}{|\mathbf{x}_1 - \mathbf{b}_1|^2} \right]_i \left[\frac{\mathbf{y}_1 - \mathbf{b}_1}{|\mathbf{y}_1 - \mathbf{b}_1|^2} \right]_j \right. \\ &\times \frac{1}{N_c^2 - 1} \left[U_{\mathbf{x}_1} U_{\mathbf{y}_1}^\dagger - U_{\mathbf{x}_1} U_{\mathbf{b}_1}^\dagger - U_{\mathbf{b}_1} U_{\mathbf{y}_1}^\dagger + \mathbb{1} \right]^{ab} \\ &\times \int d^2x_2 d^2y_2 d^2b_2 T_1(\mathbf{B}-\mathbf{b}_2) e^{-i\mathbf{k}_2 \cdot \mathbf{x}_2 + i\mathbf{k}_1 \cdot \mathbf{y}_2} \left[\frac{\mathbf{x}_2 - \mathbf{b}_2}{|\mathbf{x}_2 - \mathbf{b}_2|^2} \right]_j \left[\frac{\mathbf{y}_2 - \mathbf{b}_2}{|\mathbf{y}_2 - \mathbf{b}_2|^2} \right]_i \\ &\times \left. \frac{1}{N_c^2 - 1} \left[U_{\mathbf{x}_2} U_{\mathbf{y}_2}^\dagger - U_{\mathbf{x}_2} U_{\mathbf{b}_2}^\dagger - U_{\mathbf{b}_2} U_{\mathbf{y}_2}^\dagger + \mathbb{1} \right]^{ba} \right\rangle_{A_2} + (\mathbf{k}_2 \rightarrow -\mathbf{k}_2), \end{aligned} \quad (66)$$

where $i, j = 1, 2$ are transverse vector indices and $a, b = 1, \dots, N_c^2 - 1$ are adjoint color indices, with summation assumed over repeated indices. Here we have again separated the terms that depend on \mathbf{x}_1 , \mathbf{y}_1 , \mathbf{b}_1 from the terms that depend on \mathbf{x}_2 , \mathbf{y}_2 , \mathbf{b}_2 . Using the same trick we employed when factorizing the ‘square’ diagrams contribution, we evaluate the \mathbf{x}_1 , \mathbf{y}_1 , \mathbf{b}_1 , and \mathbf{x}_2 , \mathbf{y}_2 , \mathbf{b}_2 integrals piece by piece arriving at (after transverse vector relabeling)

$$\begin{aligned} \frac{d\sigma_{crossed}}{d^2k_1 dy_1 d^2k_2 dy_2} &= \frac{\alpha_s^2 C_F^2}{4\pi^6} \int d^2B d^2b_1 d^2b_2 d^2x_1 d^2x_2 T_1(\mathbf{B}-\mathbf{b}_1) T_1(\mathbf{B}-\mathbf{b}_2) \\ &\times \left\{ \frac{1}{2} \delta_{ij} \ln \left(\frac{1}{|\mathbf{x}_1 - \mathbf{b}_1| \Lambda} \right) - \frac{[\mathbf{x}_1 - \mathbf{b}_1]_i [\mathbf{x}_1 - \mathbf{b}_1]_j}{2|\mathbf{x}_1 - \mathbf{b}_1|^2} - i \left[\frac{\mathbf{k}_1}{k_1^2} \right]_i \left[\frac{\mathbf{x}_1 - \mathbf{b}_1}{|\mathbf{x}_1 - \mathbf{b}_1|^2} \right]_j - i \left[\frac{\mathbf{x}_1 - \mathbf{b}_1}{|\mathbf{x}_1 - \mathbf{b}_1|^2} \right]_i \left[\frac{\mathbf{k}_2}{k_2^2} \right]_j \right\} \\ &\times \left\{ \frac{1}{2} \delta_{ij} \ln \left(\frac{1}{|\mathbf{x}_2 - \mathbf{b}_2| \Lambda} \right) - \frac{[\mathbf{x}_2 - \mathbf{b}_2]_i [\mathbf{x}_2 - \mathbf{b}_2]_j}{2|\mathbf{x}_2 - \mathbf{b}_2|^2} - i \left[\frac{\mathbf{k}_1}{k_1^2} \right]_i \left[\frac{\mathbf{x}_2 - \mathbf{b}_2}{|\mathbf{x}_2 - \mathbf{b}_2|^2} \right]_j - i \left[\frac{\mathbf{x}_2 - \mathbf{b}_2}{|\mathbf{x}_2 - \mathbf{b}_2|^2} \right]_i \left[\frac{\mathbf{k}_2}{k_2^2} \right]_j \right\} \\ &\times e^{-i\mathbf{k}_1 \cdot (\mathbf{x}_1 - \mathbf{b}_2) - i\mathbf{k}_2 \cdot (\mathbf{x}_2 - \mathbf{b}_1)} \frac{1}{(N_c^2 - 1)^2} \left\langle \text{Tr} \left[\left(\mathbb{1} - U_{\mathbf{x}_1} U_{\mathbf{b}_1}^\dagger \right) \left(\mathbb{1} - U_{\mathbf{x}_2} U_{\mathbf{b}_2}^\dagger \right) \right] \right\rangle_{A_2} + (\mathbf{k}_2 \rightarrow -\mathbf{k}_2), \end{aligned} \quad (67)$$

where we have employed

$$\int d^2b \left[\frac{\mathbf{x} - \mathbf{b}}{|\mathbf{x} - \mathbf{b}|^2} \right]_i \left[\frac{\mathbf{y} - \mathbf{b}}{|\mathbf{y} - \mathbf{b}|^2} \right]_j = \pi \left\{ \delta_{ij} \ln \left(\frac{1}{|\mathbf{x} - \mathbf{y}| \Lambda} \right) - \frac{[\mathbf{x} - \mathbf{y}]_i [\mathbf{x} - \mathbf{y}]_j}{|\mathbf{x} - \mathbf{y}|^2} \right\} \quad (68)$$

along with other, more common, two-dimensional integrals (see, e.g., Appendix A.2 of [27] for a list of useful integrals).

To proceed we rewrite Eq. (67) as

$$\begin{aligned}
\frac{d\sigma_{crossed}}{d^2k_1 dy_1 d^2k_2 dy_2} &= \frac{\alpha_s^2 C_F^2}{4^3 \pi^6} \frac{1}{k_1^4 k_2^4} \int d^2B d^2b_1 d^2b_2 d^2x_1 d^2x_2 e^{-i\mathbf{k}_1 \cdot (\mathbf{x}_1 - \mathbf{b}_2) - i\mathbf{k}_2 \cdot (\mathbf{x}_2 - \mathbf{b}_1)} \\
&\times \left\{ \left[\overleftarrow{\nabla}_{x_1}^2 \overleftarrow{\nabla}_{b_1}^2 \nabla_{x_1}^i \nabla_{x_1}^j + \overleftarrow{\nabla}_{b_1}^2 \overleftarrow{\nabla}_{x_1}^i \nabla_{x_1}^j \nabla_{x_1}^2 - \overleftarrow{\nabla}_{x_1}^2 \overleftarrow{\nabla}_{b_1}^j \nabla_{x_1}^i \nabla_{x_1}^2 \right] (\mathbf{x}_1 - \mathbf{b}_1)^2 \ln \left(\frac{1}{|\mathbf{x}_1 - \mathbf{b}_1| \Lambda} \right) T_1(\mathbf{B} - \mathbf{b}_1) \right\} \\
&\times \left\{ \left[\overleftarrow{\nabla}_{x_2}^2 \overleftarrow{\nabla}_{b_2}^2 \nabla_{x_2}^i \nabla_{x_2}^j - \overleftarrow{\nabla}_{x_2}^2 \overleftarrow{\nabla}_{b_2}^i \nabla_{x_2}^j \nabla_{x_2}^2 + \overleftarrow{\nabla}_{b_2}^2 \overleftarrow{\nabla}_{x_2}^j \nabla_{x_2}^i \nabla_{x_2}^2 \right] (\mathbf{x}_2 - \mathbf{b}_2)^2 \ln \left(\frac{1}{|\mathbf{x}_2 - \mathbf{b}_2| \Lambda} \right) T_1(\mathbf{B} - \mathbf{b}_2) \right\} \\
&\times \frac{1}{(N_c^2 - 1)^2} \left\langle \text{Tr} \left[\left(\mathbb{1} - U_{x_1} U_{b_1}^\dagger \right) \left(\mathbb{1} - U_{x_2} U_{b_2}^\dagger \right) \right] \right\rangle_{A_2} + (\mathbf{k}_2 \rightarrow -\mathbf{k}_2), \tag{69}
\end{aligned}$$

where ∇ 's denote transverse coordinate derivatives and the left arrow over ∇ indicates that the derivative is acting on the exponential to the left of the curly brackets.

Notice the non-trivial transverse index structure in Eq. (69): this drastically alters the factorized form of the expression, as compared to, say, Eq. (65). Inverting Fourier transforms in Eqs. (46) and (50), employing Eq. (43), and substituting the results into Eq. (69) yields, after a fair bit of algebra,

$$\begin{aligned}
\frac{d\sigma_{crossed}}{d^2k_1 dy_1 d^2k_2 dy_2} &= \left(\frac{2\alpha_s}{C_F} \right)^2 \frac{1}{k_1^2 k_2^2} \int d^2B d^2b_1 d^2b_2 \int d^2q_1 d^2q_2 \frac{\mathcal{K}(\mathbf{b}_1, \mathbf{b}_2, \mathbf{k}_1, \mathbf{k}_2, \mathbf{q}_1, \mathbf{q}_2)}{N_c^2 - 1} \\
&\times \left\langle \frac{d\phi_{A_1}(\mathbf{q}_1, y=0)}{d^2(\mathbf{B} - \mathbf{b}_1)} \right\rangle_{A_1} \left\langle \frac{d\phi_{A_1}(\mathbf{q}_2, y=0)}{d^2(\mathbf{B} - \mathbf{b}_2)} \right\rangle_{A_1} \left\langle \frac{d\phi_{A_2}^Q(\mathbf{k}_1 - \mathbf{q}_1, \mathbf{k}_2 - \mathbf{q}_2, y \approx y_1 \approx y_2)}{d^2b_1 d^2b_2} \right\rangle_{A_2} + (\mathbf{k}_2 \rightarrow -\mathbf{k}_2), \tag{70}
\end{aligned}$$

where the ‘‘coefficient function’’ is defined as

$$\begin{aligned}
\mathcal{K}(\mathbf{b}_1, \mathbf{b}_2, \mathbf{k}_1, \mathbf{k}_2, \mathbf{q}_1, \mathbf{q}_2) &= \frac{1}{q_1^2 q_2^2 (\mathbf{k}_1 - \mathbf{q}_1)^2 (\mathbf{k}_2 - \mathbf{q}_2)^2} e^{-i(\mathbf{k}_1 - \mathbf{k}_2) \cdot (\mathbf{b}_1 - \mathbf{b}_2)} \{ k_1^2 k_2^2 (\mathbf{q}_1 \cdot \mathbf{q}_2)^2 \\
&- k_1^2 (\mathbf{q}_1 \cdot \mathbf{q}_2) [(\mathbf{k}_2 \cdot \mathbf{q}_1) q_2^2 + (\mathbf{k}_2 \cdot \mathbf{q}_2) q_1^2 - q_1^2 q_2^2] \\
&- k_2^2 (\mathbf{q}_1 \cdot \mathbf{q}_2) [(\mathbf{k}_1 \cdot \mathbf{q}_1) q_2^2 + (\mathbf{k}_1 \cdot \mathbf{q}_2) q_1^2 - q_1^2 q_2^2] \\
&+ q_1^2 q_2^2 [(\mathbf{k}_1 \cdot \mathbf{q}_1)(\mathbf{k}_2 \cdot \mathbf{q}_2) + (\mathbf{k}_1 \cdot \mathbf{q}_2)(\mathbf{k}_2 \cdot \mathbf{q}_1)] \} \tag{71}
\end{aligned}$$

with $q_i = |\mathbf{q}_i|$, $k_i = |\mathbf{k}_i|$.

Inserting Eq. (65) and Eq. (70) into Eq. (1) we arrive at the k_T -factorized form for the two gluon production cross section in heavy-light ion collisions

$$\begin{aligned}
\frac{d\sigma}{d^2k_1 dy_1 d^2k_2 dy_2} &= \left(\frac{2\alpha_s}{C_F} \right)^2 \frac{1}{k_1^2 k_2^2} \int d^2B d^2b_1 d^2b_2 \int d^2q_1 d^2q_2 \left\langle \frac{d\phi_{A_1}(\mathbf{q}_1, y=0)}{d^2(\mathbf{B} - \mathbf{b}_1)} \right\rangle_{A_1} \left\langle \frac{d\phi_{A_1}(\mathbf{q}_2, y=0)}{d^2(\mathbf{B} - \mathbf{b}_2)} \right\rangle_{A_1} \\
&\times \left\{ \left\langle \frac{d\phi_{A_2}^D(\mathbf{q}_1 - \mathbf{k}_1, \mathbf{q}_2 - \mathbf{k}_2, y)}{d^2b_1 d^2b_2} \right\rangle_{A_2} + \left[\frac{\mathcal{K}(\mathbf{b}_1, \mathbf{b}_2, \mathbf{k}_1, \mathbf{k}_2, \mathbf{q}_1, \mathbf{q}_2)}{N_c^2 - 1} \left\langle \frac{d\phi_{A_2}^Q(\mathbf{q}_1 - \mathbf{k}_1, \mathbf{q}_2 - \mathbf{k}_2, y)}{d^2b_1 d^2b_2} \right\rangle_{A_2} + (\mathbf{k}_2 \rightarrow -\mathbf{k}_2) \right] \right\} \tag{72}
\end{aligned}$$

with $y \approx y_1 \approx y_2$ in the curly brackets. Eq. (72) is the main result of this Section.

Notice that Eq. (72) has all of the properties we expected: it contains the convolution over the impact parameters \mathbf{B} , \mathbf{b}_1 , and \mathbf{b}_2 along with different two-gluon distribution functions. As advertised, Eq. (72) also contains a ‘‘coefficient function’’ associated with the factorized form of ‘crossed’ diagrams.

The convolution over impact parameters in Eq. (72) appears to imply that the 2-gluon production cross section is sensitive to the b -dependence of the one- and two-gluon distributions ϕ , ϕ^D , ϕ^Q . From Eqs. (47), (48), and (50) we see that the b -dependence of those gluon distributions is related to that of the dipole, double-trace and quadrupole operators. It is known that any perturbative approach, such as the CGC formalism employed here, cannot describe correctly the b -dependence of scattering amplitudes in peripheral collisions due to the importance of non-perturbative effects [88]. It, therefore, appears that the two-gluon production cross-section is also sensitive to the non-perturbative large- b physics. Note, however, that this conclusion also applies to the single-gluon production in Eq. (41), since the impact parameter integral in Eq. (42) is also sensitive to large- b physics. Recent studies [89] appear to indicate that this sensitivity to non-perturbative effects at the periphery is not very strong, and may be negligible at high energies.

Unfortunately the factorization expression (72) is different from that used in [17–19]. The expression in those references was motivated by extrapolation of the dilute–dilute scattering case to the dense–dense scattering by analogy

with the single-gluon production Eq. (41). While our result is valid only for the dense-dilute scattering, we can conclude that the extrapolation suggested in [12, 13, 17–19] does not work in the dense-dilute case, and is, therefore, unlikely to be valid in the dense-dense scattering case either.

Just like Eq. (65), the expression (72) is not projectile-target symmetric. While this is natural due to the asymmetric treatment of the target and projectile in our dense-dilute scattering approximation, this asymmetry also means that a simple generalization to the case of nucleus-nucleus scattering along the lines of what was done with Eq. (41) in [44, 45, 90, 91] appears to be impossible for Eq. (72).

The factorized form of the two-gluon production cross section (72) contains a few interesting properties. If we look at the large- N_c limit the 'crossed' diagrams contribution can be neglected and, using Eq. (53), the two-gluon singlet distribution function factorizes into two single gluon distribution functions,

$$\frac{d\sigma}{d^2k_1 dy_1 d^2k_2 dy_2} \Big|_{\text{large-}N_c} = \left(\frac{2\alpha_s}{C_F}\right)^2 \frac{1}{k_1^2 k_2^2} \int d^2B d^2b_1 d^2b_2 \int d^2q_1 d^2q_2 \times \left\langle \frac{d\phi_{A_1}(\mathbf{q}_1, y=0)}{d^2(\mathbf{B}-\mathbf{b}_1)} \right\rangle_{A_1} \left\langle \frac{d\phi_{A_1}(\mathbf{q}_2, y=0)}{d^2(\mathbf{B}-\mathbf{b}_2)} \right\rangle_{A_1} \left\langle \frac{d\phi_{A_2}(\mathbf{q}_1-\mathbf{k}_1, y)}{d^2b_1} \right\rangle_{A_2} \left\langle \frac{d\phi_{A_2}(\mathbf{q}_2-\mathbf{k}_2, y)}{d^2b_2} \right\rangle_{A_2}. \quad (73)$$

This equation can only generate correlations between the two gluons through the convolution over the impact parameters, which are geometric correlations [1]. This form does not contain the information needed to, say, calculate the correlation function (16), since for that one needs terms that are subleading in the large- N_c limit.

Another interesting property is that we can isolate the part of the cross-section that gives rise to HBT correlations [85]. Due to the nature of HBT correlations, the only way the correlations can be generated is through interference effects. Thus only the 'crossed' diagrams contribute. In addition, for the correlation to be pure HBT, the two produced gluons should have the same colors (to be identical particles): imposing same-color requirement on the 'crossed' diagrams is equivalent to the projection employed in arriving at Eq. (61). We conclude that the only part of the quadrupole two-gluon distribution function (50) that contributes to HBT correlations is the portion that can be factorized into two single-gluon distributions shown in (61). With the help of Eq. (61) the HBT part of the two-gluon production cross-section can be written as

$$\frac{d\sigma_{HBT}}{d^2k_1 dy_1 d^2k_2 dy_2} = \left(\frac{2\alpha_s}{C_F}\right)^2 \frac{1}{k_1^2 k_2^2} \int d^2B d^2b_1 d^2b_2 \int d^2q_1 d^2q_2 \frac{\mathcal{K}(\mathbf{b}_1, \mathbf{b}_2, \mathbf{k}_1, \mathbf{k}_2, \mathbf{q}_1, \mathbf{q}_2)}{N_c^2 - 1} \times \left\langle \frac{d\phi_{A_1}(\mathbf{q}_1, y=0)}{d^2(\mathbf{B}-\mathbf{b}_1)} \right\rangle_{A_1} \left\langle \frac{d\phi_{A_1}(\mathbf{q}_2, y=0)}{d^2(\mathbf{B}-\mathbf{b}_2)} \right\rangle_{A_1} \left\langle \frac{d\phi_{A_2}(\mathbf{q}_1-\mathbf{k}_1, y)}{d^2b_1} \right\rangle_{A_2} \left\langle \frac{d\phi_{A_2}(\mathbf{q}_2-\mathbf{k}_2, y)}{d^2b_2} \right\rangle_{A_2} + (\mathbf{k}_2 \rightarrow -\mathbf{k}_2). \quad (74)$$

To summarize this Section let us stress that we were able to find a factorized form for the two-gluon production cross section in heavy-light ion collisions, given by Eq. (72). It had to be written in a different form than that of the single gluon production cross-section (41). In particular, in Eq. (72) we have a convolution over the impact parameters which requires that the distribution functions have to be written as differentials with respect to impact parameters, that is as gluon Wigner distributions. There was also a ‘‘coefficient function’’ factor (71) that was associated with the interference effects included in the 'crossed' diagrams. These facts may have important implications for k_T -factorization when it comes to multi-gluon cross-sections and could possibly give insight into the nature of k_T -factorization in general.

VI. ENERGY DEPENDENCE OF THE CORRELATIONS

Our goal now is to study the energy and rapidity dependence of the correlator in Eq. (13). As mentioned before, we are working in the regime where the rapidities of the produced gluons, y_1, y_2 , are sufficiently close to the rapidity of the projectile Y such that no small- x evolution needs to be included in the $[y_1, y_2]$ and $[y_2, Y]$ rapidity intervals (for $y_2 > y_1$). This implies that $|y_1 - y_2| \ll 1/\alpha_s$ and $0 < Y - y_{1,2} \ll 1/\alpha_s$. Taking the rapidity of the target to be 0, we see that the results of [1] outlined above apply to the case when Y, y_1 , and y_2 are all large enough to necessitate the inclusion of small- x evolution in the rapidity interval between the target and the produced gluons. Since, from the standpoint of the leading-logarithmic small- x evolution, the rapidities of the gluons and the projectile are close enough to be considered identical, $y_1 \approx y_2 \approx Y$, including the evolution between the gluons and the projectile would only generate the dependence of the cross section (1) on the net rapidity interval Y (or, equivalently, on the center-of-mass energy of the collision), without producing any additional y_1 and y_2 dependence of the cross section. To generate the latter one has to include the small- x evolution between the two gluons and between the gluons and the projectile: this is left for future work. Therefore, here we will not distinguish between the energy and rapidity dependence of the cross section (1), since the two are identical in the approximation used.

In the leading- $\ln 1/x$ approximation, the effects of the nonlinear BK/JIMWLK evolution are included in the cross section (1) by simply evolving the Wilson-line correlators in Eqs. (2) and (3) up to rapidity Y . The corresponding evolution equations can be easily obtained by applying the JIMWLK evolution to the correlators. The results are listed in the Appendix, with the evolution equations for the gluon dipole, gluon quadrupole, and the double-trace operator given by the Eqs. (A3), (A5), and (A7) respectively. Unfortunately none of these equations is a closed integro-differential equation: their right-hand-sides contain higher-order Wilson-line correlators, which in turn would obey other evolution equations, involving yet higher-order correlators, etc., forming the whole infinite tower of the Balitsky hierarchy [36, 37]. Unfortunately the hierarchy by itself can not be solved neither numerically nor analytically: instead one can solve the JIMWLK functional evolution equation numerically, and construct all the correlators by averaging the corresponding operators over all color field configurations [92–94].

Instead, here we will try to evaluate the energy dependence of the cross section (1) by using an approximate analytic method, based on the Gaussian truncation of the JIMWLK evolution [93, 95]. It is based on the observation that relations between different Wilson line correlators calculated in the MV model remain approximately valid for JIMWLK-evolved correlators. For instance, as was shown in [93], the relation

$$S_G(\mathbf{x}_1, \mathbf{x}_2, Y) = [S_{q\bar{q}}(\mathbf{x}_1, \mathbf{x}_2, Y)]^{N_c/C_F} \quad (75)$$

between the adjoint and fundamental ($S_{q\bar{q}}$) dipole S -matrices, valid strictly-speaking only in the MV model (that is, at $Y = 0$), is also preserved (with high accuracy, but not exactly) by the leading- $\ln 1/x$ JIMWLK evolution. In fact, both dipole S -matrices in Eq. (75) can be well approximated if one writes

$$S_{q\bar{q}}(\mathbf{x}_1, \mathbf{x}_2, Y) = [S_{BK}(\mathbf{x}_1, \mathbf{x}_2, Y)]^{2C_F/N_c}, \quad (76)$$

where S_{BK} is found from the BK evolution equation,

$$\partial_Y S_{BK}(\mathbf{x}, \mathbf{y}, Y) = \frac{\alpha_s N_c}{2\pi^2} \int d^2z \frac{(\mathbf{x} - \mathbf{y})^2}{(\mathbf{x} - \mathbf{z})^2 (\mathbf{y} - \mathbf{z})^2} [S_{BK}(\mathbf{x}, \mathbf{z}, Y) S_{BK}(\mathbf{z}, \mathbf{y}, Y) - S_{BK}(\mathbf{x}, \mathbf{y}, Y)]. \quad (77)$$

In the large- N_c approximation for which the BK equation is valid, Eq. (76) reduces to $S_{q\bar{q}} = S_{BK}$, a relation which also seems to hold well numerically if $S_{q\bar{q}}$ is found using JIMWLK evolution [92]. However, the full Eq. (76) provides an even better numerical agreement between JIMWLK-evolved $S_{q\bar{q}}$ and BK-evolved S_{BK} [93].

The validity of the Gaussian truncation for higher-order correlators of Wilson lines was studied numerically in [94], while analytic arguments in support of the Gaussian approximation have been proposed in [96, 97].

Here we will assume that the Gaussian truncation is valid, and apply it to determine the energy dependence of the two-gluon production cross section (1). While the exact analytic solution of the BK equation is not known, a good approximation exists immediately outside the saturation region [98, 99]

$$N(\mathbf{x}_1, \mathbf{x}_2, Y) \propto [|\mathbf{x}_1 - \mathbf{x}_2| Q_s(Y)]^{1+2i\nu_0}, \quad (78)$$

where the (imaginary part of the) dipole forward scattering amplitude is

$$N(\mathbf{x}_1, \mathbf{x}_2, Y) = 1 - S_{BK}(\mathbf{x}_1, \mathbf{x}_2, Y) \quad (79)$$

and $\nu_0 \approx -0.1275i$. The approximate solution (78) was derived in the limit where the impact-parameter dependence of the dipole scattering amplitude could be neglected. The proportionality (78) becomes an equality if one includes an energy-dependent prefactor [98, 99], though its energy dependence is much slower than that of the factor shown in Eq. (78): as we neglect this prefactor, we have to remember that all our conclusions here will be valid up to a factor which may vary slowly with energy. The solution (78) is valid in the extended geometric scaling region, $1/k_{geom} \lesssim |\mathbf{x}_1 - \mathbf{x}_2| \lesssim 1/Q_s(Y)$, with $k_{geom} \approx Q_s^2(Y)/Q_s(0) \gg Q_s(Y)$ [98]. There the BK equation (77) is linearized in the powers of the dipole amplitude N , and the resulting BFKL equation is solved with an IR saturation boundary [99].

To find the gluon dipole S matrix we use Eqs. (75) and (76) to write

$$\begin{aligned} 1 - S_G(\mathbf{x}_1, \mathbf{x}_2, Y) &= 1 - [S_{BK}(\mathbf{x}_1, \mathbf{x}_2, Y)]^2 = 2N(\mathbf{x}_1, \mathbf{x}_2, Y) - [N(\mathbf{x}_1, \mathbf{x}_2, Y)]^2 \\ &\approx 2N(\mathbf{x}_1, \mathbf{x}_2, Y) \propto [|\mathbf{x}_1 - \mathbf{x}_2| Q_s(Y)]^{1+2i\nu_0}. \end{aligned} \quad (80)$$

Comparing this to Eq. (11) and postulating the latter to be valid at all rapidities (thus defining Γ_G for $Y \neq 0$), we conclude that, in this linearized regime,

$$\Gamma_G(\mathbf{x}_1, \mathbf{x}_2, Y) \approx 1 - S_G(\mathbf{x}_1, \mathbf{x}_2, Y) \propto (|\mathbf{x}_1 - \mathbf{x}_2| Q_s(Y))^{1+2i\nu_0}. \quad (81)$$

We now want to determine the energy-dependence of the two-gluon production cross section in Eqs. (2) and (3) outside the saturation region, that is for $k_1, k_2 \gg Q_{s2}(Y)$. From the experience with the single inclusive gluon production [79, 100, 101] it appears that the behavior of the cross section in the $k_1, k_2 \approx Q_{s2}(Y)$ regime (at the edge of the saturation region) is qualitatively similar to that for $k_1, k_2 \gg Q_{s2}(Y)$ (outside the saturation region). We, therefore, hope that by studying the energy-dependence of two-gluon production at $k_1, k_2 \gg Q_{s2}(Y)$ we would obtain a good estimate of the energy dependence in other kinematic regions as well.

Let us begin with the 'square' diagram case. Employing the results of the previous Section we see that, for Eq. (64) the $k_1, k_2 \gg Q_{s2}(Y)$ limit implies that \mathbf{x}_1 is close to \mathbf{b}_1 while \mathbf{x}_2 is close to \mathbf{b}_2 . It is also a good approximation to assume that the two pairs of points, $\mathbf{x}_1, \mathbf{b}_1$ and $\mathbf{x}_2, \mathbf{b}_2$, are close to each other. To justify this assume that $\mathbf{x}_1, \mathbf{b}_1$ and $\mathbf{x}_2, \mathbf{b}_2$ are far apart, further away than $1/Q_{s2}(Y)$. Using the Gaussian truncation along with Eq. (32) we can evaluate the connected part of the double-trace operator as proportional to

$$(D_2 - D_3)^2 \left(\frac{1}{D_2} + \frac{1}{D_3} \right), \quad (82)$$

where

$$D_1 = -\Gamma_G(\mathbf{x}_1, \mathbf{b}_1, Y) - \Gamma_G(\mathbf{x}_2, \mathbf{b}_2, Y) \ll 1 \quad (83a)$$

$$D_2 = -\Gamma_G(\mathbf{x}_1, \mathbf{x}_2, Y) - \Gamma_G(\mathbf{b}_1, \mathbf{b}_2, Y) \gg 1 \quad (83b)$$

$$D_3 = -\Gamma_G(\mathbf{x}_1, \mathbf{b}_2, Y) - \Gamma_G(\mathbf{b}_1, \mathbf{x}_2, Y) \gg 1. \quad (83c)$$

Since for very large dipoles (with sizes much larger than $1/Q_{s2}(Y)$) the S -matrix is given by the Levin-Tuchin formula [102]

$$S_G(\mathbf{x}_1, \mathbf{x}_2, Y) \propto e^{-\text{const} \ln^2(|\mathbf{x}_1 - \mathbf{x}_2| Q_{s2}(Y))} \quad (84)$$

we see that

$$\Gamma_G(\mathbf{x}_1, \mathbf{x}_2, Y) \sim \ln^2(|\mathbf{x}_1 - \mathbf{x}_2| Q_{s2}(Y)) \quad (85)$$

is a slowly varying function of rapidity Y . Using this in Eq. (82) we conclude that at large separations between $\mathbf{x}_1, \mathbf{b}_1$ and $\mathbf{x}_2, \mathbf{b}_2$ the connected part of the double-trace operator is a slowly-varying function of energy, proportional to powers of the logarithm of energy. As we will see shortly, the contribution where $\mathbf{x}_1, \mathbf{b}_1$ and $\mathbf{x}_2, \mathbf{b}_2$ are close to each other grows as a power of energy, and is thus dominant at high energies. Therefore, we can neglect the region where $\mathbf{x}_1, \mathbf{b}_1$ and $\mathbf{x}_2, \mathbf{b}_2$ are far apart, and concentrate on the region where all four transverse vectors in the double-trace operator are within $1/Q_{s2}(Y)$ from each other.

Applying the Gaussian truncation, we see that to assess the energy dependence of the cross section in Eq. (2) we have to expand the double-trace operators in it to the lowest non-trivial order in Γ_G (or, equivalently, in D_1, D_2 , and D_3 defined in Eq. (9), but now for any rapidity Y), and then use Eq. (81) to obtain the explicit dependence of the cross sections on $Q_{s2}(Y)$. Namely we need to take Eqs. (8) and (9) and expand Δ to the lowest non-trivial order in Γ_G , and then substitute Γ_G from Eq. (81) to obtain the energy dependence of the double-trace correlator. Using the result in Eq. (2) would then give the energy dependence of the two-gluon production cross section. However, the expansion of Eq. (2) to the lowest order in D_i 's was already constructed in [1] in order to reproduce the lowest-order correlation function (16) from [8, 11, 12]. We can, therefore, use the results of the expansion from [1] simply replacing

$$\Gamma_G(\mathbf{x}_1, \mathbf{x}_2, Y=0) = \frac{(\mathbf{x}_1 - \mathbf{x}_2)^2 Q_{s2}^2}{4} \ln \frac{1}{|\mathbf{x}_1 - \mathbf{x}_2| \Lambda} = Q_{s2}^2 \int \frac{d^2 l}{2\pi} \frac{1}{|l|^4} \left(1 - e^{i l \cdot (\mathbf{x}_1 - \mathbf{x}_2)} \right) \quad (86)$$

by

$$\Gamma_G(\mathbf{x}_1, \mathbf{x}_2, Y) \propto (|\mathbf{x}_1 - \mathbf{x}_2| Q_{s2}(Y))^{1+2i\nu_0} = c_0 Q_s^{1+2i\nu_0}(Y) \int \frac{d^2 l}{2\pi} \frac{1}{|l|^{3+2i\nu_0}} \left(1 - e^{i l \cdot (\mathbf{x}_1 - \mathbf{x}_2)} \right) \quad (87)$$

where

$$c_0 = -2^{2+2i\nu_0} \frac{\Gamma\left(\frac{3}{2} + i\nu_0\right)}{\Gamma\left(-\frac{1}{2} - i\nu_0\right)} \approx 1.1255. \quad (88)$$

We see that the primary differences between the two functions in Eqs. (86) and (87) is that the momentum in the denominator along with the saturation scale are now taken to a different power while the saturation scale is also rapidity-dependent.

With a good accuracy the rapidity dependence of the saturation scale can be factored from the impact parameter dependence. Concentrating on the powers of energy only, we write [22, 98]

$$Q_{s2}^2(Y) = e^{\lambda Y} Q_{s2}^2(\mathbf{b}) \quad (89)$$

with $\lambda > 0$ a known quantity, the exact value of which is not important to us here.

Proceeding to evaluate the energy-dependence of the correlated part of Eq. (2) we now employ the fact that at the lowest quasi-classical order the interaction term in it (the sum of all the Δ 's in the square brackets of Eq. (22)) can be written as

$$\begin{aligned} Int_{square}(\mathbf{x}_1, \mathbf{y}_1, \mathbf{b}_1, \mathbf{x}_2, \mathbf{y}_2, \mathbf{b}_2) &= \frac{Q_{s2}^4(\mathbf{b})}{2N_c^2(2\pi)^2} \int \frac{d^2l}{l^4} \frac{d^2l'}{l'^4} e^{i\Delta_{\mathbf{b}} \cdot (\mathbf{l} - \mathbf{l}')} \\ &\times \left[(1 - e^{i\mathbf{l} \cdot \mathbf{x}_1}) (1 - e^{-i\mathbf{l}' \cdot \mathbf{y}_1}) + (1 - e^{-i\mathbf{l}' \cdot \mathbf{x}_1}) (1 - e^{i\mathbf{l} \cdot \mathbf{y}_1}) \right] \\ &\times \left[(1 - e^{-i\mathbf{l} \cdot \mathbf{x}_2}) (1 - e^{i\mathbf{l}' \cdot \mathbf{y}_2}) + (1 - e^{i\mathbf{l}' \cdot \mathbf{x}_2}) (1 - e^{-i\mathbf{l} \cdot \mathbf{y}_2}) \right] \end{aligned} \quad (90)$$

with $l = |\mathbf{l}|$, $l' = |\mathbf{l}'|$. (This expression follows from Eq. (47) in [1].) Generalizing this along the steps justifying the transition from (86) to (87) yields

$$\begin{aligned} Int_{square}(\mathbf{x}_1, \mathbf{y}_1, \mathbf{b}_1, \mathbf{x}_2, \mathbf{y}_2, \mathbf{b}_2) &\propto \frac{e^{\lambda(1+2i\nu_0)Y} Q_{s2}^{2(1+2i\nu_0)}(\mathbf{b})}{2N_c^2(2\pi)^2} \int \frac{d^2l}{l^{3+2i\nu_0}} \frac{d^2l'}{l'^{3+2i\nu_0}} e^{i\Delta_{\mathbf{b}} \cdot (\mathbf{l} - \mathbf{l}')} \\ &\times \left[(1 - e^{i\mathbf{l} \cdot \mathbf{x}_1}) (1 - e^{-i\mathbf{l}' \cdot \mathbf{y}_1}) + (1 - e^{-i\mathbf{l}' \cdot \mathbf{x}_1}) (1 - e^{i\mathbf{l} \cdot \mathbf{y}_1}) \right] \\ &\times \left[(1 - e^{-i\mathbf{l} \cdot \mathbf{x}_2}) (1 - e^{i\mathbf{l}' \cdot \mathbf{y}_2}) + (1 - e^{i\mathbf{l}' \cdot \mathbf{x}_2}) (1 - e^{-i\mathbf{l} \cdot \mathbf{y}_2}) \right]. \end{aligned} \quad (91)$$

Employing Eq. (89) we conclude that the leading energy-dependence of the connected part of the 'square' diagrams contribution to the two-gluon production cross section is

$$\left. \frac{d\sigma_{square}}{d^2k_1 dy_1 d^2k_2 dy_2} \right|_{connected} \propto e^{\lambda(1+2i\nu_0)Y}. \quad (92)$$

This power-of-energy growth also justifies the approximation made above in which we neglected large ($> 1/Q_{s2}(Y)$) transverse separations.

We now study the 'crossed' diagrams contribution in Eq. (3). Again the strategy is the same: use Gaussian truncation to relate S_G and Q in Eq. (3) to Γ_G using Eqs. (11), (12) and (9). Then use Γ_G from Eq. (81) to determine energy dependence of S_G and Q . In the end, substituting this in Eq. (3), we would obtain the energy dependence of this part of the two-gluon production cross section.

From Eq. (67) it follows that in the $k_1, k_2 \gg Q_{s2}(Y)$ region the points $\mathbf{x}_1, \mathbf{b}_2$ are close to each other and so are $\mathbf{x}_2, \mathbf{b}_1$. First assume that $\mathbf{x}_1, \mathbf{b}_2$ are also close to $\mathbf{x}_2, \mathbf{b}_1$. In such a case we can write the interaction term (the term in the second square brackets of Eq. (3)) as

$$\begin{aligned} Int_{crossed}(\mathbf{x}_1, \mathbf{y}_1, \mathbf{b}_1, \mathbf{x}_2, \mathbf{y}_2, \mathbf{b}_2) &= Q_{s2}^4 \int \frac{d^2l d^2l'}{(2\pi)^2} \frac{1}{l^4} \frac{1}{l'^4} \left\{ e^{i(\mathbf{l} - \mathbf{l}') \cdot \Delta_{\mathbf{b}}} (1 - e^{i\mathbf{l}' \cdot \tilde{\mathbf{x}}_2}) (1 - e^{-i\mathbf{l} \cdot \tilde{\mathbf{y}}_2}) \right. \\ &\times \left[\frac{1}{2} (1 - e^{-i\mathbf{l}' \cdot \tilde{\mathbf{x}}_1}) (1 - e^{i\mathbf{l} \cdot \tilde{\mathbf{y}}_1}) + (1 - e^{i\mathbf{l} \cdot \tilde{\mathbf{x}}_1}) (1 - e^{-i\mathbf{l}' \cdot \tilde{\mathbf{y}}_1}) \right] \\ &\left. + (1 - e^{i\mathbf{l} \cdot \tilde{\mathbf{x}}_1}) (1 - e^{-i\mathbf{l}' \cdot \tilde{\mathbf{x}}_2}) (1 - e^{-i\mathbf{l} \cdot \tilde{\mathbf{y}}_1}) (1 - e^{i\mathbf{l}' \cdot \tilde{\mathbf{y}}_2}) \right\} \end{aligned} \quad (93)$$

at the lowest non-trivial order in the quasi-classical approximation (cf. Eq. (56) in [1]). Using the same substitution as what led to (87) from (86) we obtain

$$\begin{aligned} Int_{crossed}(\mathbf{x}_1, \mathbf{y}_1, \mathbf{b}_1, \mathbf{x}_2, \mathbf{y}_2, \mathbf{b}_2) &\propto \frac{e^{\lambda(1+2i\nu_0)Y} Q_{s2}^{2(1+2i\nu_0)}(\mathbf{b})}{(2\pi)^2} \int \frac{d^2l}{l^{3+2i\nu_0}} \frac{d^2l'}{l'^{3+2i\nu_0}} \\ &\times \left\{ e^{i(\mathbf{l} - \mathbf{l}') \cdot \Delta_{\mathbf{b}}} (1 - e^{i\mathbf{l}' \cdot \tilde{\mathbf{x}}_2}) (1 - e^{-i\mathbf{l} \cdot \tilde{\mathbf{y}}_2}) \right. \\ &\times \left[\frac{1}{2} (1 - e^{-i\mathbf{l}' \cdot \tilde{\mathbf{x}}_1}) (1 - e^{i\mathbf{l} \cdot \tilde{\mathbf{y}}_1}) + (1 - e^{i\mathbf{l} \cdot \tilde{\mathbf{x}}_1}) (1 - e^{-i\mathbf{l}' \cdot \tilde{\mathbf{y}}_1}) \right] \\ &\left. + (1 - e^{i\mathbf{l} \cdot \tilde{\mathbf{x}}_1}) (1 - e^{-i\mathbf{l}' \cdot \tilde{\mathbf{x}}_2}) (1 - e^{-i\mathbf{l} \cdot \tilde{\mathbf{y}}_1}) (1 - e^{i\mathbf{l}' \cdot \tilde{\mathbf{y}}_2}) \right\}, \end{aligned} \quad (94)$$

such that

$$\frac{d\sigma_{crossed}}{d^2k_1 dy_1 d^2k_2 dy_2} \propto e^{\lambda(1+2i\nu_0)Y}. \quad (95)$$

To properly justify Eq. (95) we also need to consider the case when $\mathbf{x}_1, \mathbf{b}_2$ and $\mathbf{x}_2, \mathbf{b}_1$ from Eq. (67) are far apart. This is the same $D_1, D_2 \gg 1, D_3 = \text{fixed}$ regime considered earlier in the second half of Sec. IV. Using Eq. (36) we see that the Wilson-line correlator in Eq. (67) becomes

$$\begin{aligned} \left\langle \text{Tr} \left[\left(\mathbb{1} - U_{\mathbf{x}_1} U_{\mathbf{b}_1}^\dagger \right) \left(\mathbb{1} - U_{\mathbf{x}_2} U_{\mathbf{b}_2}^\dagger \right) \right] \right\rangle_{A_2}(Y) &\approx (N_c^2 - 1) [1 + S_G(\mathbf{x}_1, \mathbf{b}_2, Y) S_G(\mathbf{x}_2, \mathbf{b}_1, Y)] \\ &= (N_c^2 - 1) \left[2 + \mathcal{O} \left(e^{\lambda(1+2i\nu_0)Y} \right) \right], \end{aligned} \quad (96)$$

where we have also utilized Eq. (80). We see that the large-distance behavior in the 'crossed' diagrams case may not be negligible, but grows with energy at most just as fast as the short-distance contribution (95). (Note also that the term in Eq. (96), when used in Eq. (67), also leads to $\sim 1/\Lambda_{\text{IR}}^2$ divergence after $\Delta\mathbf{b}$ -integration, just like Eq. (39). If the saturation effects in the projectile regulate this divergence, this would generate a factor of $1/Q_{s1}^2$, which may also affect the energy-dependence of such terms.)

Combining Eqs. (92) and (95) we conclude that the net two-gluon production cross section in heavy-light ion collisions scales with the center-of-mass energy as

$$\frac{d\sigma}{d^2k_1 dy_1 d^2k_2 dy_2} \propto e^{\lambda(1+2i\nu_0)Y}. \quad (97)$$

To construct the correlator (14) we also need to calculate the energy-dependence of the cross-sections for single-gluon production. This cross-section can be written in terms of the gluon dipole forward scattering amplitude as [60]

$$\begin{aligned} \frac{d\sigma^{pA_2}}{d^2k dy d^2b} &= \frac{\alpha_s C_F}{4\pi^4} \int d^2B T_1(\mathbf{B} - \mathbf{b}) d^2x d^2y e^{-i\mathbf{k}\cdot(\mathbf{x}-\mathbf{y})} \frac{\mathbf{x} - \mathbf{b}}{|\mathbf{x} - \mathbf{b}|^2} \cdot \frac{\mathbf{y} - \mathbf{b}}{|\mathbf{y} - \mathbf{b}|^2} \\ &\times [N_G(\mathbf{x}, \mathbf{b}, y) + N_G(\mathbf{b}, \mathbf{y}, y) - N_G(\mathbf{x}, \mathbf{y}, y)]. \end{aligned} \quad (98)$$

In the $k_T \gg Q_{s2}(Y)$ approximation we use Eqs. (81) and (89) to write (see e.g. [24, 27] for details of similar integrations)

$$\frac{d\sigma^{pA_2}}{d^2k dy d^2b} \propto c_0 e^{\lambda(1+2i\nu_0)Y/2} \frac{\alpha_s C_F}{\pi^2} \frac{Q_{s2}^{1+2i\nu_0}(\mathbf{b})}{2k_T^{3+2i\nu_0}} \ln \left(\frac{k_T^2}{\Lambda^2} \right), \quad (99)$$

where we assume that $y \approx Y$, that is, the gluon is produced near the projectile in rapidity, similar to our two-gluon production case (1). We see that the denominator of the first term of the correlator (14) contains

$$\frac{d\sigma}{d^2k_1 dy_1} \frac{d\sigma}{d^2k_2 dy_2} \propto e^{\lambda(1+2i\nu_0)Y}. \quad (100)$$

Substituting Eqs. (97) and (100) into Eq. (14) we conclude that, in the leading-power approximation employed, the correlator is energy-independent,

$$C(\mathbf{k}_1, y_1, \mathbf{k}_2, y_2) = \text{const}(Y). \quad (101)$$

Therefore, our two-gluon correlations are (almost) energy-independent.

VII. SUMMARY AND OUTLOOK

In this paper we studied several properties of the two-gluon production cross section in heavy-light ion collisions in the saturation/CGC framework. We have constructed some qualitative experimental predictions. The correlations were found to be almost energy-independent. The CGC two-gluon long-range rapidity correlations are stronger in tip-on-tip $U + U$ collisions, than in the side-on-side ones. Detailed numerical predictions for the di-hadron correlation function can be constricted by using the expressions (2) and (3) further improved by including running coupling corrections, but would require a dedicated phenomenological effort.

On a more theoretical side we have constructed a new k_T -factorized form of the expression given in Eq. (72), involving two new objects: the double-trace and quadrupole two-gluon Wigner distributions (48) and (50). This is by no means a proof of factorization for two-gluon production: rather this simply is an observation that two-gluon production cross section, calculated in the approximation used above, can be written in this factorized form. It would be interesting to see whether this (or any other) factorized form would survive the inclusion of small- x evolution correction in the interval between the semi-dilute projectile and the produced gluons. This is left for the future work.

We have also shown that the part of the two-gluon production cross section given by Eq. (3) contains a power-law IR divergence, as shown in Eq. (40), despite all the target wave function saturation effects included in the expression. Luckily the azimuthal-angle dependence of the corresponding correlator is not affected by this divergence. One could hope that saturation effects in the projectile wave function would remove this divergence making the final result for the two-gluon production IR-finite.

ACKNOWLEDGMENTS

The authors are grateful to Miklos Gyulassy, Ulrich Heinz and Alfred Mueller for discussions. This research is sponsored in part by the U.S. Department of Energy under Grant No. DE-SC0004286.

APPENDIX

Perhaps the most straightforward algebraic way to obtain evolution equations for the correlators considered here is by applying JIMWLK equation [40–43] to the correlation functions. The application often involves tedious algebra, but is conceptually straightforward. Below we list the resulting leading- $\ln 1/x$ evolution equations for the expectation values of the adjoint dipole, quadrupole, and the double-trace operators (see e.g. [27] for a pedagogical presentation of the technique we used to derive the evolution equations).

The evolution equations below employ the following kernel,

$$\mathcal{K}_{\mathbf{x}\mathbf{z}\mathbf{y}} \equiv \frac{\alpha_s N_c}{\pi^2} \frac{(\mathbf{z} - \mathbf{x}) \cdot (\mathbf{z} - \mathbf{y})}{|\mathbf{z} - \mathbf{x}|^2 |\mathbf{z} - \mathbf{y}|^2}. \quad (\text{A1})$$

Defining the following expectation values of the Wilson line correlators (normalized to one for the case of no interaction, $U = 1 = U^\dagger$)

$$S_{\mathbf{x}_1\mathbf{x}_2}^G \equiv \frac{1}{N_c^2 - 1} \langle \text{Tr}[U_{\mathbf{x}_1} U_{\mathbf{x}_2}^\dagger] \rangle \quad (\text{A2a})$$

$$S_{\mathbf{x}_1\mathbf{x}_2\mathbf{x}_3\mathbf{x}_4}^{(4,dip)} \equiv \frac{1}{N_c(N_c^2 - 1)} \langle \text{Tr}[T^a U_{\mathbf{x}_1} U_{\mathbf{x}_2}^\dagger T^a U_{\mathbf{x}_3} U_{\mathbf{x}_4}^\dagger] \rangle \quad (\text{A2b})$$

with T^a the $SU(N_c)$ generators in the adjoint representation, we write the evolution equation for the adjoint dipole correlator,

$$\begin{aligned} \partial_Y S_{\mathbf{x}_1\mathbf{x}_2}^G = & \int d^2z \left[(\mathcal{K}_{\mathbf{x}_1\mathbf{z}\mathbf{x}_2} - \mathcal{K}_{\mathbf{x}_1\mathbf{z}\mathbf{x}_1} - \mathcal{K}_{\mathbf{x}_2\mathbf{z}\mathbf{x}_2}) S_{\mathbf{x}_1\mathbf{x}_2}^G - (\mathcal{K}_{\mathbf{x}_1\mathbf{z}\mathbf{x}_2} - \mathcal{K}_{\mathbf{x}_1\mathbf{z}\mathbf{x}_1}) S_{\mathbf{z}\mathbf{x}_1\mathbf{x}_1\mathbf{x}_2}^{(4,dip)} \right. \\ & \left. - (\mathcal{K}_{\mathbf{x}_1\mathbf{z}\mathbf{x}_2} - \mathcal{K}_{\mathbf{x}_2\mathbf{z}\mathbf{x}_2}) S_{\mathbf{x}_2\mathbf{z}\mathbf{x}_1\mathbf{x}_2}^{(4,dip)} + \mathcal{K}_{\mathbf{x}_1\mathbf{z}\mathbf{x}_2} S_{\mathbf{x}_2\mathbf{x}_1\mathbf{x}_1\mathbf{x}_2}^{(4,dip)} \right]. \quad (\text{A3}) \end{aligned}$$

To write down the evolution equation for the quadrupole correlator we will need the following definitions (also normalized to one for the no-interaction case):

$$Q_{\mathbf{x}_1\mathbf{x}_2\mathbf{x}_3\mathbf{x}_4} \equiv \frac{1}{N_c^2 - 1} \langle \text{Tr}[U_{\mathbf{x}_1} U_{\mathbf{x}_2}^\dagger U_{\mathbf{x}_3} U_{\mathbf{x}_4}^\dagger] \rangle \quad (\text{A4a})$$

$$S_{\mathbf{x}_1\mathbf{x}_2\mathbf{x}_3\mathbf{x}_4\mathbf{x}_5\mathbf{x}_6}^{(6,quad-1)} \equiv \frac{1}{N_c(N_c^2 - 1)} \langle [U_{\mathbf{x}_1} U_{\mathbf{x}_2}^\dagger]^{ab} \text{Tr}[T^a U_{\mathbf{x}_3} U_{\mathbf{x}_4}^\dagger T^b U_{\mathbf{x}_5} U_{\mathbf{x}_6}^\dagger] \rangle \quad (\text{A4b})$$

$$S_{\mathbf{x}_1\mathbf{x}_2\mathbf{x}_3\mathbf{x}_4\mathbf{x}_5\mathbf{x}_6}^{(6,quad-2)} \equiv \frac{1}{N_c(N_c^2 - 1)} \langle \text{Tr}[T^a U_{\mathbf{x}_1} U_{\mathbf{x}_2}^\dagger T^a U_{\mathbf{x}_3} U_{\mathbf{x}_4}^\dagger U_{\mathbf{x}_5} U_{\mathbf{x}_6}^\dagger] \rangle. \quad (\text{A4c})$$

The adjoint quadrupole evolution equation reads

$$\begin{aligned}
\partial_Y Q_{\mathbf{x}_1 \mathbf{x}_2 \mathbf{x}_3 \mathbf{x}_4} = & \int d^2 z \left[(\mathcal{K}_{\mathbf{x}_1 \mathbf{z} \mathbf{x}_4} + \mathcal{K}_{\mathbf{x}_2 \mathbf{z} \mathbf{x}_3} - \mathcal{K}_{\mathbf{x}_1 \mathbf{z} \mathbf{x}_1} - \mathcal{K}_{\mathbf{x}_2 \mathbf{z} \mathbf{x}_2} - \mathcal{K}_{\mathbf{x}_3 \mathbf{z} \mathbf{x}_3} - \mathcal{K}_{\mathbf{x}_4 \mathbf{z} \mathbf{x}_4}) Q_{\mathbf{x}_1 \mathbf{x}_2 \mathbf{x}_3 \mathbf{x}_4} \right. \\
& + (\mathcal{K}_{\mathbf{x}_1 \mathbf{z} \mathbf{x}_2} + \mathcal{K}_{\mathbf{x}_3 \mathbf{z} \mathbf{x}_4} - \mathcal{K}_{\mathbf{x}_1 \mathbf{z} \mathbf{x}_3} - \mathcal{K}_{\mathbf{x}_2 \mathbf{z} \mathbf{x}_4}) S_{\mathbf{x}_1 \mathbf{x}_2 \mathbf{x}_3 \mathbf{x}_4}^{(4,dip)} \\
& + (\mathcal{K}_{\mathbf{x}_1 \mathbf{z} \mathbf{x}_3} - \mathcal{K}_{\mathbf{x}_1 \mathbf{z} \mathbf{x}_2}) S_{\mathbf{x}_1 \mathbf{z} \mathbf{x}_1 \mathbf{x}_2 \mathbf{x}_3 \mathbf{x}_4}^{(6,quad-1)} + \mathcal{K}_{\mathbf{x}_1 \mathbf{z} \mathbf{x}_2} S_{\mathbf{x}_1 \mathbf{x}_2 \mathbf{x}_1 \mathbf{x}_2 \mathbf{x}_3 \mathbf{x}_4}^{(6,quad-1)} \\
& + (\mathcal{K}_{\mathbf{x}_1 \mathbf{z} \mathbf{x}_3} - \mathcal{K}_{\mathbf{x}_3 \mathbf{z} \mathbf{x}_4}) S_{\mathbf{z} \mathbf{x}_3 \mathbf{x}_1 \mathbf{x}_2 \mathbf{x}_3 \mathbf{x}_4}^{(6,quad-1)} - \mathcal{K}_{\mathbf{x}_1 \mathbf{z} \mathbf{x}_3} S_{\mathbf{x}_1 \mathbf{x}_3 \mathbf{x}_1 \mathbf{x}_2 \mathbf{x}_3 \mathbf{x}_4}^{(6,quad-1)} \\
& + (\mathcal{K}_{\mathbf{x}_2 \mathbf{z} \mathbf{x}_4} - \mathcal{K}_{\mathbf{x}_1 \mathbf{z} \mathbf{x}_2}) S_{\mathbf{z} \mathbf{x}_2 \mathbf{x}_1 \mathbf{x}_2 \mathbf{x}_3 \mathbf{x}_4}^{(6,quad-1)} + \mathcal{K}_{\mathbf{x}_3 \mathbf{z} \mathbf{x}_4} S_{\mathbf{x}_4 \mathbf{x}_3 \mathbf{x}_1 \mathbf{x}_2 \mathbf{x}_3 \mathbf{x}_4}^{(6,quad-1)} \\
& + (\mathcal{K}_{\mathbf{x}_2 \mathbf{z} \mathbf{x}_4} - \mathcal{K}_{\mathbf{x}_3 \mathbf{z} \mathbf{x}_4}) S_{\mathbf{x}_4 \mathbf{z} \mathbf{x}_1 \mathbf{x}_2 \mathbf{x}_3 \mathbf{x}_4}^{(6,quad-1)} - \mathcal{K}_{\mathbf{x}_2 \mathbf{z} \mathbf{x}_4} S_{\mathbf{x}_4 \mathbf{x}_2 \mathbf{x}_1 \mathbf{x}_2 \mathbf{x}_3 \mathbf{x}_4}^{(6,quad-1)} \\
& + (\mathcal{K}_{\mathbf{x}_1 \mathbf{z} \mathbf{x}_1} - \mathcal{K}_{\mathbf{x}_1 \mathbf{z} \mathbf{x}_4}) S_{\mathbf{z} \mathbf{x}_1 \mathbf{x}_1 \mathbf{x}_2 \mathbf{x}_3 \mathbf{x}_4}^{(6,quad-2)} + (\mathcal{K}_{\mathbf{x}_4 \mathbf{z} \mathbf{x}_4} - \mathcal{K}_{\mathbf{x}_1 \mathbf{z} \mathbf{x}_4}) S_{\mathbf{x}_4 \mathbf{z} \mathbf{x}_1 \mathbf{x}_2 \mathbf{x}_3 \mathbf{x}_4}^{(6,quad-2)} \\
& + \mathcal{K}_{\mathbf{x}_1 \mathbf{z} \mathbf{x}_4} S_{\mathbf{x}_4 \mathbf{x}_1 \mathbf{x}_1 \mathbf{x}_2 \mathbf{x}_3 \mathbf{x}_4}^{(6,quad-2)} \\
& + (\mathcal{K}_{\mathbf{x}_2 \mathbf{z} \mathbf{x}_2} - \mathcal{K}_{\mathbf{x}_2 \mathbf{z} \mathbf{x}_3}) S_{\mathbf{x}_2 \mathbf{z} \mathbf{x}_3 \mathbf{x}_4 \mathbf{x}_1 \mathbf{x}_2}^{(6,quad-2)} + (\mathcal{K}_{\mathbf{x}_3 \mathbf{z} \mathbf{x}_3} - \mathcal{K}_{\mathbf{x}_2 \mathbf{z} \mathbf{x}_3}) S_{\mathbf{z} \mathbf{x}_3 \mathbf{x}_3 \mathbf{x}_4 \mathbf{x}_1 \mathbf{x}_2}^{(6,quad-2)} \\
& \left. + \mathcal{K}_{\mathbf{x}_2 \mathbf{z} \mathbf{x}_3} S_{\mathbf{x}_2 \mathbf{x}_3 \mathbf{x}_3 \mathbf{x}_4 \mathbf{x}_1 \mathbf{x}_2}^{(6,quad-2)} \right]. \tag{A5}
\end{aligned}$$

Finally, for the evolution of the double-trace operator we need the following definitions:

$$D_{\mathbf{x}_1 \mathbf{x}_2 \mathbf{x}_3 \mathbf{x}_4} \equiv \frac{1}{(N_c^2 - 1)^2} \langle \text{Tr}[U_{\mathbf{x}_1} U_{\mathbf{x}_2}^\dagger] \text{Tr}[U_{\mathbf{x}_3} U_{\mathbf{x}_4}^\dagger] \rangle \tag{A6a}$$

$$S_{\mathbf{x}_1 \mathbf{x}_2 \mathbf{x}_3 \mathbf{x}_4}^{(4,double)} \equiv \frac{1}{N_c (N_c^2 - 1)^2} \langle \text{Tr}[T^a U_{\mathbf{x}_1} U_{\mathbf{x}_2}^\dagger] \text{Tr}[T^a U_{\mathbf{x}_3} U_{\mathbf{x}_4}^\dagger] \rangle \tag{A6b}$$

$$S_{\mathbf{x}_1 \mathbf{x}_2 \mathbf{x}_3 \mathbf{x}_4 \mathbf{x}_5 \mathbf{x}_6}^{(6,double-1)} \equiv \frac{1}{N_c (N_c^2 - 1)^2} \langle [U_{\mathbf{x}_1} U_{\mathbf{x}_2}^\dagger]^{ab} \text{Tr}[T^a U_{\mathbf{x}_3} U_{\mathbf{x}_4}^\dagger] \text{Tr}[T^b U_{\mathbf{x}_5} U_{\mathbf{x}_6}^\dagger] \rangle \tag{A6c}$$

$$S_{\mathbf{x}_1 \mathbf{x}_2 \mathbf{x}_3 \mathbf{x}_4 \mathbf{x}_5 \mathbf{x}_6}^{(6,double-2)} \equiv \frac{1}{N_c (N_c^2 - 1)^2} \langle \text{Tr}[T^a U_{\mathbf{x}_1} U_{\mathbf{x}_2}^\dagger T^a U_{\mathbf{x}_3} U_{\mathbf{x}_4}^\dagger] \text{Tr}[U_{\mathbf{x}_5} U_{\mathbf{x}_6}^\dagger] \rangle. \tag{A6d}$$

(Note that while $D_{\mathbf{x}_1 \mathbf{x}_2 \mathbf{x}_3 \mathbf{x}_4}$ and $S_{\mathbf{x}_1 \mathbf{x}_2 \mathbf{x}_3 \mathbf{x}_4 \mathbf{x}_5 \mathbf{x}_6}^{(6,double-2)}$ are normalized to one in the no-interactions case, $S_{\mathbf{x}_1 \mathbf{x}_2 \mathbf{x}_3 \mathbf{x}_4}^{(4,double)}$ and $S_{\mathbf{x}_1 \mathbf{x}_2 \mathbf{x}_3 \mathbf{x}_4 \mathbf{x}_5 \mathbf{x}_6}^{(6,double-1)}$ actually vanish for $U = U^\dagger = 1$, such that their normalization is arbitrary, fixed here to match the normalization of the other correlators.) Using the correlators in (A6) we obtain the evolution equation for the adjoint double-trace operator

$$\begin{aligned}
\partial_Y D_{\mathbf{x}_1 \mathbf{x}_2 \mathbf{x}_3 \mathbf{x}_4} = & \int d^2 z \left[(\mathcal{K}_{\mathbf{x}_1 \mathbf{z} \mathbf{x}_2} + \mathcal{K}_{\mathbf{x}_3 \mathbf{z} \mathbf{x}_4} - \mathcal{K}_{\mathbf{x}_1 \mathbf{z} \mathbf{x}_1} - \mathcal{K}_{\mathbf{x}_2 \mathbf{z} \mathbf{x}_2} - \mathcal{K}_{\mathbf{x}_3 \mathbf{z} \mathbf{x}_3} - \mathcal{K}_{\mathbf{x}_4 \mathbf{z} \mathbf{x}_4}) D_{\mathbf{x}_1 \mathbf{x}_2 \mathbf{x}_3 \mathbf{x}_4} \right. \\
& + (\mathcal{K}_{\mathbf{x}_1 \mathbf{z} \mathbf{x}_4} + \mathcal{K}_{\mathbf{x}_2 \mathbf{z} \mathbf{x}_3} - \mathcal{K}_{\mathbf{x}_1 \mathbf{z} \mathbf{x}_3} - \mathcal{K}_{\mathbf{x}_2 \mathbf{z} \mathbf{x}_4}) S_{\mathbf{x}_1 \mathbf{x}_2 \mathbf{x}_3 \mathbf{x}_4}^{(4,double)} \\
& + (\mathcal{K}_{\mathbf{x}_1 \mathbf{z} \mathbf{x}_3} - \mathcal{K}_{\mathbf{x}_1 \mathbf{z} \mathbf{x}_4}) S_{\mathbf{x}_1 \mathbf{z} \mathbf{x}_1 \mathbf{x}_2 \mathbf{x}_3 \mathbf{x}_4}^{(6,double-1)} + \mathcal{K}_{\mathbf{x}_1 \mathbf{z} \mathbf{x}_4} S_{\mathbf{x}_1 \mathbf{x}_4 \mathbf{x}_1 \mathbf{x}_2 \mathbf{x}_3 \mathbf{x}_4}^{(6,double-1)} \\
& + (\mathcal{K}_{\mathbf{x}_1 \mathbf{z} \mathbf{x}_3} - \mathcal{K}_{\mathbf{x}_2 \mathbf{z} \mathbf{x}_3}) S_{\mathbf{z} \mathbf{x}_3 \mathbf{x}_1 \mathbf{x}_2 \mathbf{x}_3 \mathbf{x}_4}^{(6,double-1)} - \mathcal{K}_{\mathbf{x}_1 \mathbf{z} \mathbf{x}_3} S_{\mathbf{x}_1 \mathbf{x}_3 \mathbf{x}_1 \mathbf{x}_2 \mathbf{x}_3 \mathbf{x}_4}^{(6,double-1)} \\
& + (\mathcal{K}_{\mathbf{x}_2 \mathbf{z} \mathbf{x}_4} - \mathcal{K}_{\mathbf{x}_2 \mathbf{z} \mathbf{x}_3}) S_{\mathbf{x}_2 \mathbf{z} \mathbf{x}_1 \mathbf{x}_2 \mathbf{x}_3 \mathbf{x}_4}^{(6,double-1)} + \mathcal{K}_{\mathbf{x}_2 \mathbf{z} \mathbf{x}_3} S_{\mathbf{x}_2 \mathbf{x}_3 \mathbf{x}_1 \mathbf{x}_2 \mathbf{x}_3 \mathbf{x}_4}^{(6,double-1)} \\
& + (\mathcal{K}_{\mathbf{x}_2 \mathbf{z} \mathbf{x}_4} - \mathcal{K}_{\mathbf{x}_1 \mathbf{z} \mathbf{x}_4}) S_{\mathbf{z} \mathbf{x}_4 \mathbf{x}_1 \mathbf{x}_2 \mathbf{x}_3 \mathbf{x}_4}^{(6,double-1)} - \mathcal{K}_{\mathbf{x}_2 \mathbf{z} \mathbf{x}_4} S_{\mathbf{x}_2 \mathbf{x}_4 \mathbf{x}_1 \mathbf{x}_2 \mathbf{x}_3 \mathbf{x}_4}^{(6,double-1)} \\
& + (\mathcal{K}_{\mathbf{x}_1 \mathbf{z} \mathbf{x}_1} - \mathcal{K}_{\mathbf{x}_1 \mathbf{z} \mathbf{x}_2}) S_{\mathbf{z} \mathbf{x}_1 \mathbf{x}_1 \mathbf{x}_2 \mathbf{x}_3 \mathbf{x}_4}^{(6,double-2)} + (\mathcal{K}_{\mathbf{x}_2 \mathbf{z} \mathbf{x}_2} - \mathcal{K}_{\mathbf{x}_1 \mathbf{z} \mathbf{x}_2}) S_{\mathbf{x}_2 \mathbf{z} \mathbf{x}_1 \mathbf{x}_2 \mathbf{x}_3 \mathbf{x}_4}^{(6,double-2)} \\
& + \mathcal{K}_{\mathbf{x}_1 \mathbf{z} \mathbf{x}_2} S_{\mathbf{x}_2 \mathbf{x}_1 \mathbf{x}_1 \mathbf{x}_2 \mathbf{x}_3 \mathbf{x}_4}^{(6,double-2)} \\
& + (\mathcal{K}_{\mathbf{x}_3 \mathbf{z} \mathbf{x}_3} - \mathcal{K}_{\mathbf{x}_3 \mathbf{z} \mathbf{x}_4}) S_{\mathbf{z} \mathbf{x}_3 \mathbf{x}_3 \mathbf{x}_4 \mathbf{x}_1 \mathbf{x}_2}^{(6,double-2)} + (\mathcal{K}_{\mathbf{x}_4 \mathbf{z} \mathbf{x}_4} - \mathcal{K}_{\mathbf{x}_3 \mathbf{z} \mathbf{x}_4}) S_{\mathbf{x}_4 \mathbf{z} \mathbf{x}_3 \mathbf{x}_4 \mathbf{x}_1 \mathbf{x}_2}^{(6,double-2)} \\
& \left. + \mathcal{K}_{\mathbf{x}_3 \mathbf{z} \mathbf{x}_4} S_{\mathbf{x}_4 \mathbf{x}_3 \mathbf{x}_3 \mathbf{x}_4 \mathbf{x}_1 \mathbf{x}_2}^{(6,double-2)} \right]. \tag{A7}
\end{aligned}$$

None of the equations (A3), (A5), and (A7) are closed equations: they include higher-order Wilson line correlators on their right-hand sides, as expected from the equations in Balitsky hierarchy [36, 37].

[1] Y. V. Kovchegov and D. E. Wertepny, *Long-Range Rapidity Correlations in Heavy-Light Ion Collisions*, *Nucl.Phys.* **A906** (2013) 50–83, [arXiv:1212.1195].

- [2] **STAR** Collaboration, J. Adams *et. al.*, *Distributions of charged hadrons associated with high transverse momentum particles in $p + p$ and $Au + Au$ collisions at $s_{NN}^{1/2} = 200$ GeV*, *Phys. Rev. Lett.* **95** (2005) 152301, [[nucl-ex/0501016](#)].
- [3] **PHENIX** Collaboration, A. Adare *et. al.*, *Dihadron azimuthal correlations in $Au+Au$ collisions at $\sqrt{s_{NN}}=200$ GeV*, *Phys. Rev.* **C78** (2008) 014901, [[arXiv:0801.4545](#)].
- [4] **PHOBOS** Collaboration, B. Alver *et. al.*, *High transverse momentum triggered correlations over a large pseudorapidity acceptance in $Au+Au$ collisions at $\sqrt{s_{NN}}=200$ GeV*, *Phys. Rev. Lett.* **104** (2010) 062301, [[arXiv:0903.2811](#)].
- [5] **STAR Collaboration** Collaboration, B. Abelev *et. al.*, *Long range rapidity correlations and jet production in high energy nuclear collisions*, *Phys.Rev.* **C80** (2009) 064912, [[arXiv:0909.0191](#)].
- [6] N. Armesto, L. McLerran, and C. Pajares, *Long Range Forward-Backward Correlations and the Color Glass Condensate*, *Nucl.Phys.* **A781** (2007) 201–208, [[hep-ph/0607345](#)].
- [7] N. Armesto, M. Braun, and C. Pajares, *On the long-range correlations in hadron-nucleus collisions*, *Phys.Rev.* **C75** (2007) 054902, [[hep-ph/0702216](#)].
- [8] A. Dumitru, F. Gelis, L. McLerran, and R. Venugopalan, *Glasma flux tubes and the near side ridge phenomenon at RHIC*, *Nucl. Phys.* **A810** (2008) 91–108, [[arXiv:0804.3858](#)].
- [9] S. Gavin, L. McLerran, and G. Moschelli, *Long Range Correlations and the Soft Ridge in Relativistic Nuclear Collisions*, *Phys. Rev.* **C79** (2009) 051902, [[arXiv:0806.4718](#)].
- [10] F. Gelis, T. Lappi, and R. Venugopalan, *High energy factorization in nucleus-nucleus collisions. 3. Long range rapidity correlations*, *Phys.Rev.* **D79** (2009) 094017, [[arXiv:0810.4829](#)].
- [11] K. Dusling, F. Gelis, T. Lappi, and R. Venugopalan, *Long range two-particle rapidity correlations in $A+A$ collisions from high energy QCD evolution*, *Nucl. Phys.* **A836** (2010) 159–182, [[arXiv:0911.2720](#)].
- [12] A. Dumitru, K. Dusling, F. Gelis, J. Jalilian-Marian, T. Lappi, *et. al.*, *The Ridge in proton-proton collisions at the LHC*, *Phys.Lett.* **B697** (2011) 21–25, [[arXiv:1009.5295](#)].
- [13] A. Dumitru and J. Jalilian-Marian, *Two-particle correlations in high energy collisions and the gluon four-point function*, *Phys. Rev.* **D81** (2010) 094015, [[arXiv:1001.4820](#)].
- [14] A. Kovner and M. Lublinsky, *Angular Correlations in Gluon Production at High Energy*, *Phys.Rev.* **D83** (2011) 034017, [[arXiv:1012.3398](#)].
- [15] A. Kovner and M. Lublinsky, *On Angular Correlations and High Energy Evolution*, *Phys.Rev.* **D84** (2011) 094011, [[arXiv:1109.0347](#)].
- [16] A. Kovner and M. Lublinsky, *Angular and long range rapidity correlations in particle production at high energy*, *Int.J.Mod.Phys.* **E22** (2013) 1330001, [[arXiv:1211.1928](#)].
- [17] K. Dusling and R. Venugopalan, *Evidence for BFKL and saturation dynamics from di-hadron spectra at the LHC*, [arXiv:1210.3890](#).
- [18] K. Dusling and R. Venugopalan, *Explanation of systematics of CMS $p+Pb$ high multiplicity di-hadron data at $\sqrt{s_{NN}} = 5.02$ TeV*, [arXiv:1211.3701](#).
- [19] K. Dusling and R. Venugopalan, *Azimuthal collimation of long range rapidity correlations by strong color fields in high multiplicity hadron-hadron collisions*, *Phys.Rev.Lett.* **108** (2012) 262001, [[arXiv:1201.2658](#)].
- [20] Y. V. Kovchegov, E. Levin, and L. D. McLerran, *Large scale rapidity correlations in heavy ion collisions*, *Phys.Rev.* **C63** (2001) 024903, [[hep-ph/9912367](#)].
- [21] E. Levin and A. H. Rezaeian, *The Ridge from the BFKL evolution and beyond*, *Phys.Rev.* **D84** (2011) 034031, [[arXiv:1105.3275](#)].
- [22] L. V. Gribov, E. M. Levin, and M. G. Ryskin, *Semihard Processes in QCD*, *Phys. Rept.* **100** (1983) 1–150.
- [23] E. Iancu and R. Venugopalan, *The color glass condensate and high energy scattering in QCD*, [hep-ph/0303204](#).
- [24] J. Jalilian-Marian and Y. V. Kovchegov, *Saturation physics and deuteron gold collisions at RHIC*, *Prog. Part. Nucl. Phys.* **56** (2006) 104–231, [[hep-ph/0505052](#)].
- [25] H. Weigert, *Evolution at small x_{bj} : The Color Glass Condensate*, *Prog. Part. Nucl. Phys.* **55** (2005) 461–565, [[hep-ph/0501087](#)].
- [26] F. Gelis, E. Iancu, J. Jalilian-Marian, and R. Venugopalan, *The Color Glass Condensate*, *Ann.Rev.Nucl.Part.Sci.* **60** (2010) 463–489, [[arXiv:1002.0333](#)].
- [27] Y. V. Kovchegov and E. Levin, *Quantum Chromodynamics at High Energy*. Cambridge University Press, 2012.
- [28] **CMS** Collaboration, V. Khachatryan *et. al.*, *Observation of Long-Range Near-Side Angular Correlations in Proton-Proton Collisions at the LHC*, *JHEP* **09** (2010) 091, [[arXiv:1009.4122](#)].
- [29] **CMS Collaboration** Collaboration, S. Chatrchyan *et. al.*, *Observation of long-range near-side angular correlations in proton-lead collisions at the LHC*, [arXiv:1210.5482](#).
- [30] **ALICE Collaboration** Collaboration, B. Abelev *et. al.*, *Long-range angular correlations on the near and away side in $p - Pb$ collisions at $\sqrt{s_{NN}} = 5.02$ TeV*, [arXiv:1212.2001](#).
- [31] **CMS Collaboration** Collaboration, S. Chatrchyan *et. al.*, *Multiplicity and transverse momentum dependence of two- and four-particle correlations in pPb and $PbPb$ collisions*, *Phys.Lett.* **B724** (2013) 213–240, [[arXiv:1305.0609](#)].
- [32] A. H. Mueller, *Small x Behavior and Parton Saturation: A QCD Model*, *Nucl. Phys.* **B335** (1990) 115.
- [33] L. D. McLerran and R. Venugopalan, *Green's functions in the color field of a large nucleus*, *Phys. Rev.* **D50** (1994) 2225–2233, [[hep-ph/9402335](#)].
- [34] L. D. McLerran and R. Venugopalan, *Gluon distribution functions for very large nuclei at small transverse momentum*, *Phys. Rev.* **D49** (1994) 3352–3355, [[hep-ph/9311205](#)].
- [35] L. D. McLerran and R. Venugopalan, *Computing quark and gluon distribution functions for very large nuclei*, *Phys. Rev.*

- D49** (1994) 2233–2241, [[hep-ph/9309289](#)].
- [36] I. Balitsky, *Operator expansion for high-energy scattering*, *Nucl. Phys.* **B463** (1996) 99–160, [[hep-ph/9509348](#)].
- [37] I. Balitsky, *Factorization and high-energy effective action*, *Phys. Rev.* **D60** (1999) 014020, [[hep-ph/9812311](#)].
- [38] Y. V. Kovchegov, *Small- x F_2 structure function of a nucleus including multiple pomeron exchanges*, *Phys. Rev.* **D60** (1999) 034008, [[hep-ph/9901281](#)].
- [39] Y. V. Kovchegov, *Unitarization of the BFKL pomeron on a nucleus*, *Phys. Rev.* **D61** (2000) 074018, [[hep-ph/9905214](#)].
- [40] J. Jalilian-Marian, A. Kovner, and H. Weigert, *The Wilson renormalization group for low x physics: Gluon evolution at finite parton density*, *Phys. Rev.* **D59** (1998) 014015, [[hep-ph/9709432](#)].
- [41] J. Jalilian-Marian, A. Kovner, A. Leonidov, and H. Weigert, *The Wilson renormalization group for low x physics: Towards the high density regime*, *Phys. Rev.* **D59** (1998) 014014, [[hep-ph/9706377](#)].
- [42] E. Iancu, A. Leonidov, and L. D. McLerran, *The renormalization group equation for the color glass condensate*, *Phys. Lett.* **B510** (2001) 133–144.
- [43] E. Iancu, A. Leonidov, and L. D. McLerran, *Nonlinear gluon evolution in the color glass condensate. I*, *Nucl. Phys.* **A692** (2001) 583–645, [[hep-ph/0011241](#)].
- [44] J. L. Albacete, *Particle multiplicities in Lead-Lead collisions at the LHC from non-linear evolution with running coupling*, *Phys. Rev. Lett.* **99** (2007) 262301, [[0707.2545](#)].
- [45] J. L. Albacete and A. Dumitru, *A model for gluon production in heavy-ion collisions at the LHC with rcBK unintegrated gluon densities*, [arXiv:1011.5161](#).
- [46] J. L. Albacete, N. Armesto, J. G. Milhano, P. Quiroga-Arias, and C. A. Salgado, *AAMQS: A non-linear QCD analysis of new HERA data at small- x including heavy quarks*, *Eur. Phys. J.* **C71** (2011) 1705, [[arXiv:1012.4408](#)].
- [47] I. I. Balitsky, *Quark Contribution to the Small- x Evolution of Color Dipole*, *Phys. Rev. D* **75** (2007) 014001, [[hep-ph/0609105](#)].
- [48] E. Gardi, J. Kuokkanen, K. Rummukainen, and H. Weigert, *Running coupling and power corrections in nonlinear evolution at the high-energy limit*, *Nucl. Phys.* **A784** (2007) 282–340, [[hep-ph/0609087](#)].
- [49] Y. Kovchegov and H. Weigert, *Triumvirate of Running Couplings in Small- x Evolution*, *Nucl. Phys. A* **784** (2007) 188–226, [[hep-ph/0609090](#)].
- [50] W. A. Horowitz and Y. V. Kovchegov, *Running Coupling Corrections to High Energy Inclusive Gluon Production*, *Nucl. Phys.* **A849** (2011) 72–97, [[arXiv:1009.0545](#)].
- [51] S. J. Brodsky, G. P. Lepage, and P. B. Mackenzie, *On the elimination of scale ambiguities in perturbative quantum chromodynamics*, *Phys. Rev.* **D28** (1983) 228.
- [52] I. Balitsky and G. A. Chirilli, *Next-to-leading order evolution of color dipoles*, *Phys. Rev.* **D77** (2008) 014019, [[arXiv:0710.4330](#)].
- [53] A. Kovner, L. D. McLerran, and H. Weigert, *Gluon production at high transverse momentum in the mclerran-venugopalan model of nuclear structure functions*, *Phys. Rev.* **D52** (1995) 3809–3814, [[hep-ph/9505320](#)].
- [54] A. Kovner, L. D. McLerran, and H. Weigert, *Gluon production from nonAbelian Weizsacker-Williams fields in nucleus-nucleus collisions*, *Phys. Rev.* **D52** (1995) 6231–6237, [[hep-ph/9502289](#)].
- [55] Y. V. Kovchegov and D. H. Rischke, *Classical gluon radiation in ultrarelativistic nucleus nucleus collisions*, *Phys. Rev.* **C56** (1997) 1084–1094, [[hep-ph/9704201](#)].
- [56] Y. V. Kovchegov and A. H. Mueller, *Gluon production in current nucleus and nucleon nucleus collisions in a quasi-classical approximation*, *Nucl. Phys.* **B529** (1998) 451–479, [[hep-ph/9802440](#)].
- [57] A. Dumitru and L. D. McLerran, *How protons shatter colored glass*, *Nucl. Phys.* **A700** (2002) 492–508, [[hep-ph/0105268](#)].
- [58] A. Krasnitz, Y. Nara, and R. Venugopalan, *Classical gluodynamics of high energy nuclear collisions: An erratum and an update*, *Nucl. Phys.* **A727** (2003) 427–436, [[hep-ph/0305112](#)].
- [59] T. Lappi, *Production of gluons in the classical field model for heavy ion collisions*, *Phys. Rev.* **C67** (2003) 054903, [[hep-ph/0303076](#)].
- [60] Y. V. Kovchegov and K. Tuchin, *Inclusive gluon production in dis at high parton density*, *Phys. Rev.* **D65** (2002) 074026, [[hep-ph/0111362](#)].
- [61] A. Kovner and M. Lublinsky, *One gluon, two gluon: Multigluon production via high energy evolution*, *JHEP* **11** (2006) 083, [[hep-ph/0609227](#)].
- [62] J. Jalilian-Marian and Y. V. Kovchegov, *Inclusive two-gluon and valence quark-gluon production in DIS and pA* , *Phys. Rev.* **D70** (2004) 114017, [[hep-ph/0405266](#)].
- [63] M. A. Braun, *Inclusive jet production on the nucleus in the perturbative QCD with $N_c \rightarrow \infty$* , *Phys. Lett.* **B483** (2000) 105–114, [[hep-ph/0003003](#)].
- [64] R. Baier, A. Kovner, M. Nardi, and U. A. Wiedemann, *Particle correlations in saturated QCD matter*, *Phys. Rev.* **D72** (2005) 094013, [[hep-ph/0506126](#)].
- [65] E. Iancu and D. Triantafyllopoulos, *JIMWLK evolution for multi-particle production in Langevin form*, [arXiv:1307.1559](#).
- [66] T. Lappi, S. Srednyak, and R. Venugopalan, *Non-perturbative computation of double inclusive gluon production in the Glasma*, *JHEP* **1001** (2010) 066, [[arXiv:0911.2068](#)].
- [67] A. Bzdak, B. Schenke, P. Tribedy, and R. Venugopalan, *Initial state geometry and the role of hydrodynamics in proton-proton, proton-nucleus and deuteron-nucleus collisions*, *Phys. Rev.* **C87** (2013) 064906, [[arXiv:1304.3403](#)].
- [68] U. W. Heinz and A. Kuhlman, *Anisotropic flow and jet quenching in ultrarelativistic $U + U$ collisions*, *Phys. Rev. Lett.* **94** (2005) 132301, [[nucl-th/0411054](#)].

- [69] A. J. Kuhlman and U. W. Heinz, *Multiplicity distribution and source deformation in full-overlap U+U collisions*, *Phys.Rev.* **C72** (2005) 037901, [[nucl-th/0506088](#)].
- [70] A. Kuhlman, U. W. Heinz, and Y. V. Kovchegov, *Gluon saturation effects in relativistic U + U collisions*, *Phys. Lett.* **B638** (2006) 171–177, [[nucl-th/0604038](#)].
- [71] F. Gelis, T. Lappi, and R. Venugopalan, *High energy factorization in nucleus-nucleus collisions*, *Phys.Rev.* **D78** (2008) 054019, [[arXiv:0804.2630](#)].
- [72] F. Gelis, T. Lappi, and R. Venugopalan, *High energy factorization in nucleus-nucleus collisions. II. Multigluon correlations*, *Phys.Rev.* **D78** (2008) 054020, [[arXiv:0807.1306](#)].
- [73] L. Frankfurt, M. Strikman, and C. Weiss, *Dijet production as a centrality trigger for pp collisions at CERN LHC*, *Phys.Rev.* **D69** (2004) 114010, [[hep-ph/0311231](#)].
- [74] L. Frankfurt, M. Strikman, and C. Weiss, *Transverse nucleon structure and diagnostics of hard parton-parton processes at LHC*, *Phys.Rev.* **D83** (2011) 054012, [[arXiv:1009.2559](#)].
- [75] B. Alver and G. Roland, *Collision geometry fluctuations and triangular flow in heavy-ion collisions*, *Phys.Rev.* **C81** (2010) 054905, [[arXiv:1003.0194](#)].
- [76] J. Jalilian-Marian, A. Kovner, L. D. McLerran, and H. Weigert, *The intrinsic glue distribution at very small x*, *Phys. Rev.* **D55** (1997) 5414–5428, [[hep-ph/9606337](#)].
- [77] Y. V. Kovchegov, *Non-abelian Weizsäcker-Williams field and a two-dimensional effective color charge density for a very large nucleus*, *Phys. Rev.* **D54** (1996) 5463–5469, [[hep-ph/9605446](#)].
- [78] Y. V. Kovchegov, *Quantum structure of the non-Abelian Weizsäcker-Williams field for a very large nucleus*, *Phys. Rev.* **D55** (1997) 5445–5455, [[hep-ph/9701229](#)].
- [79] D. Kharzeev, Y. V. Kovchegov, and K. Tuchin, *Cronin effect and high-p(t) suppression in p collisions*, *Phys. Rev.* **D68** (2003) 094013, [[hep-ph/0307037](#)].
- [80] E. Avsar and J. C. Collins, *Inability to find justification of a k_T -factorization formula by following chains of citations*, [arXiv:1209.1675](#).
- [81] E. P. Wigner, *On the quantum correction for thermodynamic equilibrium*, *Phys.Rev.* **40** (1932) 749–760.
- [82] A. V. Belitsky, X. Ji, and F. Yuan, *Final state interactions and gauge invariant parton distributions*, *Nucl.Phys.* **B656** (2003) 165–198, [[hep-ph/0208038](#)].
- [83] A. Accardi, J. Albacete, M. Anselmino, N. Armesto, E. Aschenauer, et al., *Electron Ion Collider: The Next QCD Frontier - Understanding the glue that binds us all*, [arXiv:1212.1701](#).
- [84] F. Dominguez, C. Marquet, B.-W. Xiao, and F. Yuan, *Universality of Unintegrated Gluon Distributions at small x*, *Phys.Rev.* **D83** (2011) 105005, [[arXiv:1101.0715](#)].
- [85] R. Hanbury Brown and R. Twiss, *A Test of a new type of stellar interferometer on Sirius*, *Nature* **178** (1956) 1046–1048.
- [86] P. Cvitanovic, *Group theory: Birdtracks, Lie's and exceptional groups*. Princeton University Press, 2008. Available online at <http://birdtracks.eu/>.
- [87] J. P. Blaizot, T. Lappi, and Y. Mehtar-Tani, *On the gluon spectrum in the glasma*, *Nucl. Phys.* **A846** (2010) 63–82, [[arXiv:1005.0955](#)].
- [88] A. Kovner and U. A. Wiedemann, *Nonlinear qcd evolution: Saturation without unitarization*, *Phys. Rev.* **D66** (2002) 051502, [[hep-ph/0112140](#)].
- [89] E. Levin, L. Lipatov, and M. Siddikov, *BFKL Pomeron with massive gluons*, [arXiv:1401.4671](#).
- [90] D. Kharzeev and E. Levin, *Manifestations of high density QCD in the first RHIC data*, *Phys. Lett.* **B523** (2001) 79–87, [[nucl-th/0108006](#)].
- [91] D. Kharzeev, E. Levin, and M. Nardi, *The onset of classical QCD dynamics in relativistic heavy ion collisions*, *Phys. Rev.* **C71** (2005) 054903, [[hep-ph/0111315](#)].
- [92] K. Rummukainen and H. Weigert, *Universal features of JIMWLK and BK evolution at small x*, *Nucl. Phys.* **A739** (2004) 183–226, [[hep-ph/0309306](#)].
- [93] Y. V. Kovchegov, J. Kuokkanen, K. Rummukainen, and H. Weigert, *Subleading- N_c corrections in non-linear small-x evolution*, *Nucl. Phys.* **A823** (2009) 47–82, [[arXiv:0812.3238](#)].
- [94] A. Dumitru, J. Jalilian-Marian, T. Lappi, B. Schenke, and R. Venugopalan, *Renormalization group evolution of multi-gluon correlators in high energy QCD*, *Phys.Lett.* **B706** (2011) 219–224, [[arXiv:1108.4764](#)].
- [95] A. Kovner and U. A. Wiedemann, *Eikonal evolution and gluon radiation*, *Phys. Rev.* **D64** (2001) 114002, [[hep-ph/0106240](#)].
- [96] E. Iancu and D. Triantafyllopoulos, *JIMWLK evolution in the Gaussian approximation*, *JHEP* **1204** (2012) 025, [[arXiv:1112.1104](#)].
- [97] E. Iancu and D. Triantafyllopoulos, *Higher-point correlations from the JIMWLK evolution*, *JHEP* **1111** (2011) 105, [[arXiv:1109.0302](#)].
- [98] E. Iancu, K. Itakura, and L. McLerran, *Geometric scaling above the saturation scale*, *Nucl. Phys.* **A708** (2002) 327–352, [[hep-ph/0203137](#)].
- [99] A. H. Mueller and D. N. Triantafyllopoulos, *The energy dependence of the saturation momentum*, *Nucl. Phys.* **B640** (2002) 331–350, [[hep-ph/0205167](#)].
- [100] D. Kharzeev, E. Levin, and L. McLerran, *Parton saturation and N(part) scaling of semi-hard processes in QCD*, *Phys. Lett.* **B561** (2003) 93–101, [[hep-ph/0210332](#)].
- [101] J. L. Albacete, N. Armesto, A. Kovner, C. A. Salgado, and U. A. Wiedemann, *Energy dependence of the Cronin effect from non-linear QCD evolution*, *Phys. Rev. Lett.* **92** (2004) 082001, [[hep-ph/0307179](#)].
- [102] E. Levin and K. Tuchin, *Solution to the evolution equation for high parton density qcd*, *Nucl. Phys.* **B573** (2000)

833–852, [hep-ph/9908317].